Analysis of the Hydrogen Gas Distribution in the Galaxy HIZSS 3

Lance Edens
Advisor: Dr. Patricia Henning

Honors Thesis
University of New Mexico
Department of Physics and Astronomy
April 21, 2006

Abstract

The dwarf galaxy HIZSS 3 was discovered by the HI Parkes Zone of Avoidance Shallow Survey (HIZSS); a project that used 21 cm observations to search for nearby galaxies hidden by the Milky Way. Out of over 100 galaxies reported in the survey, HIZSS 3 stood out as particularly interesting. Relatively close to our own galaxy, HIZSS 3 showed an odd morphology, appearing to have a small clump of gas to one side that coincided with H_α emission. Using the Very Large Array radio interferometer, we looked at the neutral hydrogen gas in this galaxy at a resolution of 12 arcseconds. Our images reveal that HIZSS 3 is in fact two separate galaxies. The larger galaxy, called HIZSS 3a, shows a fairly regular velocity field, while the smaller galaxy, called HIZSS 3b, is highly disturbed. We derived an HI mass for the galaxies to be $\approx 2.2 \times 10^7 M_\odot$ and $\approx 2.7 \times 10^6 M_\odot$ for HIZSS 3a and HIZSS 3b respectively. We used the rotation velocity of HIZSS 3a to estimate a total mass of $\approx 7.9 \times 10^8 M_\odot$. For the smaller galaxy, we used the velocity dispersion to estimate a total mass of $\approx 2.9 \times 10^7 M_\odot$. No evidence for an HI bridge between the galaxies was observed, but we did see some indication of interaction in their morphologies and kinematics. We also found that the H_α star formation region lies in the center of HIZSS 3b, but through qualitative analysis concluded that the region is probably not energetic enough to disrupt the galaxy.

Introduction

The Zone of Avoidance (ZOA) is a region of the sky where observations of external galaxies and the large-scale structure of the universe are hampered by the gas, dust, and stars of the Milky Way. Covering roughly 20% of the optical sky, the ZOA blocks short-wavelength x-ray and optical light, making for a confusing source of infrared light via radiation from warm Galactic dust. Only long-wavelength radio waves are allowed to pass through unhindered. The inability to use optical wavelengths in the ZOA has led to a lack of catalogued galaxies in that region. This problem was partially addressed by the HI Parkes Zone of Avoidance Shallow Survey (HIZSS), a project that

used the Parkes radio telescope in Australia to search for nearby galaxies hidden by the Milky Way. Observing at 21cm, Henning et al. looked for relatively close galaxies in an effort to better understand the motion of the Local Group, a collection of neighboring galaxies gravitationally bound to the Milky Way. 21cm radiation is commonly used by radio astronomers because it corresponds to the wavelength of radiation emitted by neutral hydrogen (HI). The emission is caused by hydrogen's electron transitioning its spin from an aligned to an anti-aligned state with respect to the proton's spin. Observing in the 21cm band allows observers to detect hidden spiral and dwarf galaxies (those types which typically contain neutral hydrogen), measure their redshifts, and also map the HI distribution in a galaxy; providing internal kinematical information (Henning et al. 2000).

Out of over 100 galaxies reported in the survey, one galaxy, designated HIZSS 3, appeared particularly interesting. The galaxy had a low redshift, making it the closest galaxy discovered by the Parkes ZOA survey. A follow-up study focusing on HIZSS 3, performed by Massey, Henning, and Kraan-Korteweg in 2003, included a low resolution Very Large Array (VLA) radio interferometer HI map. The VLA will be discussed in more detail later. Recently, a paper by Begum et al. was published that used the Giant Metrewave Radio telescope in India to observe HIZSS 3. Their paper included data that had a similar angular resolution to the observations presented here, but at a higher noise level (Begum et al. 2005).

Current Knowledge of HIZSS 3

HIZSS 3 is a low-mass dwarf irregular magellanic (dIm) galaxy with an average velocity of 134 km/s with respect to the Local Group. Assuming that the universe is expanding at a constant rate, with the Hubble Constant (H_0) equal to 75 km/sec Mpc^{-1} (1 pc = 3.26 light years), the equation

$$v = H_0 d$$

gives a simple relationship between velocity v and distance d. Using this equation and the above velocity of HIZSS 3, an approximate distance of 1.8 Mpc is determined, making it the closest dIm galaxy discovered in the past 25 years (Massey et al. 2003). Silva et al. (2005) made an independent measurement of the galaxy's distance using the brightness of its giant stars in the near infrared, and calculated a distance of (1.69 ± 0.07) Mpc, in excellent agreement with the earlier estimate. The Silva et al. value will be the distance used in our calculations. HIZSS 3 has a diameter of 3 kpc, with a rough HI mass estimate of 2.5×10^7 $M_\odot$ ($1\ M_\odot = 1.989 \times 10^{30}$ kg). The most interesting feature of this galaxy is the presence of an asymmetric lump of HI. This can be seen in the figure below which displays contours of observed HI emission as mapped by the VLA's D-array.

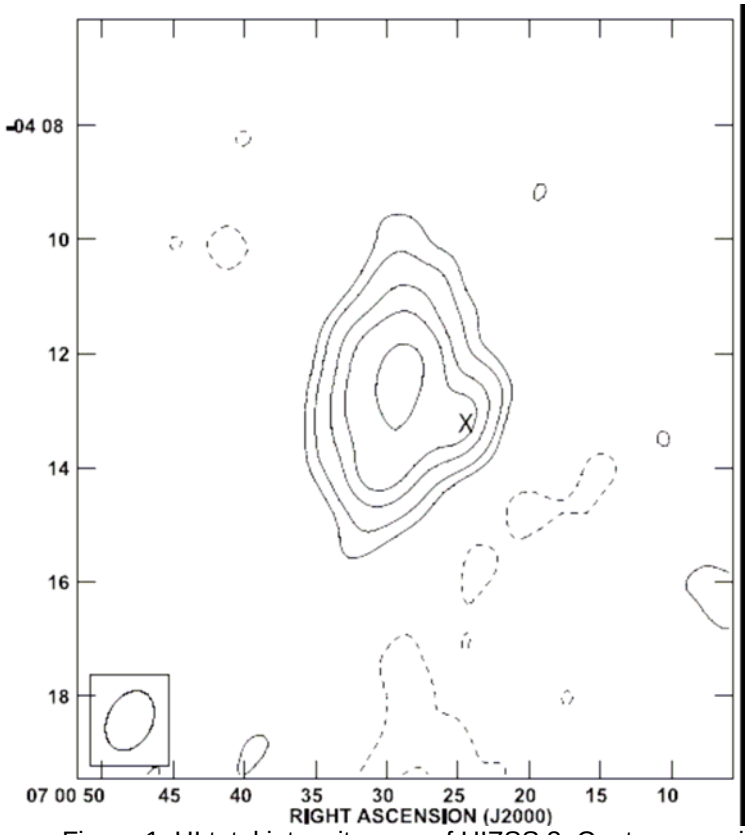

Figure 1: HI total intensity map of HIZSS 3. Contours are integrated HI emission with levels at -4, -2, 2, 4, 8, 12, and 20 times the rms noise of 1.6 x 10^{-2} Jy $beam^{-1}$. The synthesized beam is represented at the lower left-hand corner. (Massey et al. 2003)

The "X" in the above figure marks the location of an Hα source, indicating the presence of ionized hydrogen. Ionized hydrogen in turn indicates an area of star formation. The fact that the Hα emission coincides with the HI irregularity offers tantalizing clues about the nature of the irregularity, but unfortunately the resolution provided by Massey et al. is too coarse to provide any further details (Henning and Massey 2003).

VLA: Introduction

The VLA is a radio interferometer located on the Plains of San Agustin, fifty miles west of Socorro, New Mexico. Dedicated in 1980, it contains 27 antennae (plus one spare) arranged in a Y formation. Each antenna has a diameter of 25 meters (and weighs 230 tons). The array can observe at frequencies as high as 50 GHz and as low as 74 MHz. See http://www.vla.nrao.edu/genpub/overview/ for an overview of the VLA.

As an interferometer, the VLA uses its multiple antenna dishes in tandem in order to synthesize a single collecting apparatus with an equivalent diameter equal to the size of the array.

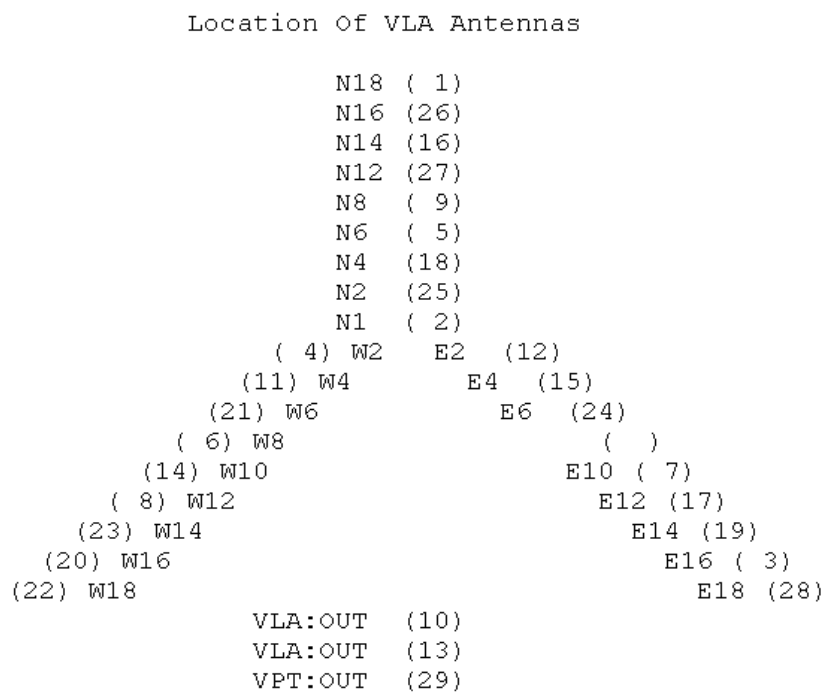

Figure 2: AIPS output of the antenna configuration of the VLA at the time of our observations. This diagram does not represent actual spacing between the individual antennas

Interferometery

In order to understand how the VLA works, let us focus on a pair of antennae with the vector $\vec{B}$ representing the distance between them. This distance is known as the baseline and it is the fundamental measuring parameter of an interferometer. The length of a baseline determines an interferometer's resolution. Short baselines are sensitive to large-angle structure while long baselines are sensitive to small-scale structure. Now let us point the two antennae at a distant source. The radiation each telescope receives from the source can be approximated as a plane wave. As the wavefront arrives at our baseline pair, it will be measured by each antenna at different times, corresponding to a geometrical delay of τ_g given by

$$\tau_g = \vec{B} \cdot \frac{\vec{s}}{c}$$

where $\vec{B}$ is the baseline vector, *c* is the speed of light, and $\vec{s}$ a vector that points toward the source, perpendicular to the wavefront (Thompson 1999). Figure 3 below provides a simple illustration of this concept.

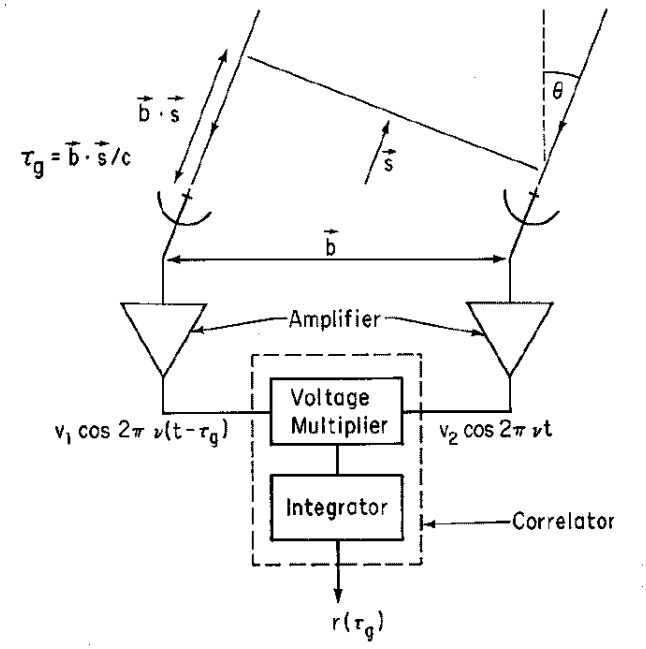

Figure 3: Simplified diagram of a single baseline pair. (Thompson 1999)

Radiation collected by each antenna is sent through filters that isolate the bandwidth dν, or range of frequencies, that is currently of interest. The voltage signals are then digitized and sent to a correlator, which contains a voltage multiplier and a time averaging unit called an integrator. In the end, what is measured by the baseline pair is a component of the visibility function, V(B), sometimes called the complex fringe visibility.

$$V(B) = \int\int A(\sigma)\, I(\sigma)\, e^{\left(i\frac{\omega}{c} B\cdot\sigma\right)}\, d\sigma$$

Here σ represents an area over the sky, A(σ) is the normalized antenna reception pattern, I(σ) is the intensity function, or brightness distribution, of the source, and the exponential describes the incoming radiation wave (Rohlfs 2004).

The brightness distribution of the source is calculated from the inverse Fourier transform of V(B), and is commonly measured in Janskys (Jy), a unit named after one of the pioneers of radio astronomy.

$$1\ \text{Jy} = 10^{-26}\ \frac{W}{m^2 \cdot Hz}$$

Measuring the baseline vector in the visibility function is accomplished using the (*u*,*v*,*w*) coordinate system. Measured in units of wavelength, u and v are baseline distances while w is the three dimensional curvature of those baselines. This coordinate system is convenient for baseline measurements and relates to the angular sky coordinates (x,y,z) by the Fourier transform

$$V(u,v,w)\, e^{-i2\pi w} = \int_{-\infty}^{\infty}\int_{-\infty}^{\infty} A(x,y)\, I(x,y)\, e^{-i2\pi(ux+vy)}\, dx\, dy$$

where A(x,y) is the effective area of the telescope , and I(x,y) is the intensity function of the source as functions of the x,y,z coordinate system (Rohlfs 2004).

For VLA observations of relatively small fields of view, such as for HIZSS 3, the w and z coordinates do not appear in the Fourier transform relation.

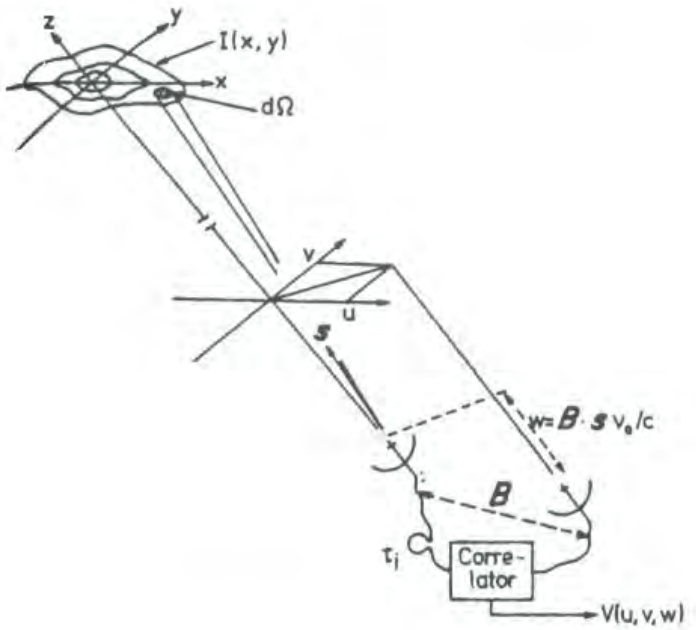

Figure 4: Geometrical relationship between (u,v,w) and (x,yz) coordinates. (Rohlfs 2004)

As shown above, the visibility function V(B) contains both an amplitude and a phase. The phase represents the time delay between each antenna pair. By common practice, the center of a source is arbitrarily set to zero phase. The distance measured from the source's center is then determined by the shift in phase. This is illustrated in Figure 5, where S_0 is the vector of zero phase, S is the distribution of the source on the sky, dΩ is the solid angle, and the vector σ is indicating the shift in phase.

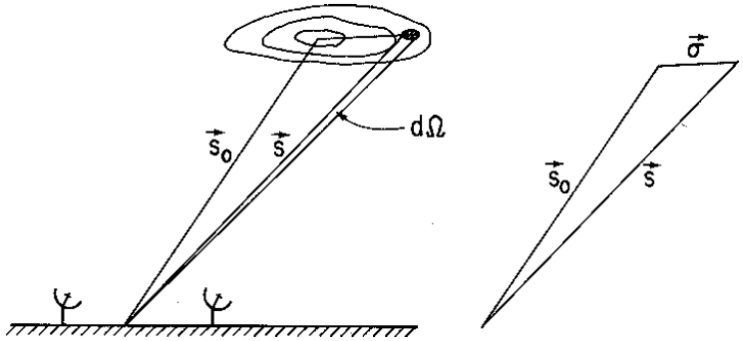

Figure 5: The position vectors that determine the distance from the source's center or point-of-zero-phase. (Thompson 1999)

The number of baselines in the interferometer determines the number of visibility measurements during a single integration time. The more points on the (*u*,*v*) plane, the

better the final result. In the case of the VLA, the 27 antennae, represented by N in the following equation, give a total number of baselines of

$$\frac{N(N-1)}{2} = \frac{(27)(26)}{2} = 351 \text{ baselines}$$

In other words, at any given instant, there are 351 visibility measurements being performed at a given frequency. As the Earth rotates, the baselines sample different angles of the sky, increasing the number of visibility measurements made on any given source (Bedding 1996).

With the multiple visibility measurements in hand, only an inverse Fourier transform is needed to find the intensity distribution of the source object. The intensity distribution, also called the surface brightness, is the power per area per frequency integrated over the source, and is what we are ultimately trying to measure.

$$I'(x, y) = A(x, y)\, I(x, y) = \int_{-\infty}^{\infty}\int_{-\infty}^{\infty} V(u, v, 0)\, e^{-i2\pi(ux+vy)}\, du\, dv$$

It is common to see the intensity function, I(x, y), modified by the beam shape A(x, y); as represented in the above equation as I′(x, y) (Rohlfs 2004). This modified intensity is given in terms of Jy/Beam.

Interferometers have two types of "beams." The primary beam is a measurement of the sky an antenna can see, analogous to its field-of-view. This beam is determined by the size of an individual antenna.

$$\text{Primary beam} \approx \frac{\lambda}{D}$$

Here D is the diameter of a single dish and λ is the wavelength. The synthesized beam is the resolution on the sky. This is determined by the span of baselines in an interferometer.

$$\text{Resolution} \approx \frac{\text{Wavelength}}{\text{Baseline length}}$$

VLA Revisited

The VLA has four different main configurations, A, B, C, and D, relating to the spacing of the individual antennas. The A configuration is the largest, with a maximum antenna separation of 36 km. The D configuration is the smallest with only a maximum antenna separation of 1 km. The Massey, Henning, and Kraan-Korteweg follow-up study of HIZSS 3 was performed using D-array. Their resolution therefore was

$$\text{Resolution} = \frac{21cm}{1x10^{5}cm} = 2.1 \text{ x } 10^{-4} \text{ radians} \approx 43"$$

We observed HIZSS 3 at 21cm using the C configuration, with a maximum baseline of 3.6 km. This means our resolution is

Resolution = $\frac{21cm}{3.6x10^5 cm} = 5.83 \text{ x } 10^{-5}$ radians ≈ 12”

So we have a little over three and a half times better resolution than the Massey, Henning, and Kraan-Korteweg study (Massey et al. 2003). Interestingly, we did not want to go too much higher on the resolution since it might “resolve out” any HI that we wished to observe. Interferometers are blind to structures which are significantly larger than the angles sampled by the shortest baselines.

Reasons to Calibrate

Spectral-line observations require three different calibrations; the flux, the phase, and the bandpass. During an observation, the telescope will image at least two calibrator sources in addition to the source of interest. The flux, or primary, calibrator is the brightest object imaged, and is typically viewed only once per observation. This calibrator is used to determine the gain and the bandpass. The gain affects the amplitude of the visibility function by causing each antenna to measure a value slightly off from the true visibility of the source. As the antennae are not exactly identical, their gains will differ slightly between each receiver. This deviation is easy to eliminate if an object of known flux is imaged during an observation. Commonly, quasars are used as primary calibrators because they are very bright, point-like objects. Bright objects are preferred because it reduces the integration time needed for a good signal-to-noise ratio.

The phase, or secondary, calibrator is used to clean up some of the effects of the atmosphere as well as to standardize the antennae measurements. The phase calibrator is usually near the object of interest; since it is imaged several times during an observational period and should have atmospheric effects that match those of the source as closely as possible. While the gain of an antenna does not vary much over a short period of time, the phase relationships between the antenna signals can vary on relatively short timescales. This is due to atmospheric changes, electronic variations in the equipment, and even terrestrial noise from objects like cell phones and cars. As mentioned above, the distance from the center of an object is determined by the phase value of the visibility function. In order for the measurements to make sense, each antenna needs to agree on where the center of the source is located. This is determined by looking at a point-source and calibrating the phase variations across the array to zero. In this manner, the incoming plane wave is artificially made to arrive at each antenna at the same time.

Spectral-line observations also include a bandpass calibration by observing an object, usually the flux calibrator, whose spectrum is known. Ideally, an antenna should respond equally to all frequencies; however, this is never the case. There is always a slight gain across frequencies, mostly due to imperfection in the antenna’s electronics, as well as atmospheric interference. The calibration procedure allows the slight differences in frequency-dependent responses to be corrected to an average value.

It is important to note that calibrators should be unresolved by the array observing them. As mentioned above, they need to appear as point-like sources without any visible structure so that the calibration correction can be set properly.

AIPS

The NRAO's Astronomical Image Processing System (AIPS) is a software package designed specifically for radio interferometric data. Used by professional astronomers across the globe, AIPS is the primary tool for calibration, analysis and display of both continuum and spectral line VLA images. Since its creation in 1978, AIPS has grown to include 405 separate tasks or applications, with over 5 megabytes of "help" text; making it an extremely versatile program. Learning to use AIPS provides valuable experience essential to work in radio astronomy (AIPS Cookbook).

In what follows, the term "flagging" refers to the process of removing data points from further processing. Any data that is considered unusable is not actually deleted from the original data set, but is simply flagged and ignored during the calibration and image processing. For example, occasionally the array is oriented in such as way that some antennas block the view of others, a process called shadowing. When shadowing occurs, the data from the blocked antenna is corrupted by the electronics of the antenna in front, and must be flagged.

Calibration Method

To calibrate our results, the middle 75% of the spectral-line data is averaged together to create a continuum-like file. Since the flux and phase calibrations apply to the entire bandwidth, the line-specific data does not add any information to the calibration, allowing the data to be averaged without affecting the quality of the calibration. The benefits of averaging are decreased computational time and the ability to utilize the same initial calibration processes for both continuum and spectral line observations. Only the middle range of the line data is used because the beginning and end channels, or frequency bins, have high noise resulting from the decreased sensitivity at the ends of the bandpass.

The AIPS program has a table of primary sources for which the flux as a function of frequency is known. In our case the quasar 3C147 (0542+498) is the primary calibrator. Once the main calibrator is selected, AIPS then knows the correct gain for the flux calibration, and the user must perform the first of three calibration runs. This first calibration utilizes a reference antenna, in our case antenna 11 (see Figure 2). It then calculates the variation in amplitude and phase for the rest of the antennas relative to the reference antenna. The choice of the reference antenna is somewhat arbitrary. However, for this array configuration looking at low elevations, a reference antenna too close to the center of the array would be missing too many data entries due to shadowing; while an antenna too far away from the center would not contain enough samplings of short baselines. This initial calibration allows for systematic errors to be manually found and flagged. Ideally, after this calibration, all the baselines should have similar amplitudes and the phase difference should be exactly or close to zero. While single odd gain fluctuations are ignored as random noise, any persistent large variance from average values shows a systematic error and should be flagged. The amount of flagging done depends on the user's preference, but a good rule of thumb is that it is better to do too little than too much and lose valuable data.

The steps in the phase calibration are very similar to those of the flux calibration. The value for the secondary calibrator, in our case 0725-009, must be entered into AIPS with the help of the VLA Calibrator manual, which can be found at www.aoc.nrao.edu/~gtaylor/calib.html. Once the position for the calibrator is given to

AIPS, it corrects for the phase difference between simultaneous baselines using the reference antenna. This process is then followed by a final calibration run that writes a complete calibration table. At this point, we used AIPS imaging commands to make a quick image that allowed us to visually confirm the calibrators to ensure that they were unresolved points.

Finally, the bandpass calibration was performed on the spectral-line data. AIPS makes this calibration step relatively simple; requiring only a visual check to confirm the bandpass appeared as expected.

Imaging

Spectral line imaging involves continuum subtraction, Fourier transforming, and deconvolution. Continuum subtraction, as the name suggests, is the process that removes the continuum emission from the data set. Without removal, the continuum emission would swamp the spectral lines, making it impossible to get any useful information about the HI from the data.

Before continuum subtraction and deconvolution take place, channels that do not contain HI line emission from the galaxy need to be determined. This is found manually by making quick, unprocessed channel maps of the data. Frequency bins, also known as channels, that contain only continuum information are called line-free channels.

Also necessary for data reduction is the calculation of the noise. An estimate of the expected noise is required by AIPS to perform the continuum subtraction and by the user in order to know how deep to deconvolve the image. Using a single baseline, the expected rms noise for that baseline is calculated with the following equation

$$\Delta I_m = \frac{k}{\sqrt{N(N-1)(N_{IF})T_{INT}\Delta\nu}}$$

where ΔI_m is the noise per time integrated in mJy, N is the number of antennas, N_{IF} is the number of integration frequencies, T_{INT} is integration time in hours, $\Delta\nu$ is the channel width, and k is a constant related to the observed frequency (AIPS Cookbook).
In our case, the above equation looked like

$$\Delta I_m = \frac{8.0}{\sqrt{2(2-1)(1)(0.00833)(0.0122)}}$$

which gave a noise of ΔI_m = 561.1 mJy for a single 30-second scan.

Once the line-free channels are found, continuum subtraction can begin. Using the specified channels, AIPS creates a linear fit to the signal in those channels and then applies that fit to the entire (u,v) data set. Essentially, AIPS uses a linear model for the continuum emission, and it simply subtracts that linear fit from the data, allowing the source information to be easily recognized. Along with the continuum subtraction, AIPS allows the additional removal of noise above a certain cutoff value, in our case eight times the noise on one baseline, which helps to clean up the image.

After the continuum has been removed, the first true images can be rendered. An image, or map, is basically a plot of the intensity function across an area of the sky. However, throughout the calibration process the data has remained in (u,v) format, representing sampling of the visibility function. As mentioned above, the data must first undergo an inverse Fourier transform to change to a coordinate system that will represent the intensity function. Quality of the image is improved by increasing the number of data

points sampled in the (u,v) plane. Once the data has been Fourier transformed, images can be produced, but they will contain artifacts resulting from the relatively sparse sampling of the (u,v) plane. To produce a perfect, artifact-free image, an infinite number of (u,v) data points are needed; something which is impossible. Therefore any real image produced will contain artifacts. Maps produced with these artifacts are called dirty images (Figure 6). In these images, artifacts such as the X-shaped sampling pattern of the VLA easily dominate the image. In order to produce nicer, more readable images, these artifacts are usually removed via a process called CLEAN.

The nonlinear CLEAN technique is the most common deconvolution method. J. Hogbom first introduced the concept of CLEAN in 1972, and today it utilizes the iterative power of computers to remove nonphysical artifacts from an image. It Fourier transforms the image data with the dirty beam element and convolves the result with a Gaussian, which represents an ideal beam. In other words, it approximates the actual, partially-known brightness distribution with a reasonable function to represent taking an infinite (u,v) sampling. CLEAN also allows various (u,v) data weights to be selected, which places emphasis on either spatial resolution or the reduction of the signal-to-noise ratio. We chose the "robust" weight, which is a middle-ground weight that does not emphasize either resolution extreme. The CLEAN process of Fourier transforming and convolving is performed on the single highest intensity peak in a given channel, removing the dirty beam elements from that peak. The process is then repeated for the next highest peak and so on until the peak intensity reaches a set level. Commonly, it is a good idea to clean to 2σ of the rms noise in images with a well-defined source, as is the case with HIZSS 3. Cleaning below 2σ in most cases only results in redistributing random noise spikes, which is a waste of time. The iterative CLEANing process is repeated for every specified channel.

While the CLEAN method is by far the most common deconvolution approach, it should be noted that there are alternative methods. For instance, the Maximum Entropy Method (MEM) is a method that is better suited than CLEAN to handle very extended sources, but is slower and used much less frequently. From the low resolution images of HIZSS 3 we know that its emission is not very extended, so this method would not be appropriate for our data.

Maps

With the data fully calibrated, Fourier transformed, and CLEANed, readable maps can finally be rendered. One type of image commonly produced is the channel map. Channel maps, usually displayed in multiple images, show the HI intensity distribution of each individual channel (for channel maps of HIZSS 3, see Appendix). The flux distribution is described by contour lines, which are chosen using the measured rms noise of the image. Channel maps can clearly display where the HI flux is located in each channel, and how it changes with frequency; allowing for easy determination of which channels contain the HI source. Observing at frequency of 1420 MHz, with a resolution of 12.3 kHz, gave us a channel map velocity resolution of 2.6 km/sec. These maps provided us with the first indication that HIZSS 3 is in fact two separate galaxies.

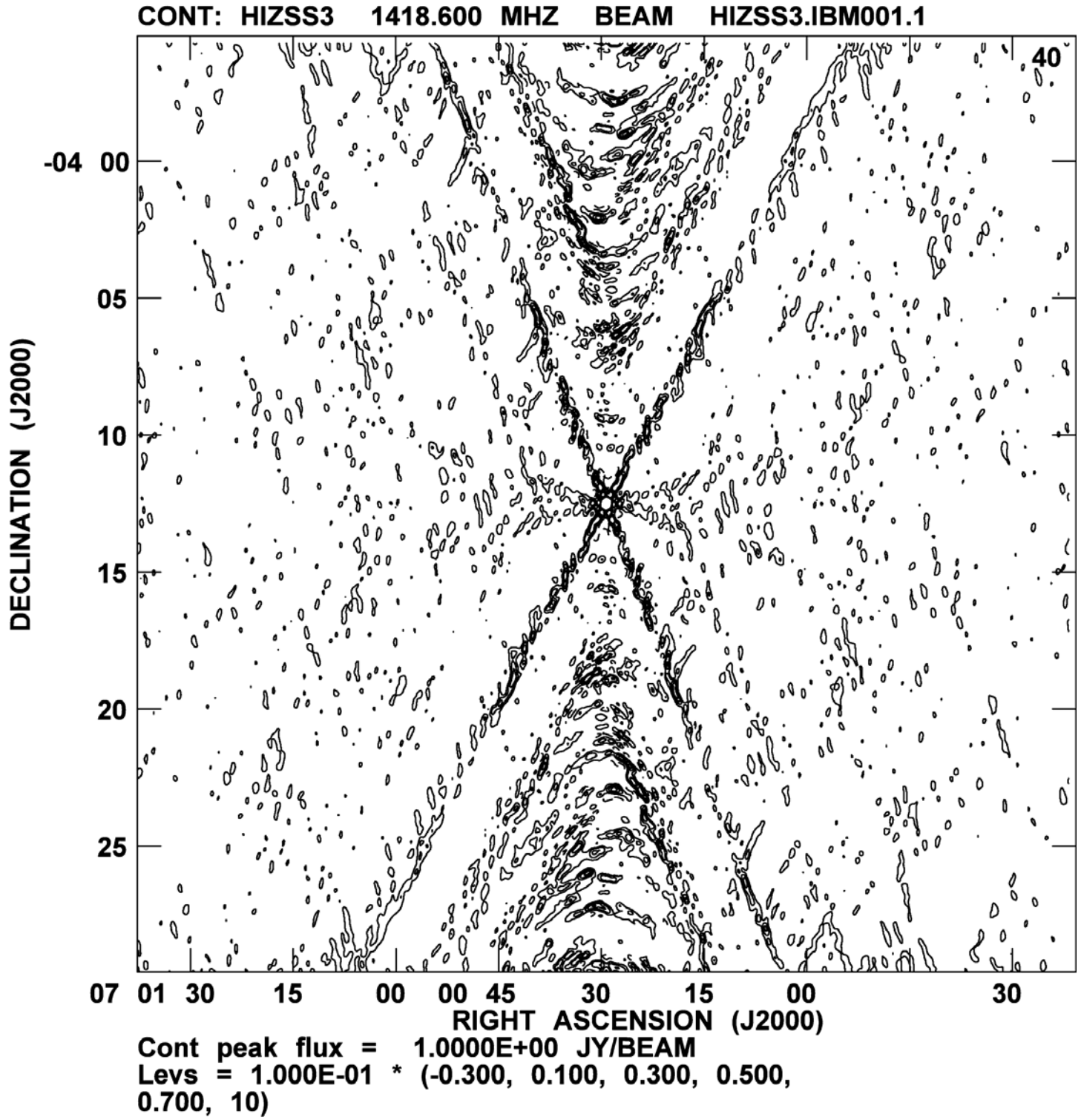

Figure 6: Dirty beam image. Contours are -3%, 3%, 5%, 7% and 100% times the central beam flux of 1 Jy.

An integrated HI map is also a commonly produced image (Figure 7). It is simply a combination of the channel maps summed into a single image. Integrated HI maps allow for an easier visual understanding of the morphology of the source, and are used to measure the total flux; which is needed in order to calculate the total HI mass.

A velocity field is a plot showing contours of constant velocity; they describe the kinematics of the galaxy. In order to produce a clean velocity field, random noise peaks need to be eliminated. To accomplish this, any signal below a set limit, in our case 2.5σ of the measured noise, is removed from the image data. The source is then manually highlighted channel by channel, resulting in the removal of all non-highlighted signals. Highlighting of the source is done by looking for signals that are continuous throughout the channel slices. With the source object clearly defined, AIPS then takes the first moment of the image, resulting in a single velocity field image.

Our velocity field of HIZSS 3 (Figure 8) is a clear indication that we have resolved two separate galaxies, named HIZSS 3a and HIZSS 3b. By using the signal highlighting program again, the two galaxies can be manually separated (Figures 9 and 10). Combing the integrated HI map and the velocity field is a good way to visualize the dynamics of the two galaxies (Figures 11 and 12).

Image Results

HIZSS 3a displays characteristics of a smoothly rotating disk galaxy. The northern region of the galaxy in Figure 9 is redshifted, while the southern region is blueshifted. HIZSS 3a also contains clumps of HI that correspond to small kinks in the velocity field (Figure 11). These clumps are asymmetrically distributed in the galaxy, favoring the side toward HIZSS 3b. The asymmetry of HIZSS 3a is easiest to see in the three-dimensional integrated HI map (Figure 13). However; for the purpose of later calculations we assume that the overall galactic disk is roughly symmetric.

HIZSS 3b is highly disturbed. Due to its small size and non-uniform velocity field, we assume that the galaxy has a spherical shape. This assumption is necessary in order to estimate its total mass, and is supported by the presence of a central HI peak (Figures 12 and 14). This central region is also the location of the galaxy's star formation region. The detection of H_α emission indicates the presence of ionized hydrogen (HII), which in turn is an indication of star formation. The HII region, detected in the earlier Massey, Henning, and Kraan-Korteweg observation, is located at Right Ascension (RA) = 7h 00m 24.57s and Declination (Dec) = −04° 13′ 13.7" (Massey at al. 2003). This location is marked in Figure 12.

Analysis

With the images in hand, analysis of the two galaxies can finally take place. The first, relatively simple calculation is the determination of the galaxies' diameters. The diameters were found using the trigonometric relation

$$D = d \, \mathrm{Sin}\theta$$

where the diameter D is determined from the distance d, and θ is the angular diameter of the galaxy. As stated above, we used a distance of (1.69 ± 0.07) Mpc. Angular diameters were found by measuring the extent of the galaxy in Right Ascension (RA) or Declination (Dec) by hand from printed maps.

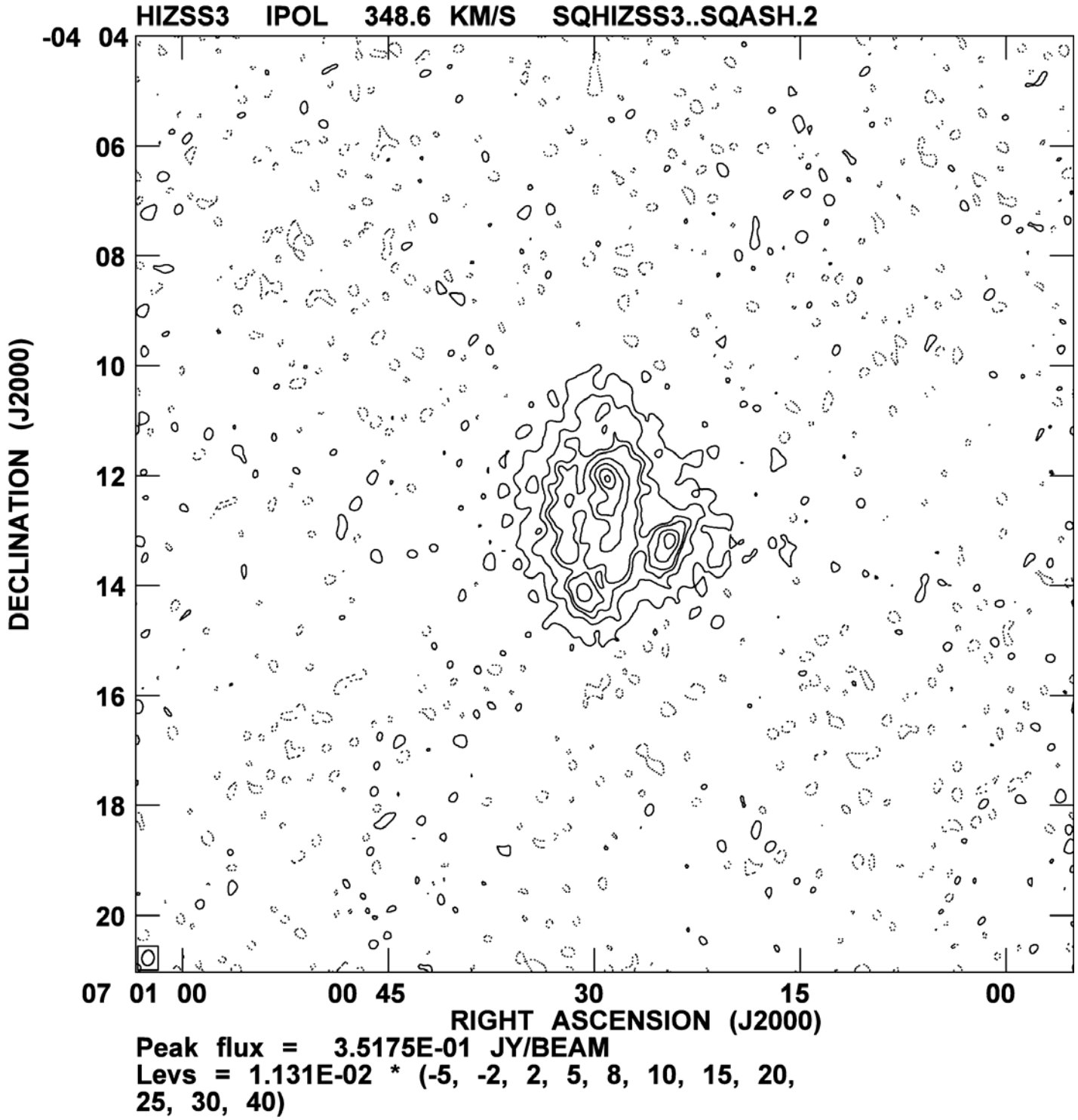

Figure 7: Integrated HI map of HIZSS 3. Flux ranges from 4.7 x 10^{-2} Jy/beam to 3.5 x 10^{-1} Jy beam^{-1} with contours 10 times the rms noise of 1.3 x 10^{-3} Jy/beam.

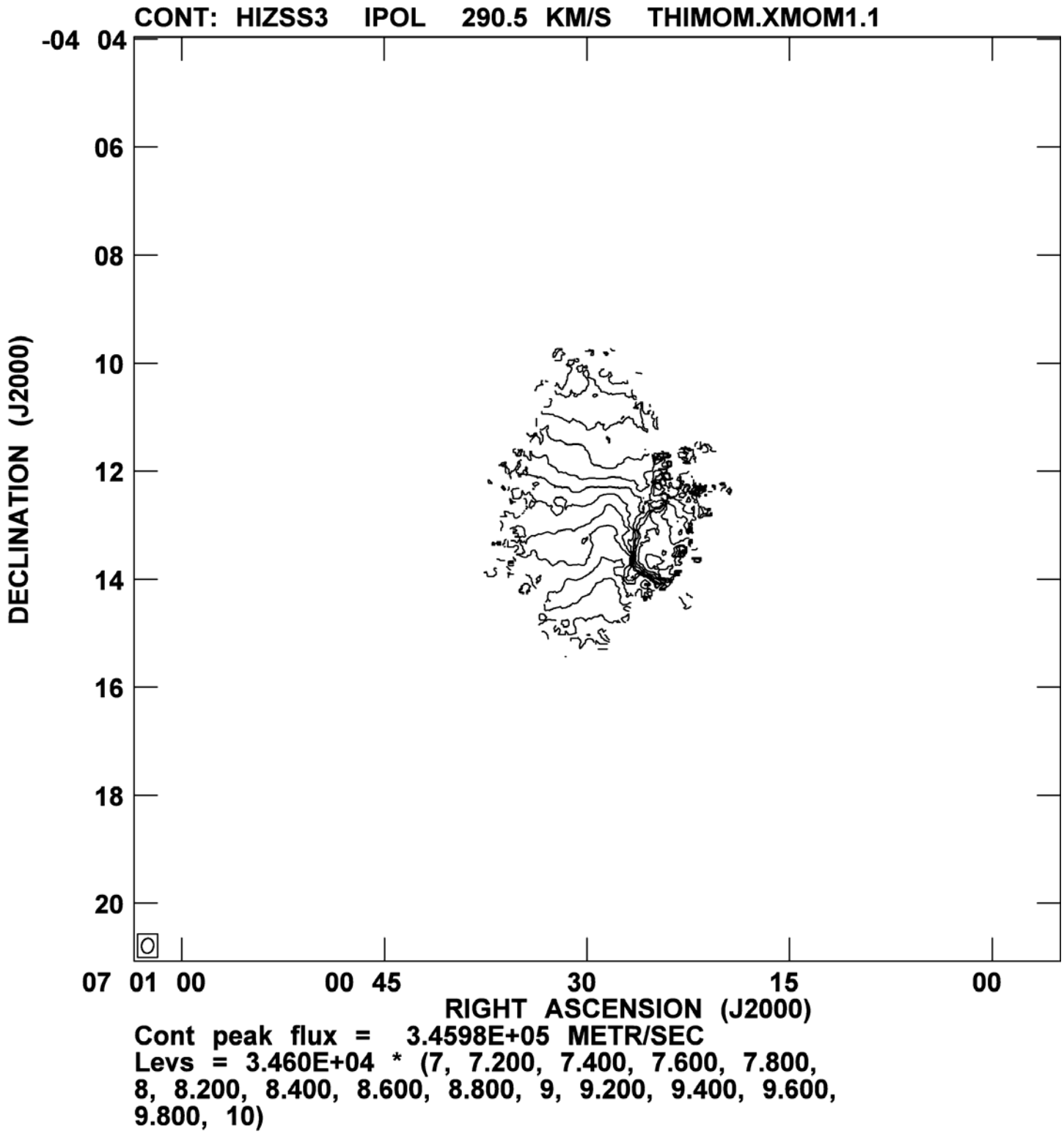

Figure 8: Velocity field of HIZSS 3. Velocity ranges from 240 km/sec to 345 km/sec with contours every 3.5 km/sec.

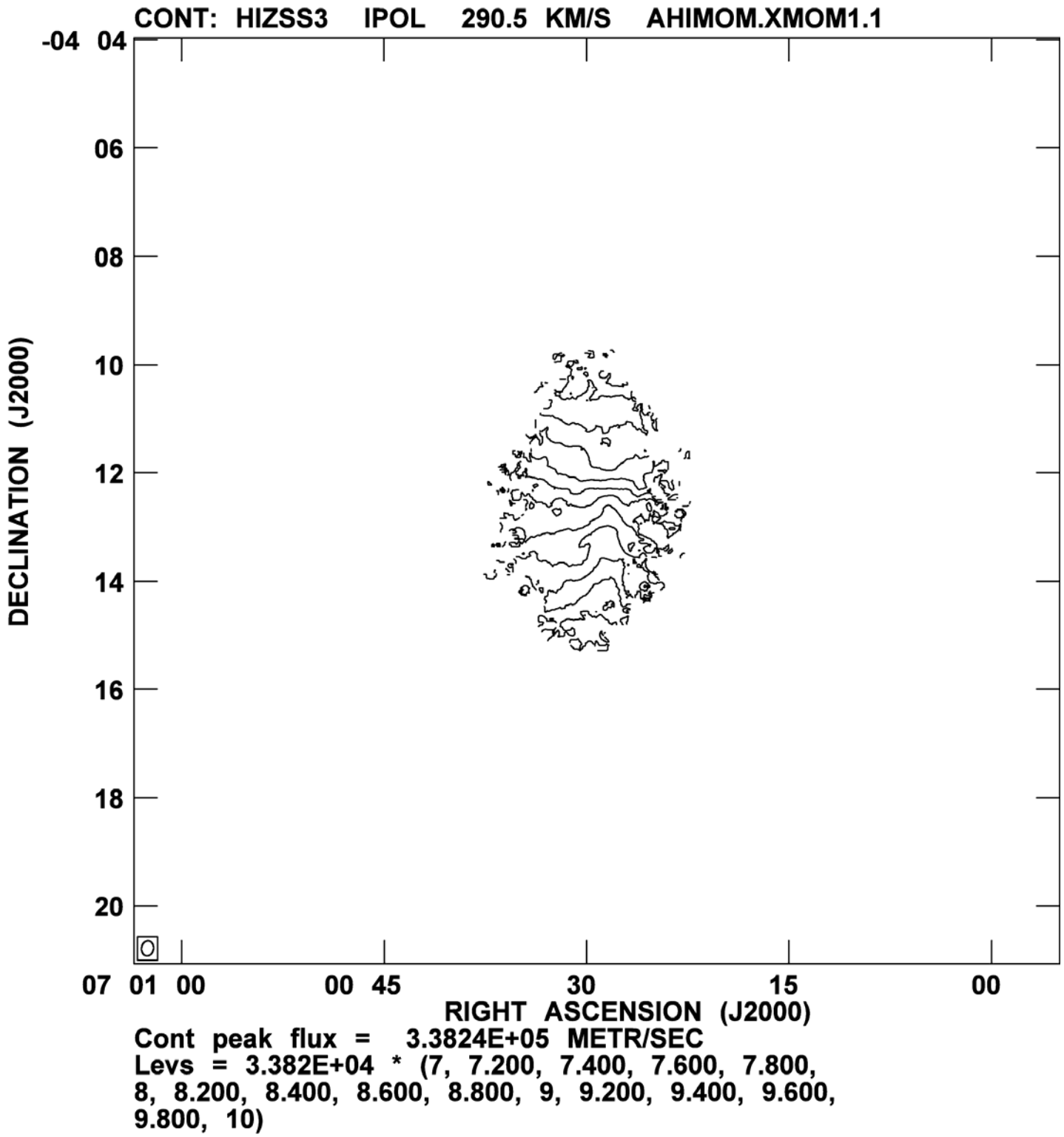

Figure 9: Velocity field of HIZSS 3a. Velocity ranges from 240 km/sec to 338 km/sec with contours every 3.4 km/sec.

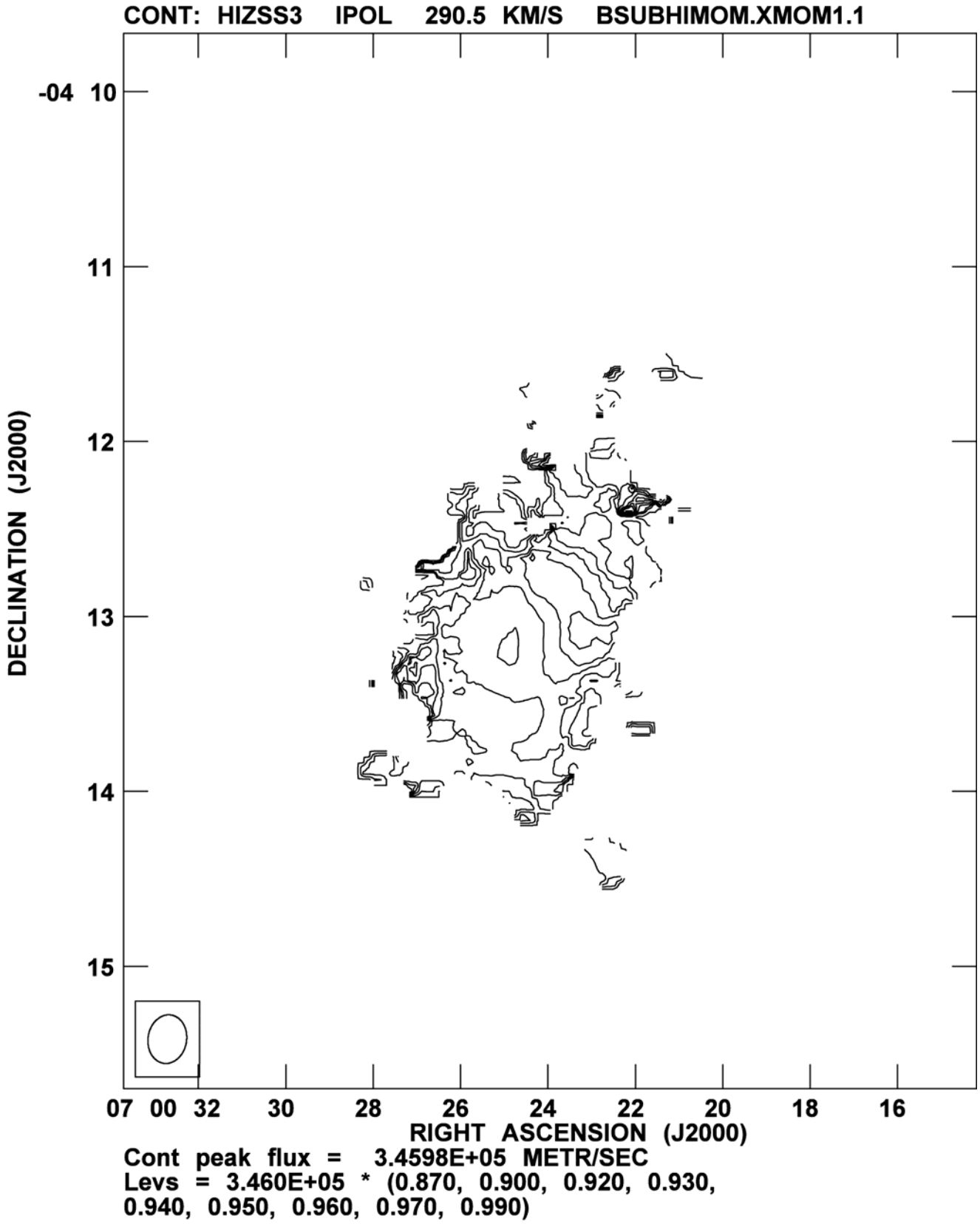

Figure 10: Velocity field of HIZSS 3b. Velocity ranges from 302 km/sec to 345 km/sec with contours every 3.5 km/sec.

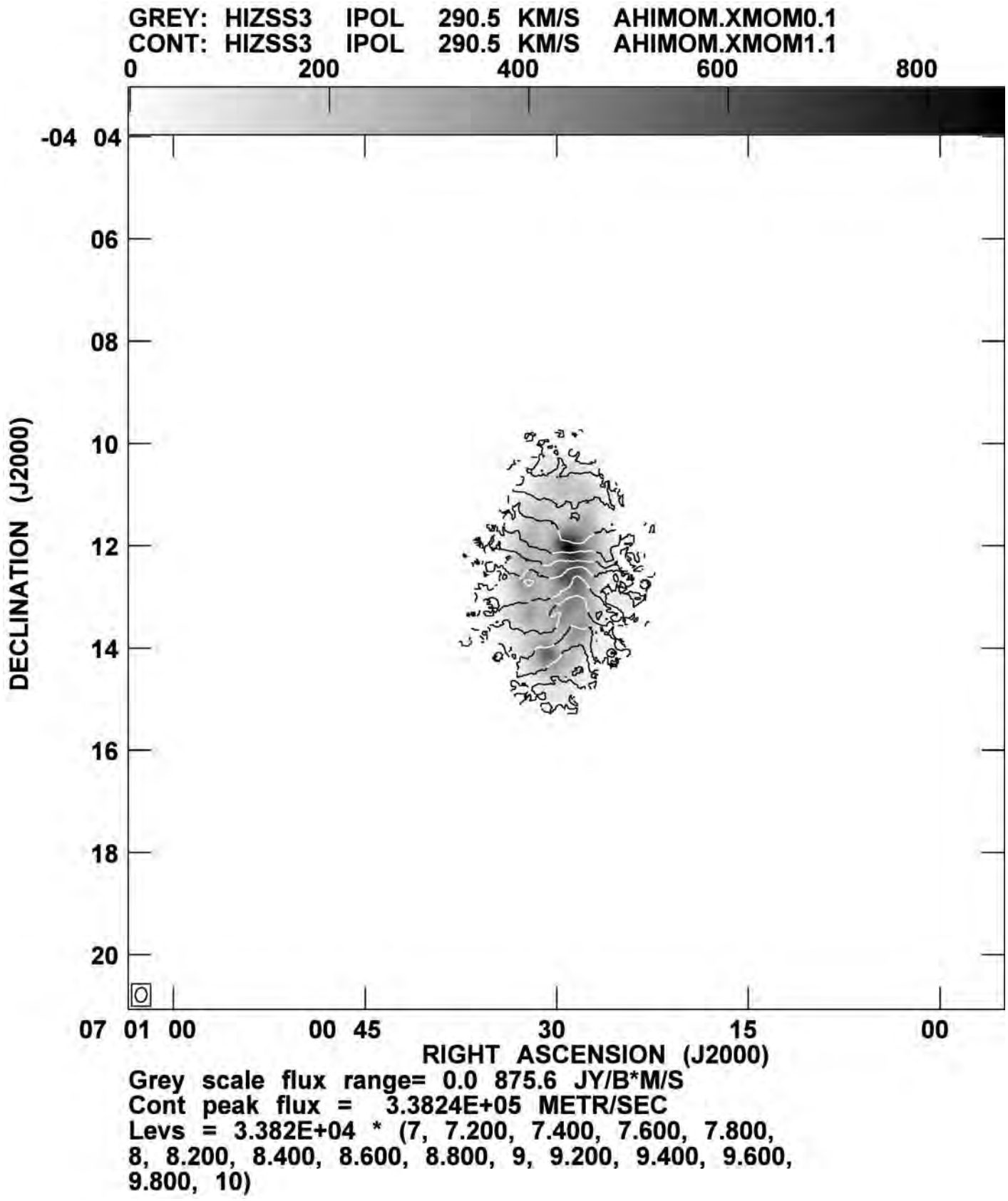

Figure 11: Combination velocity field and integrated HI map of HIZSS 3a.

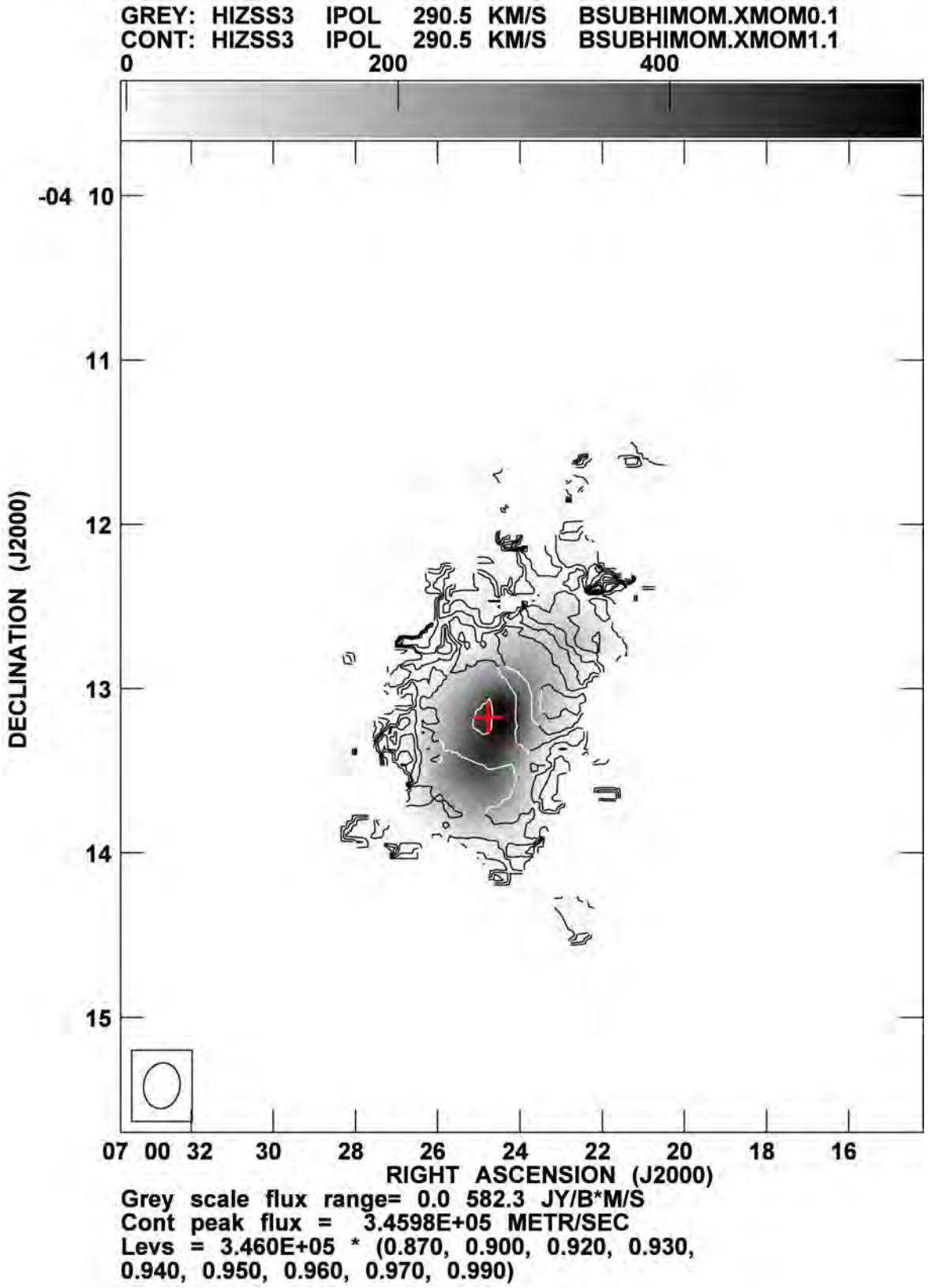

Figure 12: Combination velocity field and integrated HI map of HIZSS 3b. The cross marks a region of H_α emission, which indicates an area of star formation.

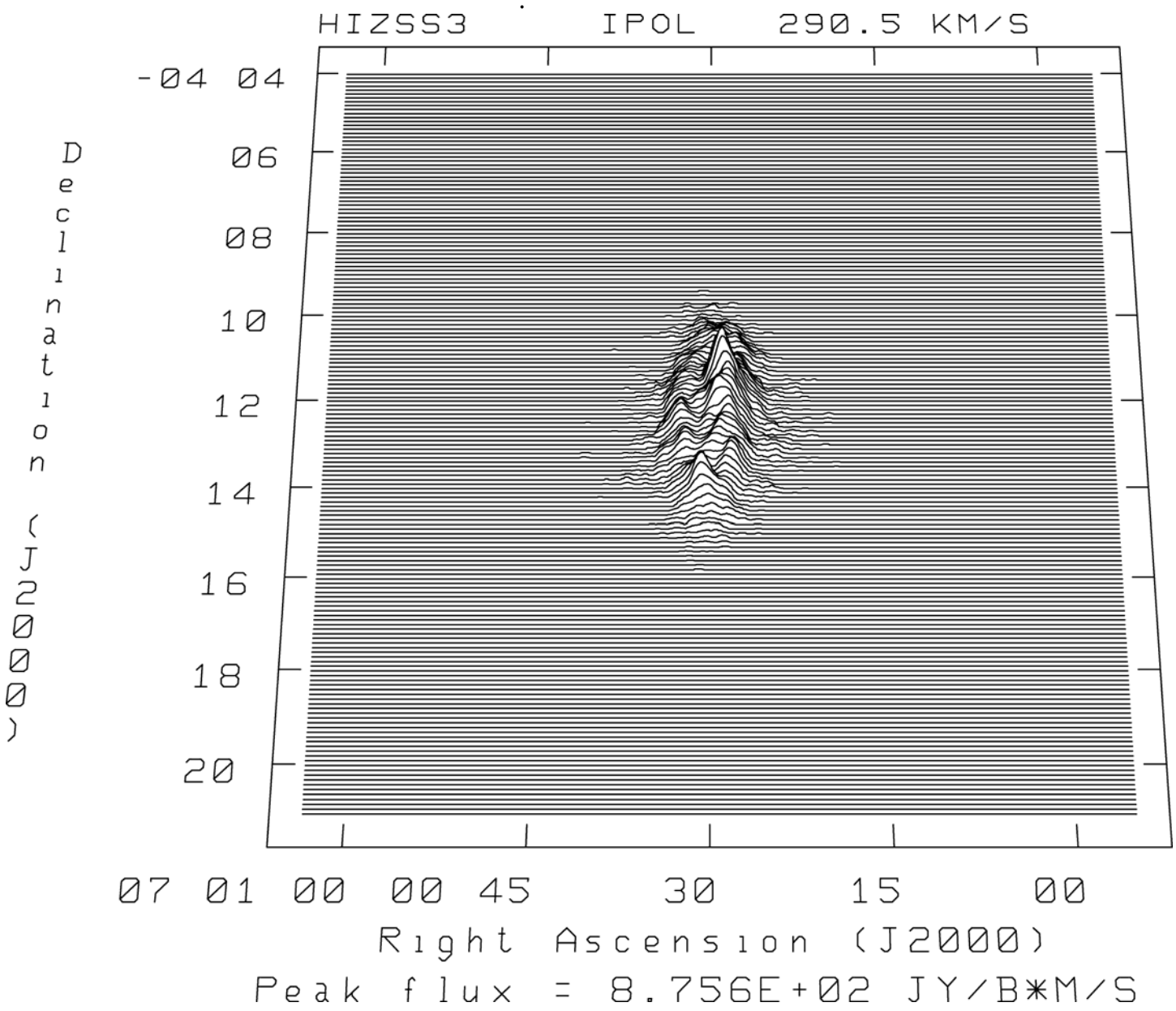

Figure 13: Three dimensional integrated HI map of HIZSS 3a. Positive Z-axis represents intensity

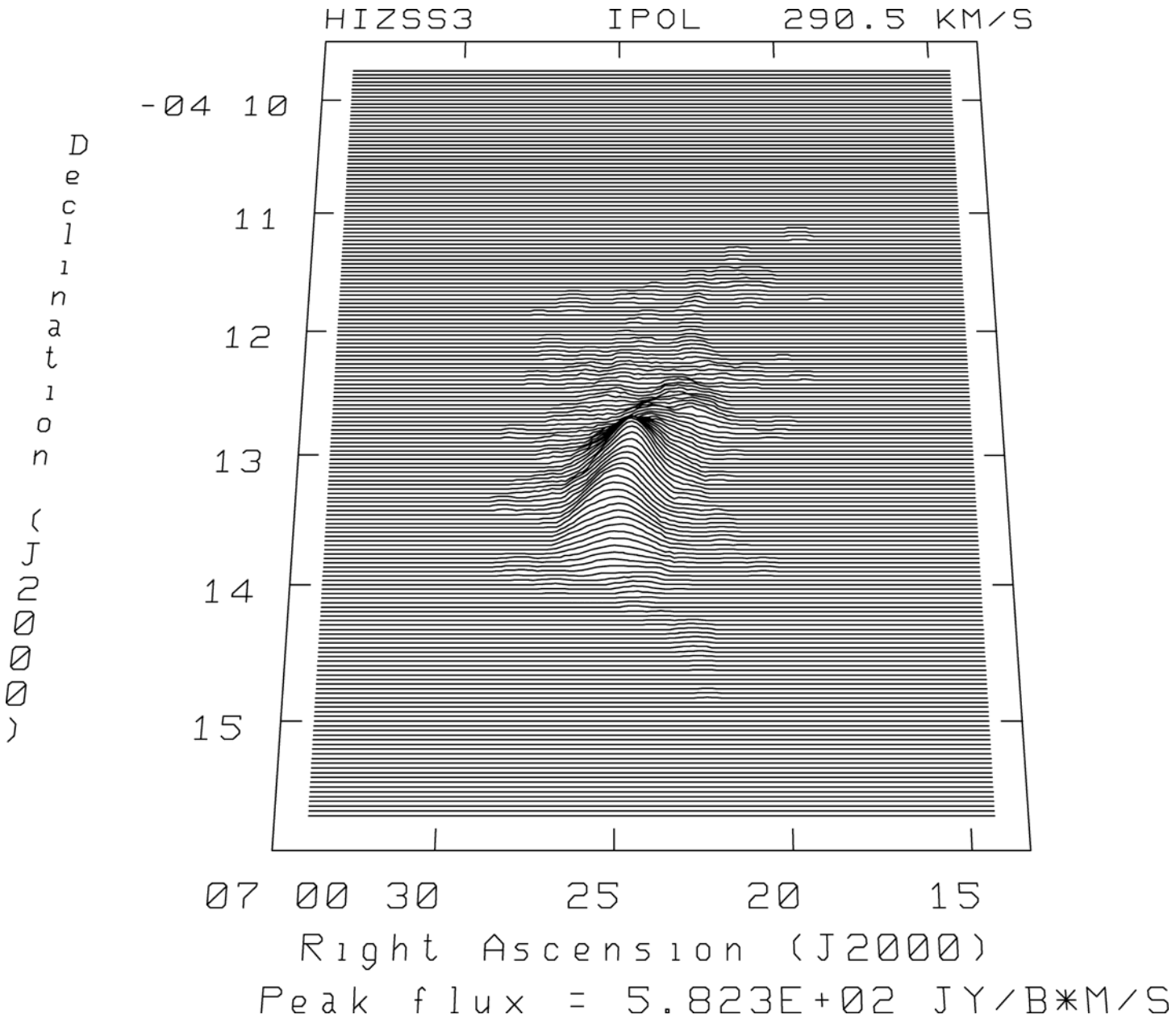

Figure 14: Three dimensional integrated HI map of HIZSS 3b. Positive Z-axis represents intensity.

For HIZSS 3a, a measured angle of 5.3 arcminutes to the 2σ rms level yields a diameter of (2.6 ± 0.11) kpc. For HIZSS 3b, a measured angle of 2.1 arcminutes to the 2σ level yields a diameter of (1.0 ± 0.04) kpc. These results, with their errors deriving from the original distance measurement, confirm that both galaxies fall into the classification of a dwarf galaxy. For reference, the Milky Way has a 50 kpc diameter (Carroll and Ostlie 1996).

Through direct measurements of the HI flux of a galaxy, the total HI mass is derived. The equation for determining the total HI mass is

$$M_{HI} = 2.356 \times 10^5 d^2 \int S_c(\nu)\, d\nu$$

where M_{HI} is the total HI mass in solar masses ($M_\odot$), d is the distance to the galaxy in Mpc, and $S_c(\nu)$ is the total HI flux integrated over all the frequency channels ν in Jy km/sec (Giovanelli and Haynes 1988). This equation comes from integrating the column densities of HI over the visible galactic area. Column density, in this case, is the number of hydrogen atoms per unit area. In order to use the above equation, we must make the assumption that the HI is optically thin, meaning that the hydrogen cloud is dispersed enough not to self-absorb its own emitted photons. While this may not be true for some dense HI regions, HI in normal galaxies generally has a low enough column density to make this assumption valid. Typically, only when galaxies are seen edge-on are corrections for self-absorption significant (Giovanelli and Haynes 1988).

To calculate the HI mass, we measured the flux to the 2.5σ level, assuming that any flux below this level is noise. This is not the case; the galaxies cannot be expected to stop arbitrarily at what we see as 2.5σ to the measured noise. Rather, 2.5σ is what we have determined as the limit to which we can accurately discern the galaxies from the noise. In doing this, we note that any HI at concentrations low enough to be labeled by us as less than 2.5σ does not contribute significantly to the total HI mass.

With the limits to the total HI mass equation in mind, the estimated values for both galaxies can be found by measuring the average galactic HI intensity. For HIZSS 3a, a total integrated flux density of (33 ± 7.7) Jy km/sec gives a total HI mass of (2.2 ± 0.52) x 10^7 $M_\odot$. For HIZSS 3b, a total integrated flux density of (4 ± 1.5) Jy km/sec gives a total HI mass of (2.7 ± 1.0) x 10^6 $M_\odot$.

HI gas only represents a small percentage of a galaxy's total mass. In order to calculate the total mass of a galaxy, its velocity measurements need to first be corrected for the galaxy's inclination, or tilt. Galaxies can lie in any orientation with respect to Earth, and the inclination of a galaxy affects how we measure the HI velocities. By convention, a galaxy that is viewed face-on is has an inclination of 0°, while galaxies viewed edge-on have an inclination of 90°. A galaxy viewed face-on would not have any radial velocity component, and hence would not show any Doppler shifted spectral lines through which internal galactic velocities could be determined. Conversely, an edge-on galaxy would only have a radial rotation velocity; the velocity difference measured across the diameter of the galaxy would then be twice the actual rotation velocity. In most instances, a galaxy's inclination will be somewhere between 0 and 90°, appearing to us as an ellipse. Any velocity measurements will need to be corrected by that galaxy's particular inclination. By assuming that all galaxies are circular disks, a relation can be set up between the galaxy's measured semi-major and semi-minor axes (a and b) and the cosine of the inclination angle i (Giovanelli and Haynes 1988).

$$\mathrm{Cos\,(i)} = \frac{b}{a}$$

In our case, the velocity field of HIZSS 3a supports the assumption that this galaxy is a disk. The same cannot be said for HIZSS 3b. This smaller galaxy does not show evidence of being a disk galaxy, so a derived inclination angle would be nonsensical. Fortunately, the inclination of HIZSS 3a can still be determined. With a semi-major axis of 2.6 kpc and a semi-minor axis of 1.8 kpc, the galaxy has an inclination angle of about 45º.

With the inclination correction to the velocity, the virial theorem can now be utilized to find the total dynamical mass of the galaxies. The virial theorem assumes that a galaxy is stable and not in the process of flying apart. By setting the kinetic energy of a revolving test mass equal to minus half the gravitational potential energy needed to keep it in a stable orbit, we can find the total mass interior to the particle's orbit.

HIZSS 3a shows a smooth velocity field with clear evidence of rotation. Since we assume the galaxy to be disked-shaped, we only need to measure its rotational velocity. This is accomplished by measuring the velocity spread between the blueshifted and redshifted ends of the galaxy, halving that value, and then correcting it for the inclination of the galaxy. With a constant that adjusts for the desired units, the total HI dynamical mass equation for HIZSS 3a is

$$M_T = 2.33 \times 10^5 \, r \left[\frac{\Delta V}{2 \sin(i)} \right]^2$$

where M_T is the total dynamical mass in $M_\odot$, r is the radius of the galaxy in kpc, i is the inclination angle, and ΔV is the velocity spread in km/sec (Giovanelli and Haynes 1988). With a rotational velocity of (51 ± 5.4) km/sec, the total dynamical mass is (7.9 ± 0.43) x 10^8 $M_\odot$.

HIZSS 3b does not show evidence of clear rotation and is assumed to be spherical, so in this case a velocity dispersion is required. We can use the virial to find its total dynamical mass, assuming an average uniform density, an isotropic velocity dispersion, and a negligible rotation. Clearly, this mass estimation is not exact, as Figure 12 shows that HIZSS 3b does not have a uniform density nor a perfectly isotropic velocity dispersion. However, the virial theorem does give a rough idea of the galactic mass. In this case, the equation is

$$M_T = 0.0154 \frac{5 r * \sigma^2}{G}$$

where M_T is the total mass in $M_\odot$, r is the radius of the galaxy in kpc, σ is the velocity dispersion in km/sec, and G is the gravitational constant in cgs units (Hoffman et al. 1996). For a velocity dispersion of 7.1 km/sec, derived from the velocity spread between several sample points, the total mass of HIZSS 3b is (2.9 ± 0.23) x 10^7 $M_\odot$.

With the dynamical masses of both galaxies determined, the HIZSS 3 system can be analyzed to see if the galaxies are gravitationally bound to each other. Using the virial theorem again, we can determine the mass required to keep both galaxies in a circular orbit about the center of mass. If the required orbital mass is within reasonable limits of the total mass of the system, then the two galaxies are assumed to be gravitationally bound. For this calculation, both the velocity of the two galaxies and their separation are

required. As we cannot know their true separation because we are limited to the single vantage point of Earth, we assume that their projected separation as measured from the galaxies' centers (Figure 8) is the correct value. The equation for the required orbital mass is

$$M_{orb} = \frac{0.4928}{3\,\pi G} r_p \Delta V^2$$

where M_{orb} is the required orbital mass in $M_\odot$, r_p is the projected separation in kpc, and ΔV is the radial velocity difference between the galaxies in km/sec (Begum at al. 2005). The velocity difference was determined from the difference in the mean velocities of each galaxy. A projected separation of (0.74 ± 0.03) kpc, and a velocity difference of 27.5 km/sec gives a M_{orb} of 4.4 x 10^8 $M_\odot$ The sum of each galaxy's dynamical mass yields a total mass of 8.2 x 10^8 $M_\odot$. Since this value is larger than the required orbital mass, we can conclude that HIZSS 3a and HIZSS 3b are gravitationally bound. This conclusion comes with the understanding that if the galaxies' true spatial separation is greater than twice their projected separation, then the system is in fact not gravitationally bound. As stated above, our conclusion is only an estimation based on the information available to us.

Conclusions

Although there is no evidence of an HI bridge between HIZSS 3a and HIZSS 3b, these galaxies do show signs of interaction. The system may be gravitationally bound and HIZSS 3a shows an HI distribution asymmetry toward HIZSS 3b. The smaller galaxy's complex kinematics may be the result of gravitational perturbation by HIZSS 3a. The star-formation region in HIZSS 3b is not an uncommon occurrence in gravitationally perturbed systems.

The presence of an HII region in HIZSS 3b raises some interesting questions about the possible evolution of the small galaxy. For example; has the star formation region produced an expanding shell of gas? Any gas shell within the galaxy should be visible in the channel maps (Appendix) as a ring that expands and then contracts through the channels. HIZSS 3b does not show evidence of an expanding sphere of gas; just the presence of a central peak of HI concentration. Another question asks: is the HII region a major contributor to the galaxy's internal dynamics? To answer this question, we first need to know the escape velocity of the galaxy. The equation for escape velocity is

$$V_e = \sqrt{\frac{2GM}{r}}$$

where V_e is the escape velocity, M is the mass of the galaxy, r is the radius of the galaxy, and G is the gravitational constant. The escape velocity of HIZSS 3b is approximately 22 km/sec. Since the velocity dispersion is only 7.1 km/sec, low compared to the escape velocity, it is unlikely the HII is driving any major internal kinematics.

HIZSS 3 System

	HIZSS 3a	HIZSS 3b
Distance	(1.69 ± 0.07) Mpc	(1.69 ± 0.07) Mpc
Diameter	(2.6 ± 0.11) kpc	(1.0 ± 0.04) kpc
Inclination	45º	NA
Integrated Flux Density	(33 ± 7.7) Jy km/sec	(4 ± 1.5) Jy km/sec
HI Mass	(2.2 ± 0.52) x 10^7 $M_\odot$	(2.7 ± 1.0) x 10^6 $M_\odot$
Total Mass	(7.9 ± 0.43) x 10^8 $M_\odot$	(2.9 ± 0.23) x 10^7 $M_\odot$

Table 1: Summary of observation results for the HIZSS 3a and HIZSS 3b galaxies.

Future Work

A possible next step in the analysis of HIZSS 3b is to determine if the star formation region could propel any gas out of the galaxy. Since the star formation region is a large source of energy to the surrounding gas, it is possible that it could provide enough kinetic energy for some gas to completely escape HIZSS 3b. According to Massey et al., the region's H_α emission line has an energy output of 1.4 x 10^{38} ergs/sec. While this is not the total energy output of the HII region, H_α is the largest contributor. The mechanism for propelling the gas must first be determined before analysis can continue. Does the energy outflow heat up the gas or push it forward in a shockwave fashion? A mathematical model is needed to convert the measured luminosity to a gas velocity in order to reach a definitive conclusion. However, on a qualitative level, the high escape velocity and low velocity dispersion gives an indication that the HII region is not energetic enough to drive gas out of HIZSS 3b.

Besides further study of HIZSS 3b's HII region, future work should include a more detailed analysis of HIZSS 3a. By using the more complicated tilted-ring method to determine HIZSS 3a's true inclination as a function of radius (Begeman 1989), the galaxy's structure, rotation curve, and response to the presence of HIZSS 3b can be studied.

Acknowledgements

I would like to thank my advisor, Professor P. Henning, for taking the time to work with me on this thesis, and for showing patience during some difficult times. I would also like to thank the Undergraduate Committee for giving me the opportunity work on and present my Senior Thesis.

References:

"AIPS Cookbook." National Radio Astronomy Observatory. NRAO. 21 Dec. 2005. <http://www.aoc.nrao.edu/aips/cook.html>.

Bedding, Timothy R. “Introduction to Interferometry.” University of Sydney: Australia, 12, Sep. 1996.

Begeman, K.C. “HI Rotation Curves of Spiral galaxies I. NGC 3198.” Astronomy and Astrophysics. 223 (3 April 1989): 47-60.

Begum, Ayesha, et al. “Resolving the mystery of the dwarf galaxy HIZSS 3.” Monthly Notices of the Royal Astronomical Society: Letters. 359 (May 2005): L53-L57.

Carroll, Bradley W and Dale A. Ostlie. Modern Astrophysics. New York: Addison-Wesley, 1996.

Giovanelli, Riccardo and Martha P. Haynes. “ Extragalactic Hydrogen.” Galactic and Extragalactic Radio Astronomy. Ed. G. L. Verschuur and K. I.Kellermann. 2nd ed. New York: Springer-Verlag, 1988.

Henning, P.A. and Philip Massey. “The HI in the Neighboring Dwarf Irregular Galaxy.” HIZSS 3” NRAO VLA Proposal. 23 Sep. 2003.

Henning, P. A., et al. “HI-Bright Galaxies in the Southern Zone of Avoidance.” The Astronomical Journal 119 (June 2000): 2686-2698.

Hoffman, G. L., et al. “Arecibo HI Mapping of a Large Sample of Dwarf Irregular Galaxies.” The Astrophysical Journal Supplement Series. 105 (Aug. 1996): 269-298

Massey, Philip, P. A. Henning, and R. C. Kraan-Korteweg. “A Neighboring Dwarf Irregular Galaxy Hidden by the Milky Way.” The Astronomical Journal 126 (Nov. 2003): 2362-2367.

Rohlfs, Kristen and Thomas L. “Interferometers and Aperture Synthesis.” Wilson.Tools of radio Astronomy. 4th Ed. Springer-Verlag: Berlin, 2004. 192-226.

Rupen, M. P. “Spectral Line Observation II: Calibration and Analysis.” Astronomical Society of the Pacific Conference Series. Ed. G. B. Taylor, C.L. Carilli, and R.A. Perley. Vol. 180. Astronomical Society of the Pacific: San Francisco.1999. 229-274

Silva, David, et al. “The Distance and Metallicity of the Newly Discovered, Nearby Irregular Galaxy HIZSS31.” The Astrophysical Journal. 623 (Jan 2005): 148-158.

Appendix

Channel maps range in velocities from 353.7 km/sec to 232.4 km/sec, with an image approximately every 2.6 km/sec. Contours were chosen to be -5, -4, -3, -2, 2, 3, 4, 7, 10, 15, 20, 25, 30, 35, and 40 times the noise of 1.1 mJy.

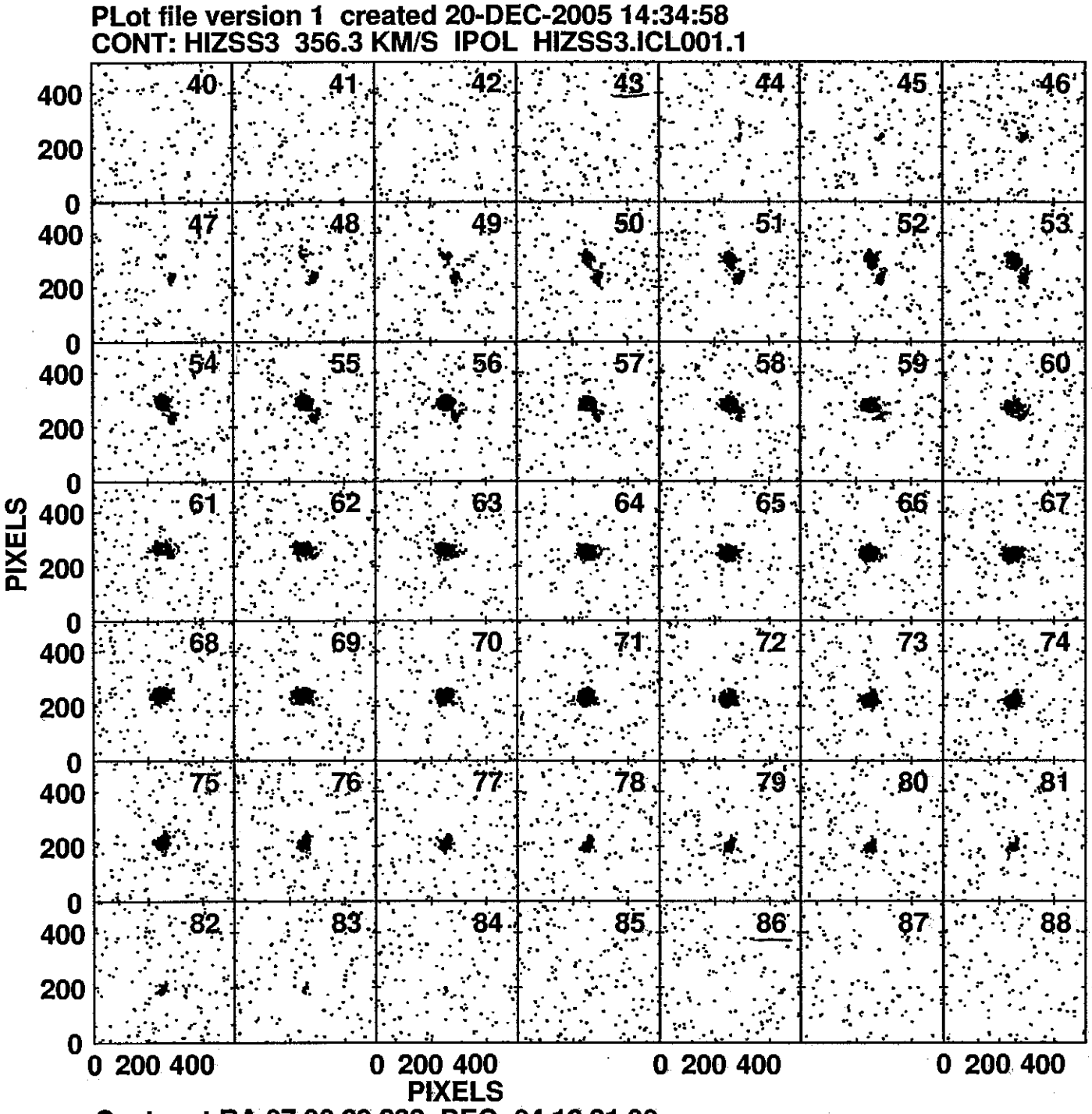
PLot file version 1 created 20-DEC-2005 14:34:58
CONT: HIZSS3 356.3 KM/S IPOL HIZSS3.ICL001.1
40 41 42 43 44 45 46
47 48 49 50 51 52 53
54 55 56 57 58 59 60
61 62 63 64 65 66 67
68 69 70 71 72 73 74
75 76 77 78 79 80 81
82 83 84 85 86 87 88
0 200 400
PIXELS
PIXELS
Center at RA 07 00 29.233 DEC -04 12 31.00
Cont peak flux = 3.7868E-02 JY/BEAM
Levs = 1.100E-03 * (-5, -4, -3, 3, 4, 5, 6, 7, 8,
9, 10, 11, 12, 13, 14, 15, 16, 17, 18, 19, 20)

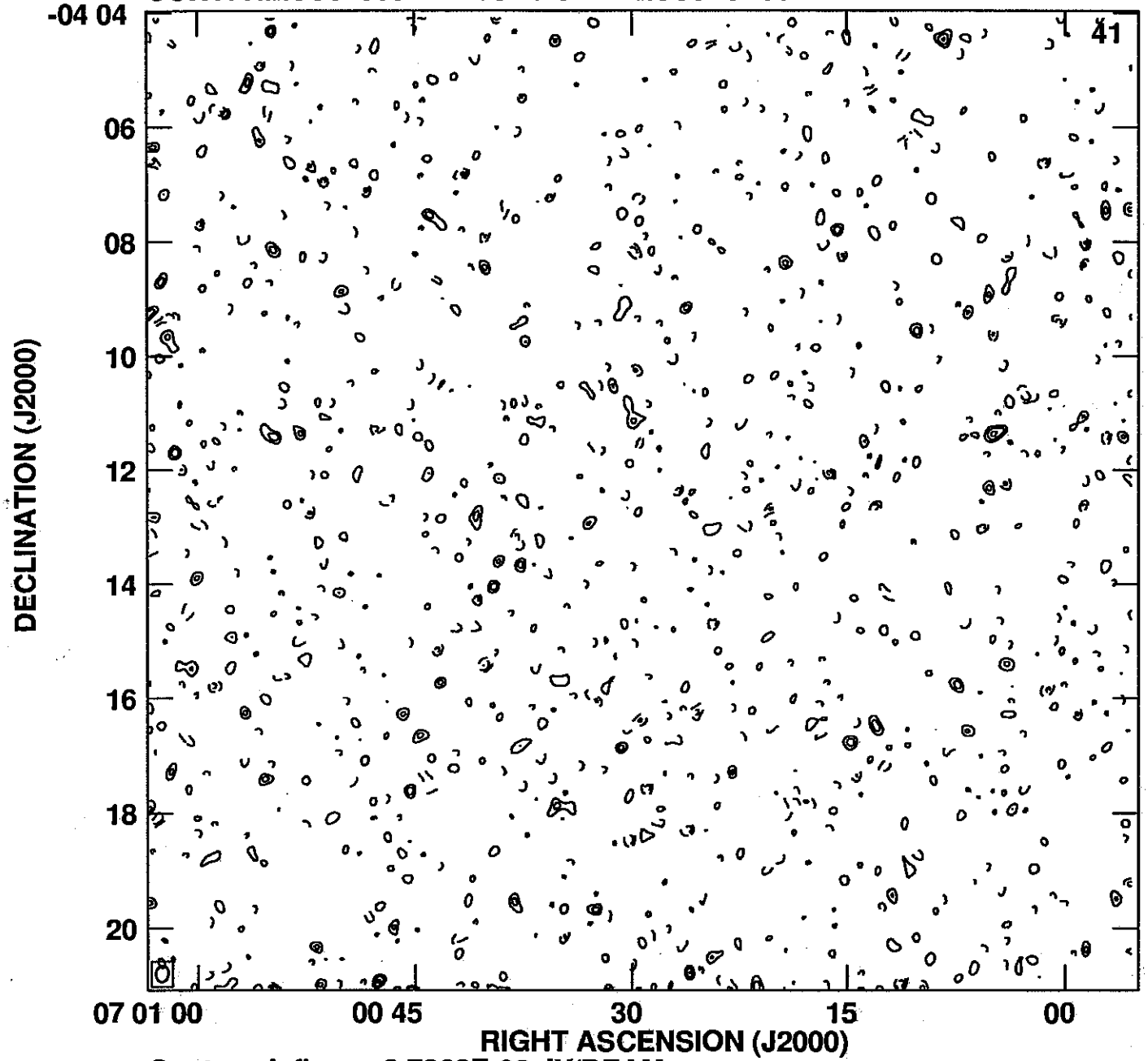
PLot file version 2 created 21-DEC-2005 14:03:18
CONT: HIZSS3 353.7 KM/S IPOL HIZSS3.ICL001.1
-04 04
06
08
10
12
14
16
18
20
41
DECLINATION (J2000)
07 01 00
00 45
30
15
00
RIGHT ASCENSION (J2000)
Cont peak flux = 3.7868E-02 JY/BEAM
Levs = 1.100E-03 * (-5, -4, -3, -2, 2, 3, 4, 7,
10, 15, 20, 25, 30, 35, 40)

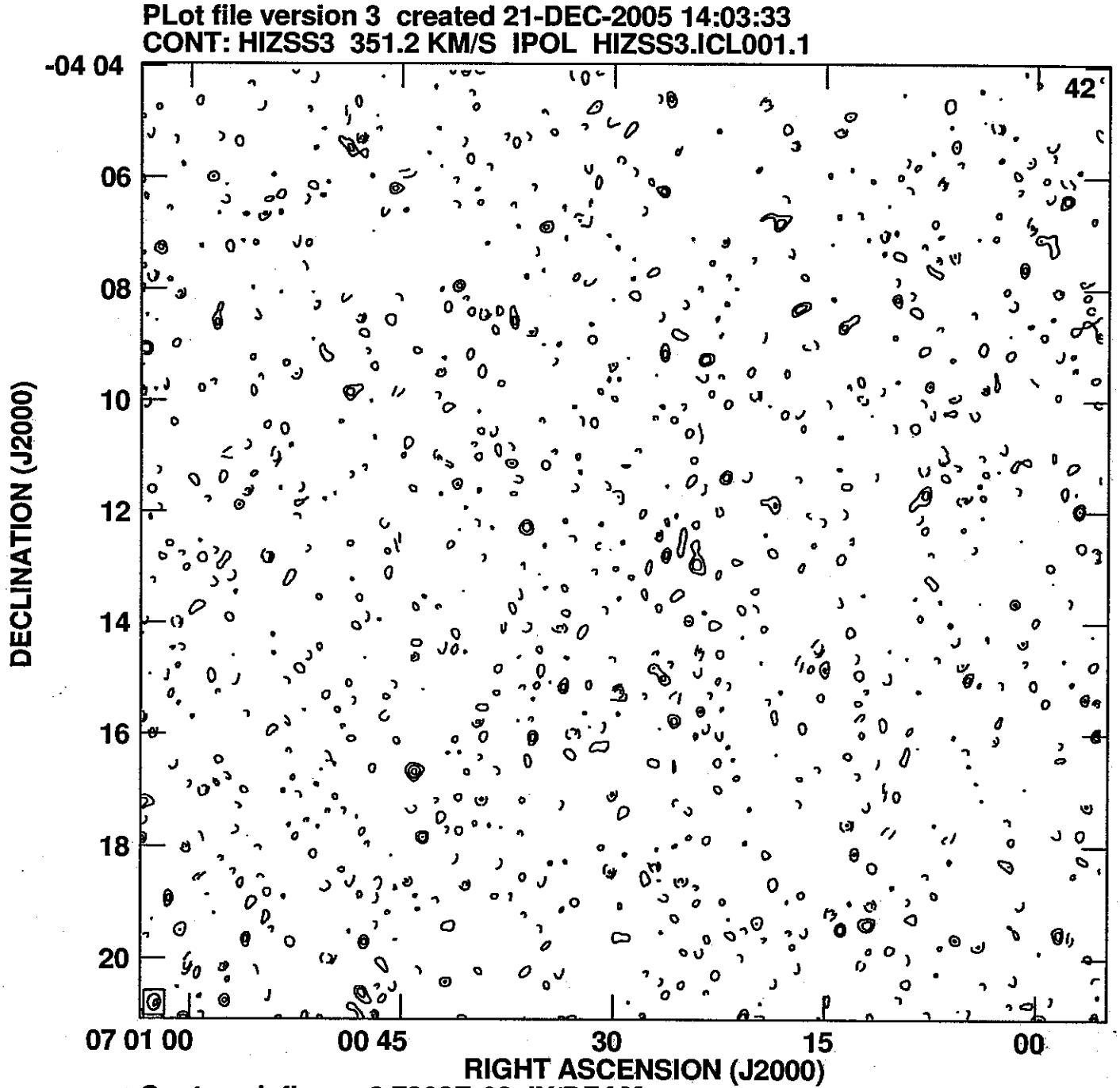
PLot file version 3 created 21-DEC-2005 14:03:33
CONT: HIZSS3 351.2 KM/S IPOL HIZSS3.ICL001.1
-04 04
06
08
10
12
14
16
18
20
42
DECLINATION (J2000)
07 01 00
00 45
30
15
00
RIGHT ASCENSION (J2000)
Cont peak flux = 3.7868E-02 JY/BEAM
Levs = 1.100E-03 * (-5, -4, -3, -2, 2, 3, 4, 7,
10, 15, 20, 25, 30, 35, 40)

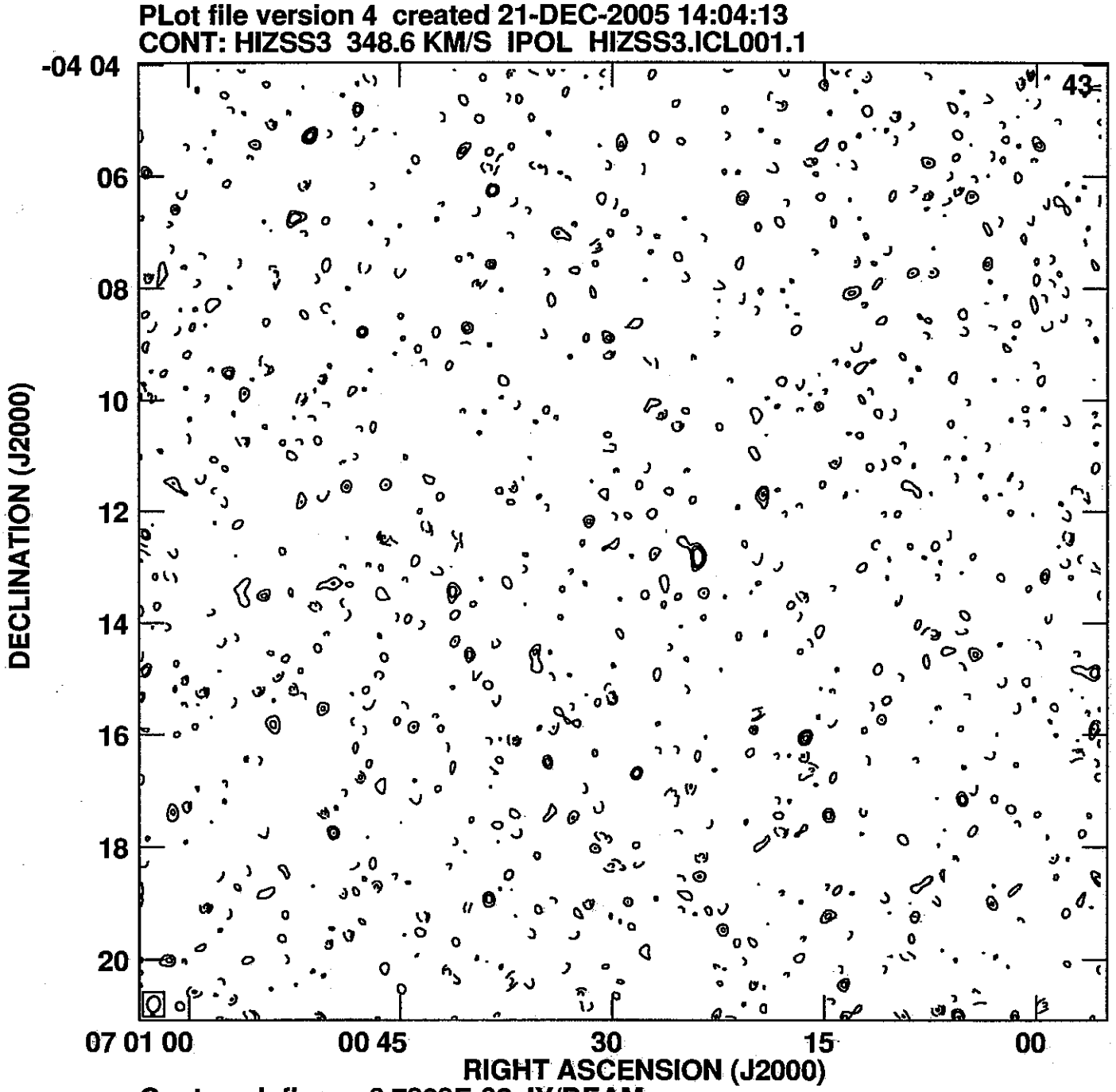
PLot file version 4 created 21-DEC-2005 14:04:13
CONT: HIZSS3 348.6 KM/S IPOL HIZSS3.ICL001.1
-04 04
43
06
08
10
12
14
16
18
20
DECLINATION (J2000)
07 01 00
00 45
30
15
00
RIGHT ASCENSION (J2000)
Cont peak flux = 3.7868E-02 JY/BEAM
Levs = 1.100E-03 * (-5, -4, -3, -2, 2, 3, 4, 7,
10, 15, 20, 25, 30, 35, 40)

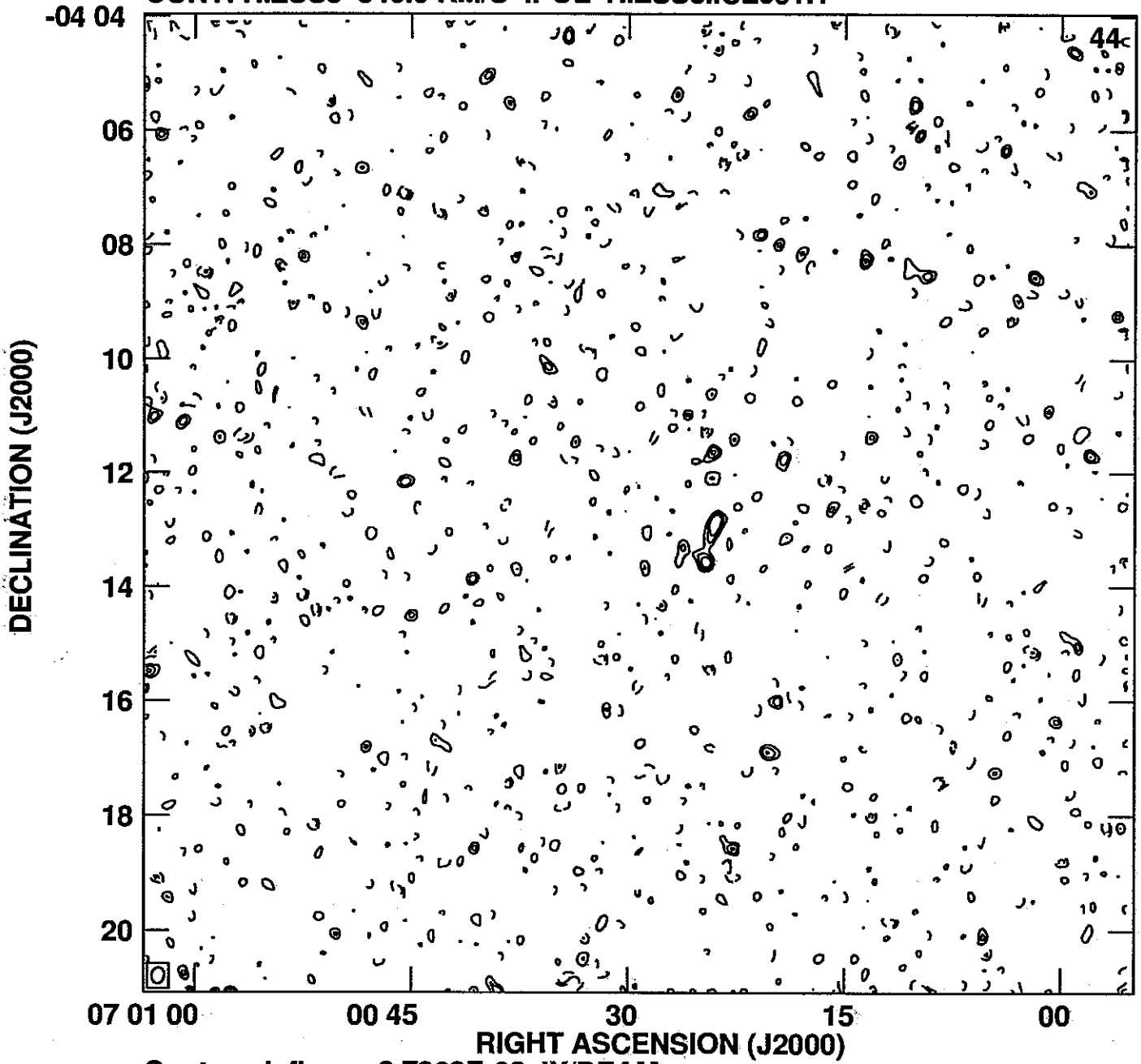
PLot file version 5 created 21-DEC-2005 14:04:19
CONT: HIZSS3 346.0 KM/S IPOL HIZSS3.ICL001.1
-04 04
06
08
10
12
14
16
18
20
DECLINATION (J2000)
07 01 00
00 45
30
15
00
RIGHT ASCENSION (J2000)
Cont peak flux = 3.7868E-02 JY/BEAM
Levs = 1.100E-03 * (-5, -4, -3, -2, 2, 3, 4, 7,
10, 15, 20, 25, 30, 35, 40)

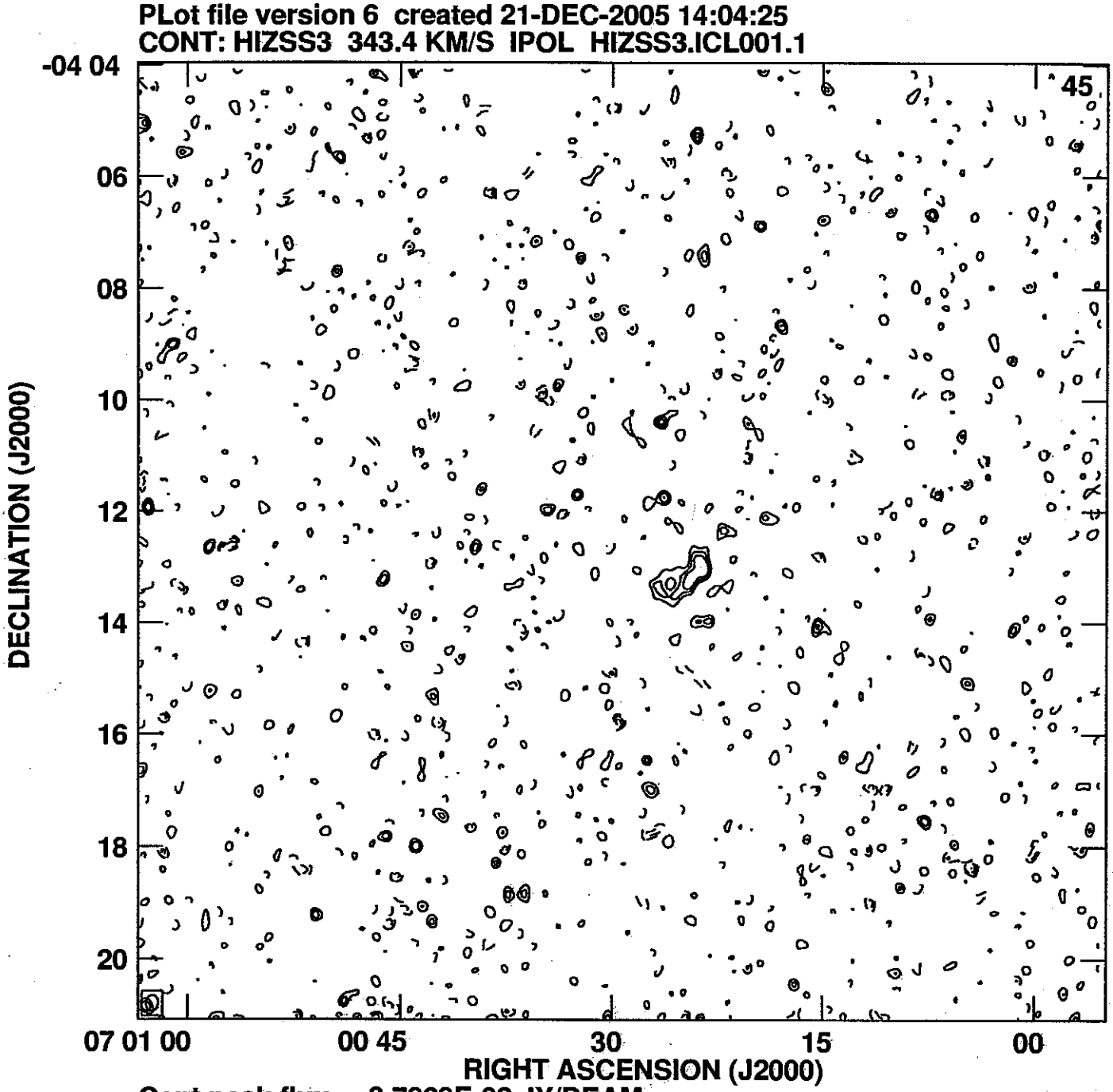
PLot file version 6 created 21-DEC-2005 14:04:25
CONT: HIZSS3 343.4 KM/S IPOL HIZSS3.ICL001.1
-04 04
45
06
08
10
12
14
16
18
20
DECLINATION (J2000)
07 01 00
00 45
30
15
00
RIGHT ASCENSION (J2000)
Cont peak flux = 3.7868E-02 JY/BEAM
Levs = 1.100E-03 * (-5, -4, -3, -2, 2, 3, 4, 7,
10, 15, 20, 25, 30, 35, 40)

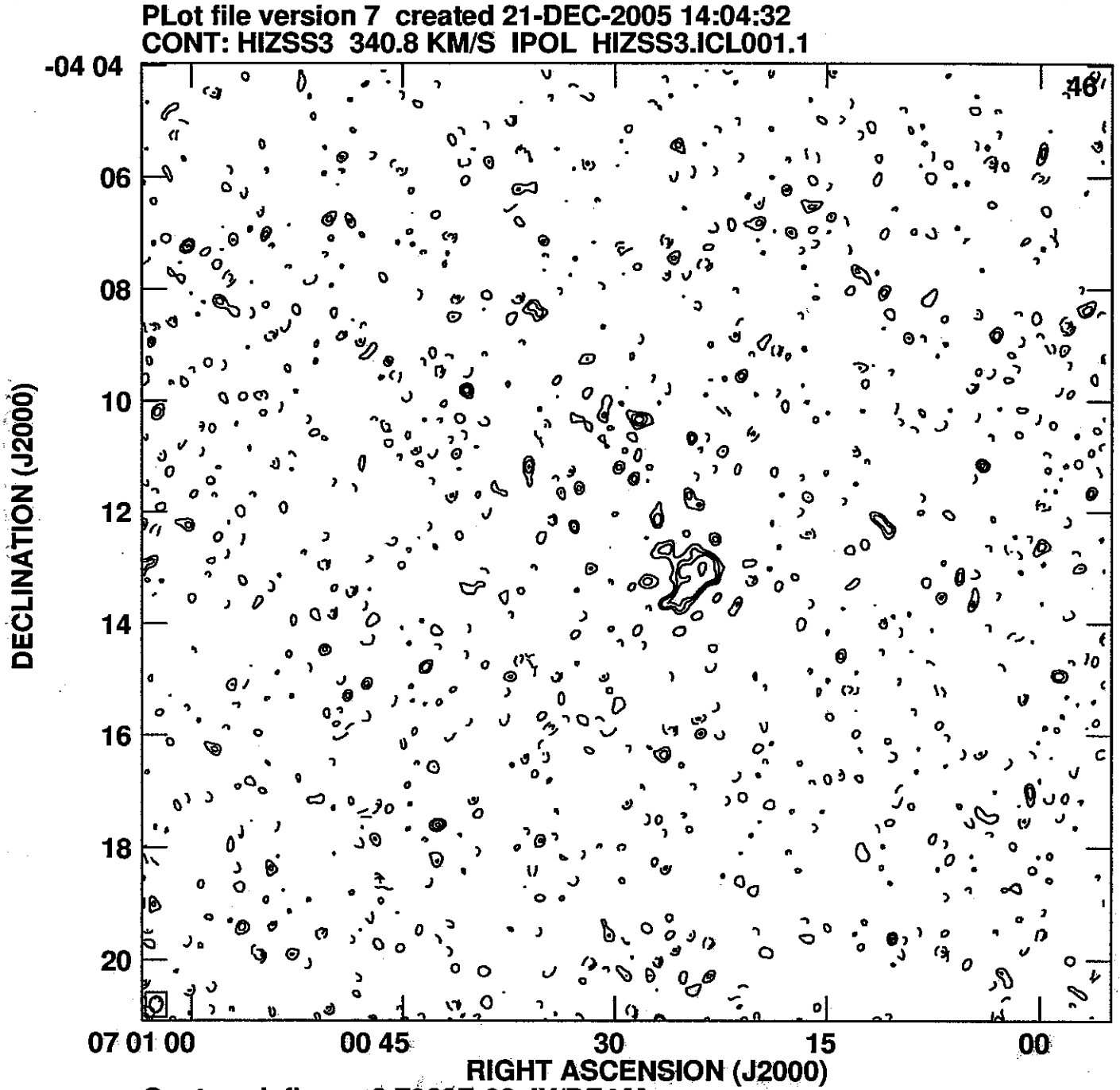
PLot file version 7 created 21-DEC-2005 14:04:32
CONT: HIZSS3 340.8 KM/S IPOL HIZSS3.ICL001.1
-04 04
06
08
10
12
14
16
18
20
46
DECLINATION (J2000)
07 01 00
00 45
30
15
00
RIGHT ASCENSION (J2000)
Cont peak flux = 3.7868E-02 JY/BEAM
Levs = 1.100E-03 * (-5, -4, -3, -2, 2, 3, 4, 7,
10, 15, 20, 25, 30, 35, 40)

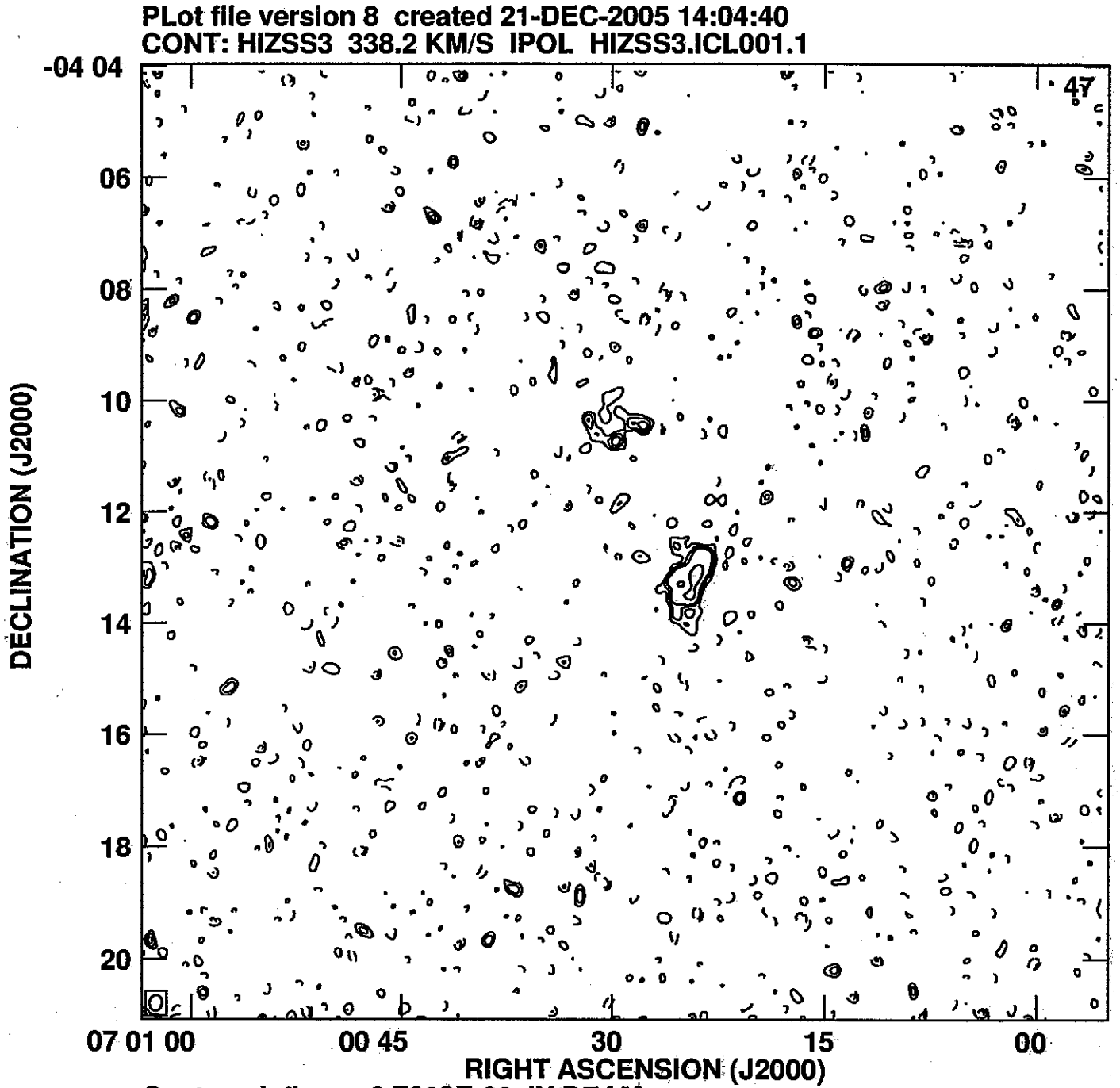
PLot file version 8 created 21-DEC-2005 14:04:40
CONT: HIZSS3 338.2 KM/S IPOL HIZSS3.ICL001.1
-04 04
06
08
10
12
14
16
18
20
47
DECLINATION (J2000)
07 01 00
00 45
30
15
00
RIGHT ASCENSION (J2000)
Cont peak flux = 3.7868E-02 JY/BEAM
Levs = 1.100E-03 * (-5, -4, -3, -2, 2, 3, 4, 7,
10, 15, 20, 25, 30, 35, 40)

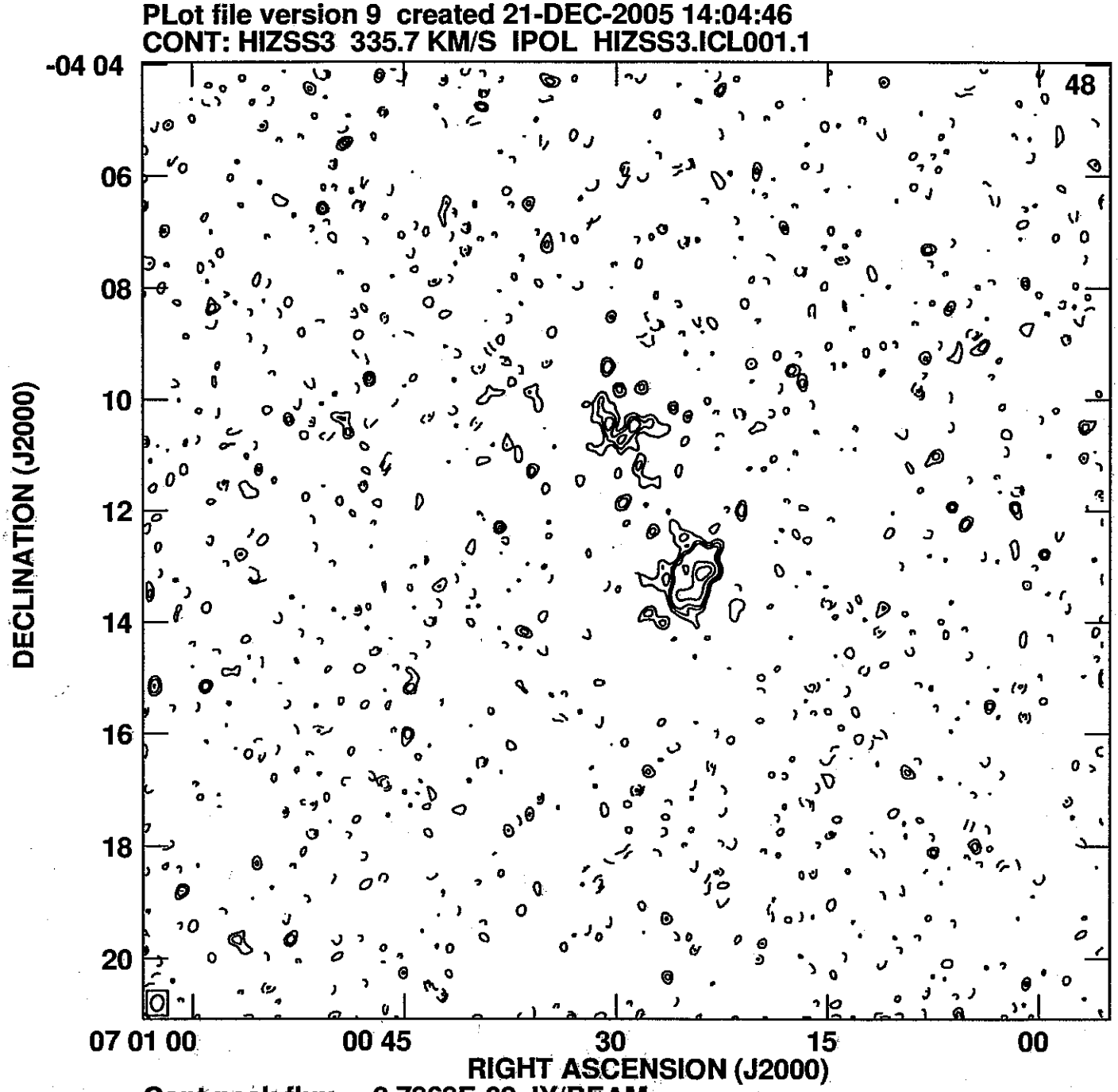
PLot file version 9 created 21-DEC-2005 14:04:46
CONT: HIZSS3 335.7 KM/S IPOL HIZSS3.ICL001.1
-04 04
48
06
08
10
12
14
16
18
20
DECLINATION (J2000)
07 01 00
00 45
30
15
00
RIGHT ASCENSION (J2000)
Cont peak flux = 3.7868E-02 JY/BEAM
Levs = 1.100E-03 * (-5, -4, -3, -2, 2, 3, 4, 7,
10, 15, 20, 25, 30, 35, 40)

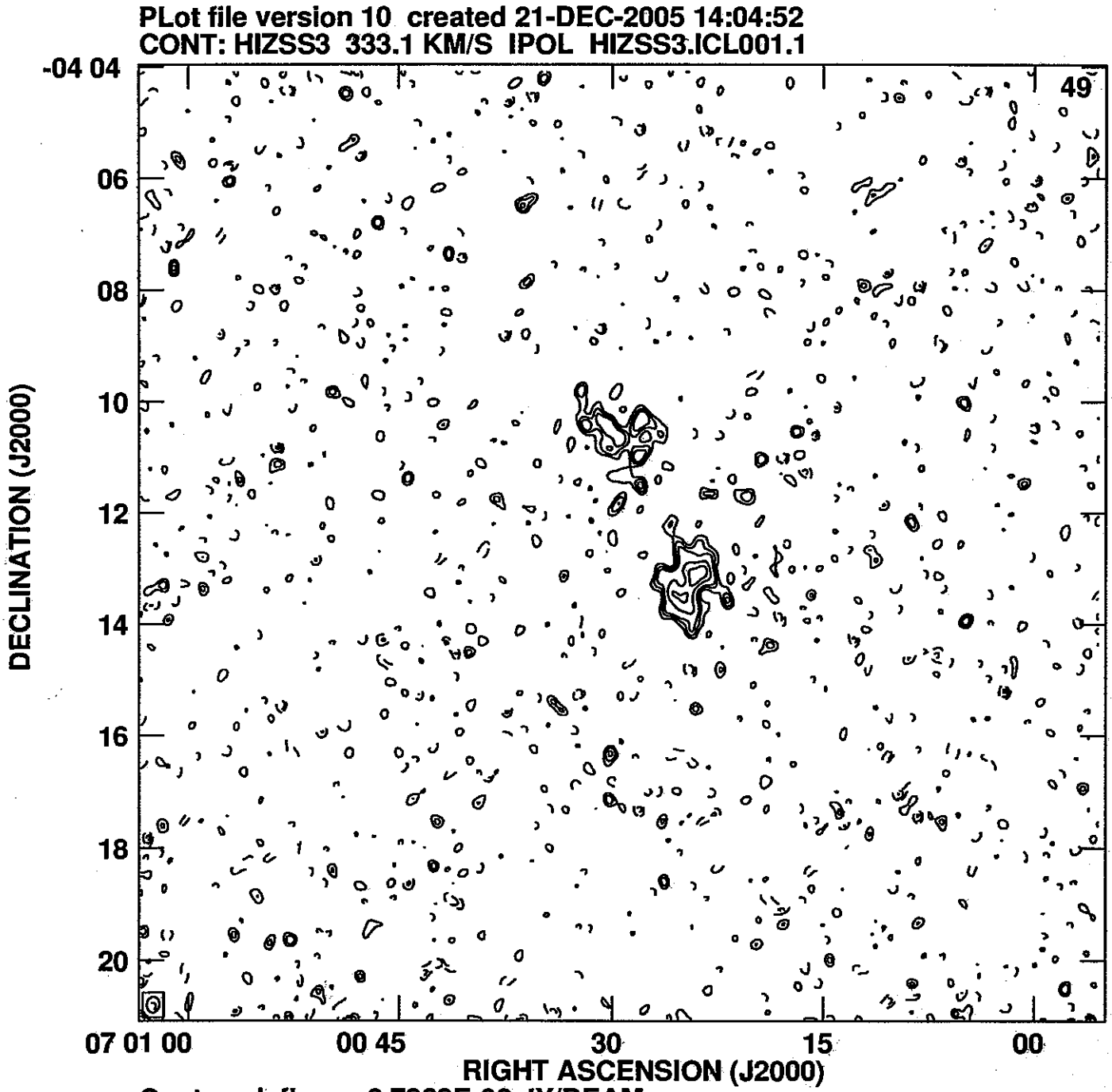
PLot file version 10 created 21-DEC-2005 14:04:52
CONT: HIZSS3 333.1 KM/S IPOL HIZSS3.ICL001.1
-04 04
49
06
08
10
12
14
16
18
20
DECLINATION (J2000)
07 01 00
00 45
30
15
00
RIGHT ASCENSION (J2000)
Cont peak flux = 3.7868E-02 JY/BEAM
Levs = 1.100E-03 * (-5, -4, -3, -2, 2, 3, 4, 7,
10, 15, 20, 25, 30, 35, 40)

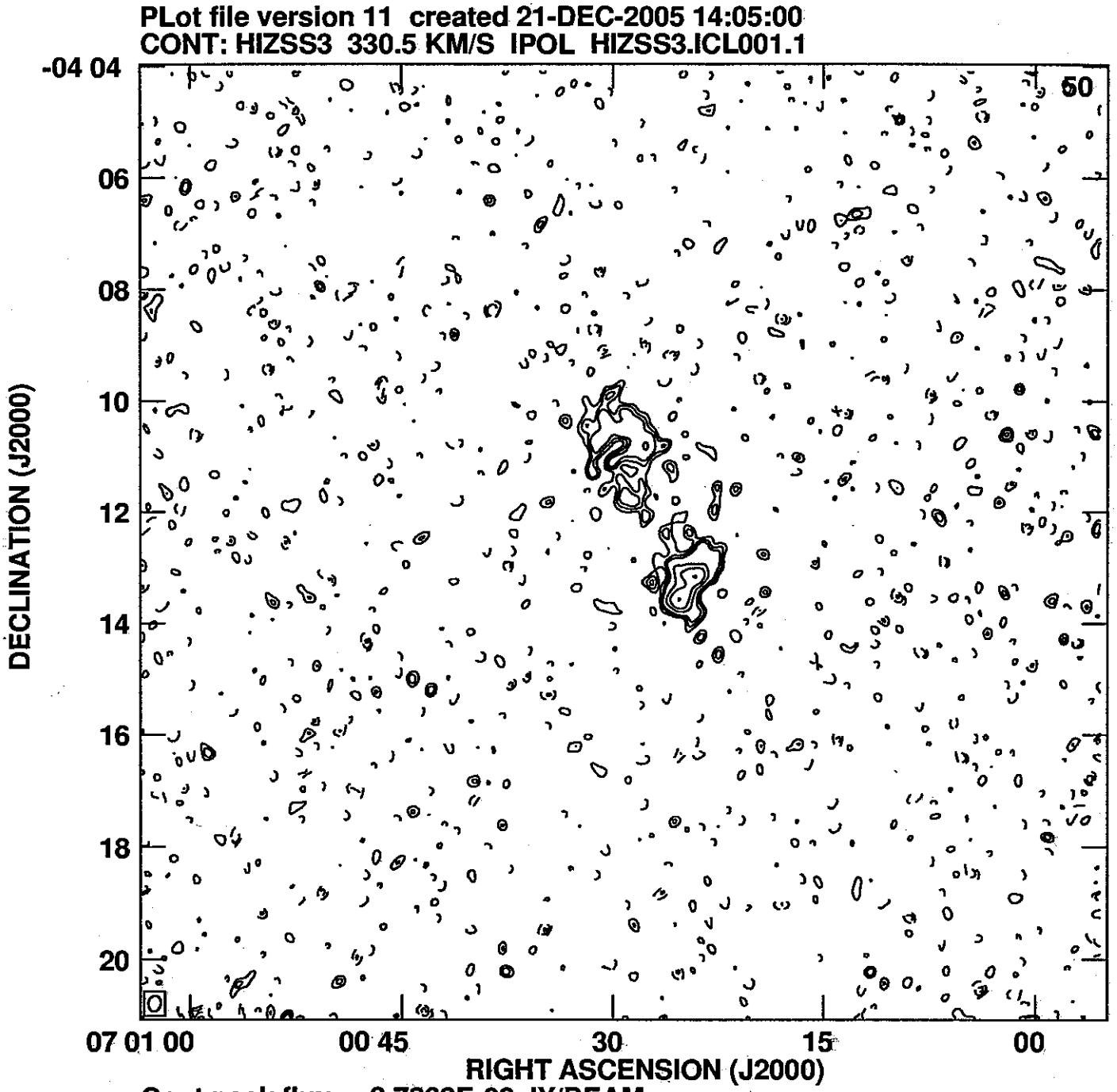
PLot file version 11 created 21-DEC-2005 14:05:00
CONT: HIZSS3 330.5 KM/S IPOL HIZSS3.ICL001.1
-04 04
50
06
08
10
12
14
16
18
20
DECLINATION (J2000)
07 01 00
00 45
30
15
00
RIGHT ASCENSION (J2000)
Cont peak flux = 3.7868E-02 JY/BEAM
Levs = 1.100E-03 * (-5, -4, -3, -2, 2, 3, 4, 7,
10, 15, 20, 25, 30, 35, 40)

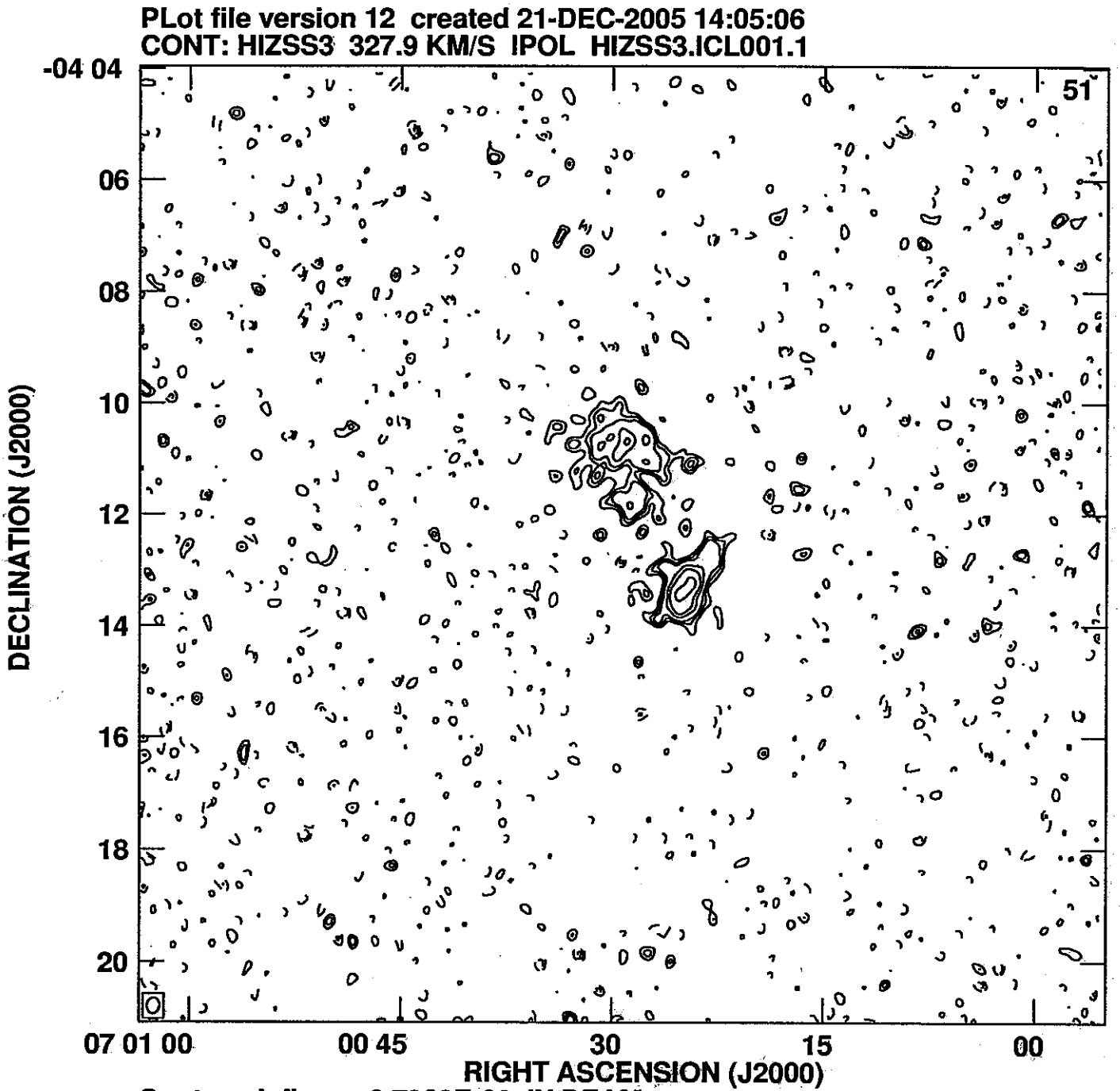
PLot file version 12 created 21-DEC-2005 14:05:06
CONT: HIZSS3 327.9 KM/S IPOL HIZSS3.ICL001.1
-04 04
06
08
10
12
14
16
18
20
51
DECLINATION (J2000)
07 01 00
00 45
30
15
00
RIGHT ASCENSION (J2000)
Cont peak flux = 3.7868E-02 JY/BEAM
Levs = 1.100E-03 * (-5, -4, -3, -2, 2, 3, 4, 7,
10, 15, 20, 25, 30, 35, 40)

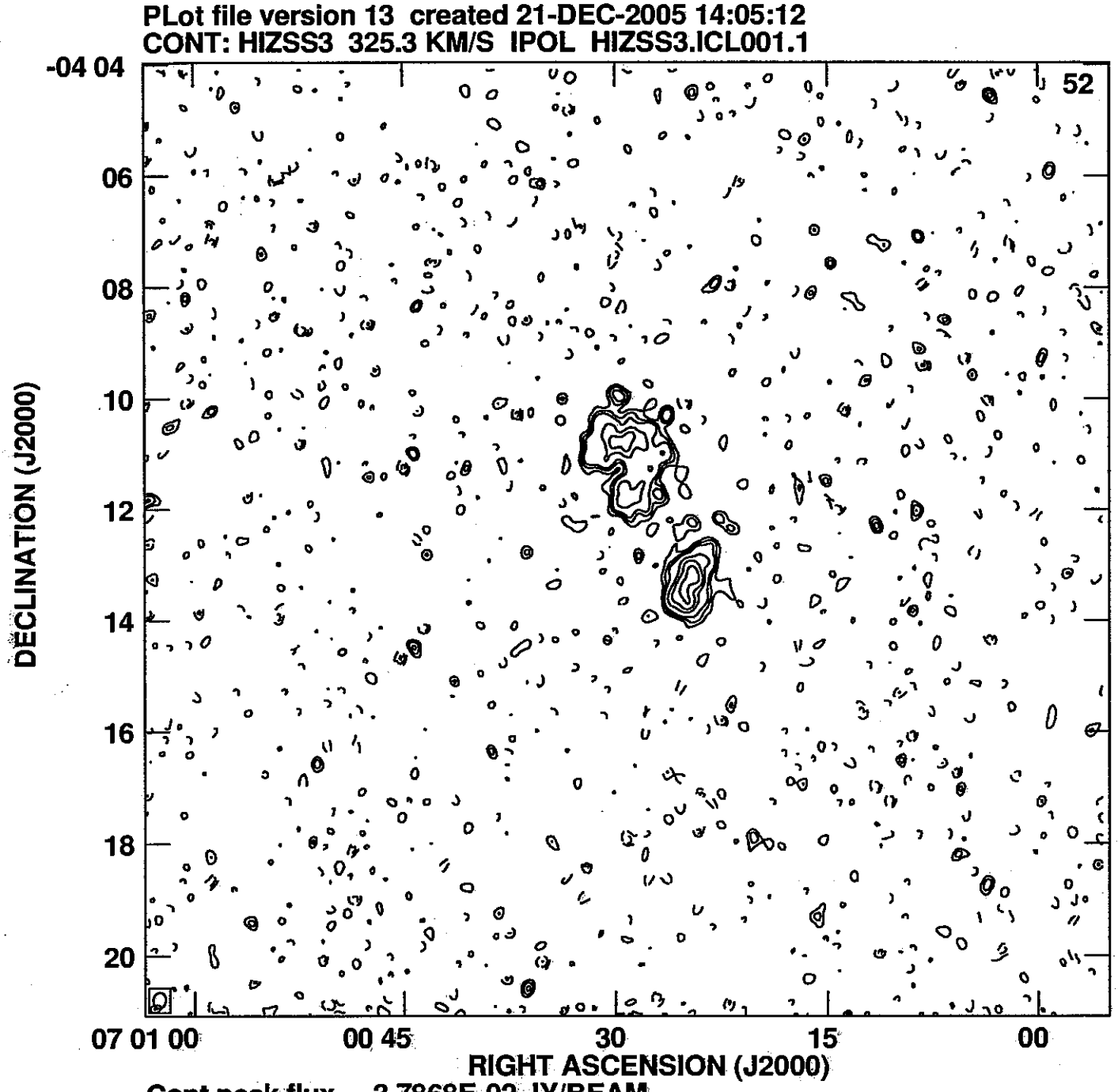
PLot file version 13 created 21-DEC-2005 14:05:12
CONT: HIZSS3 325.3 KM/S IPOL HIZSS3.ICL001.1
-04 04
06
08
10
12
14
16
18
20
52
DECLINATION (J2000)
07 01 00
00 45
30
15
00
RIGHT ASCENSION (J2000)
Cont peak flux = 3.7868E-02 JY/BEAM
Levs = 1.100E-03 * (-5, -4, -3, -2, 2, 3, 4, 7,
10, 15, 20, 25, 30, 35, 40)

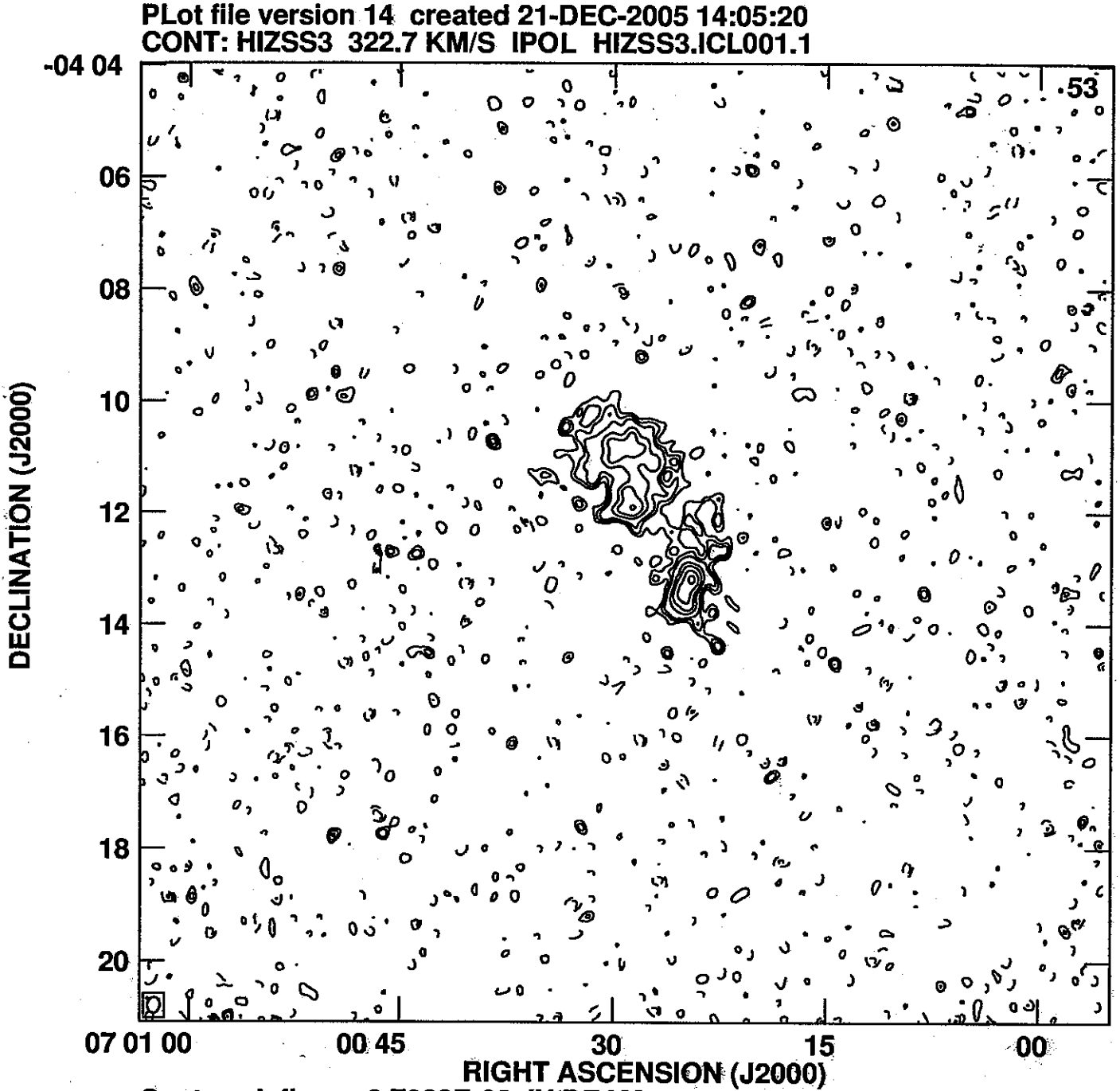
PLot file version 14 created 21-DEC-2005 14:05:20
CONT: HIZSS3 322.7 KM/S IPOL HIZSS3.ICL001.1
-04 04
06
08
10
12
14
16
18
20
.53
DECLINATION (J2000)
07 01 00
00 45
30
15
00
RIGHT ASCENSION (J2000)
Cont peak flux = 3.7868E-02 JY/BEAM
Levs = 1.100E-03 * (-5, -4, -3, -2, 2, 3, 4, 7,
10, 15, 20, 25, 30, 35, 40)

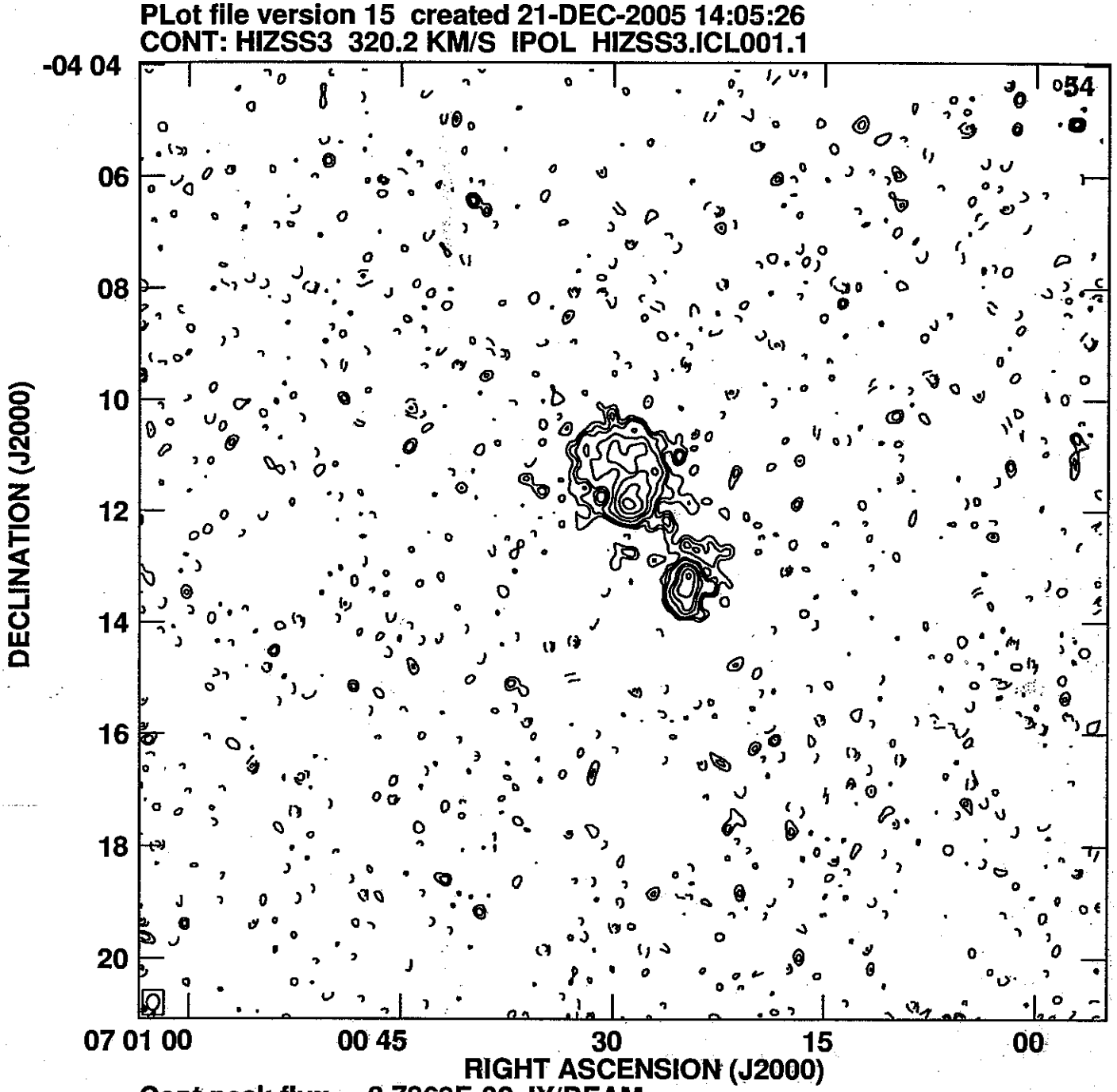
PLot file version 15 created 21-DEC-2005 14:05:26
CONT: HIZSS3 320.2 KM/S IPOL HIZSS3.ICL001.1
-04 04
06
08
10
12
14
16
18
20
54
DECLINATION (J2000)
07 01 00
00 45
30
15
00
RIGHT ASCENSION (J2000)
Cont peak flux = 3.7868E-02 JY/BEAM
Levs = 1.100E-03 * (-5, -4, -3, -2, 2, 3, 4, 7,
10, 15, 20, 25, 30, 35, 40)

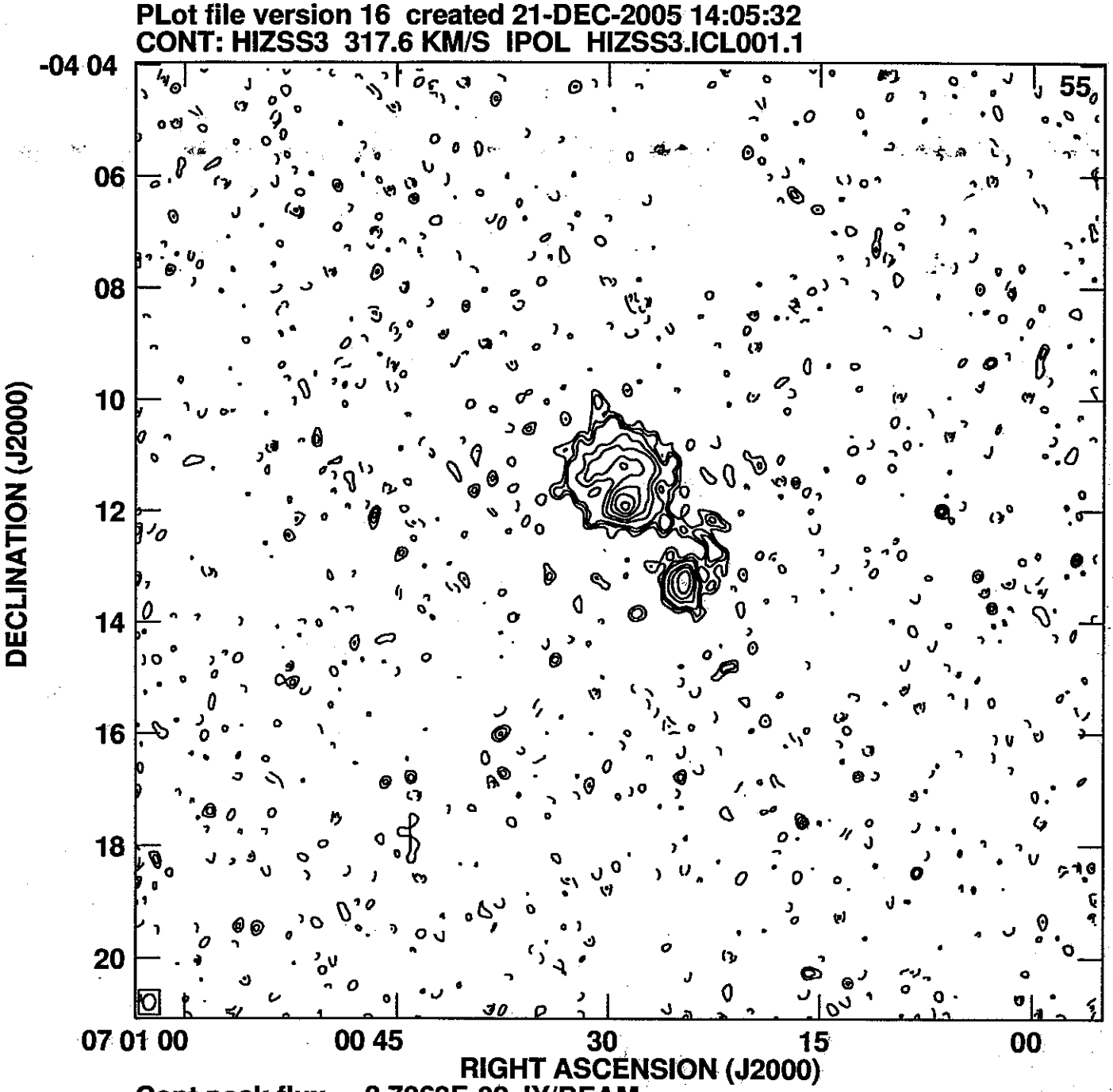
PLot file version 16 created 21-DEC-2005 14:05:32
CONT: HIZSS3 317.6 KM/S IPOL HIZSS3.ICL001.1
-04 04
55
06
08
10
12
14
16
18
20
DECLINATION (J2000)
07 01 00
00 45
30
15
00
RIGHT ASCENSION (J2000)
Cont peak flux = 3.7868E-02 JY/BEAM
Levs = 1.100E-03 * (-5, -4, -3, -2, 2, 3, 4, 7,
10, 15, 20, 25, 30, 35, 40)

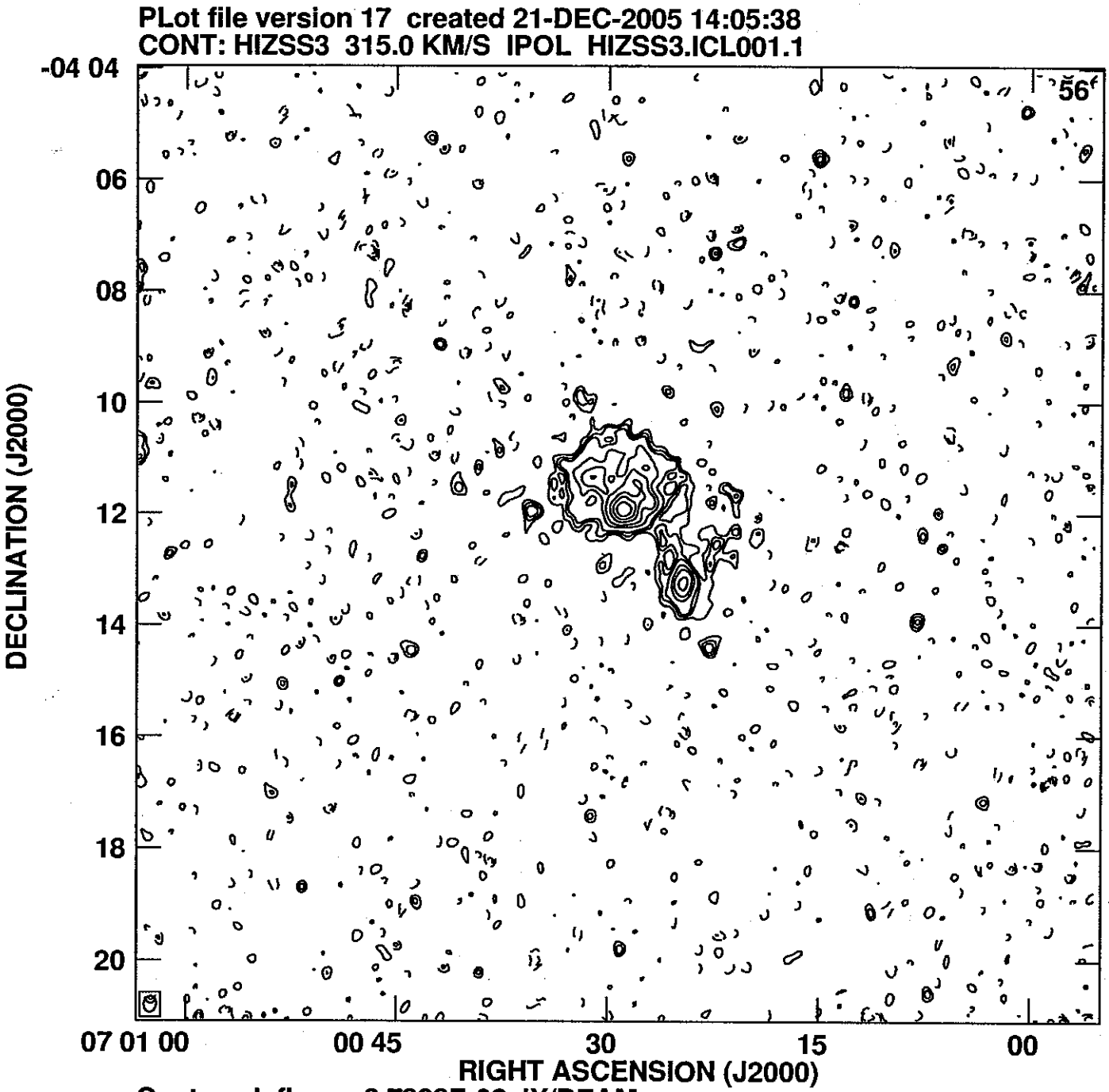
PLot file version 17 created 21-DEC-2005 14:05:38
CONT: HIZSS3 315.0 KM/S IPOL HIZSS3.ICL001.1
-04 04
06
08
10
12
14
16
18
20
56
DECLINATION (J2000)
07 01 00
00 45
30
15
00
RIGHT ASCENSION (J2000)
Cont peak flux = 3.7868E-02 JY/BEAM
Levs = 1.100E-03 * (-5, -4, -3, -2, 2, 3, 4, 7,
10, 15, 20, 25, 30, 35, 40)

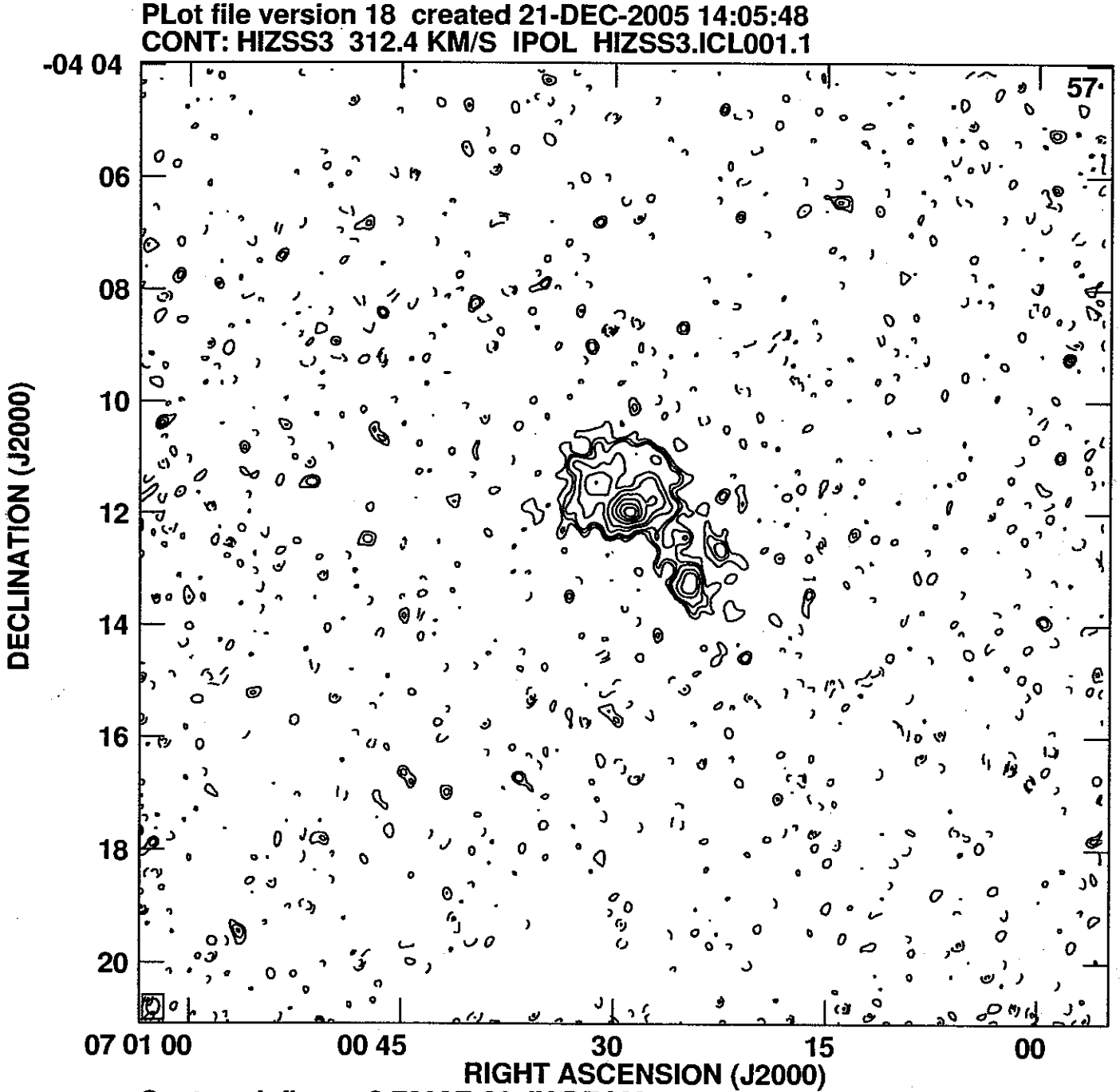
PLot file version 18 created 21-DEC-2005 14:05:48
CONT: HIZSS3 312.4 KM/S IPOL HIZSS3.ICL001.1
-04 04
06
08
10
12
14
16
18
20
57.
DECLINATION (J2000)
07 01 00
00 45
30
15
00
RIGHT ASCENSION (J2000)
Cont peak flux = 3.7868E-02 JY/BEAM
Levs = 1.100E-03 * (-5, -4, -3, -2, 2, 3, 4, 7,
10, 15, 20, 25, 30, 35, 40)

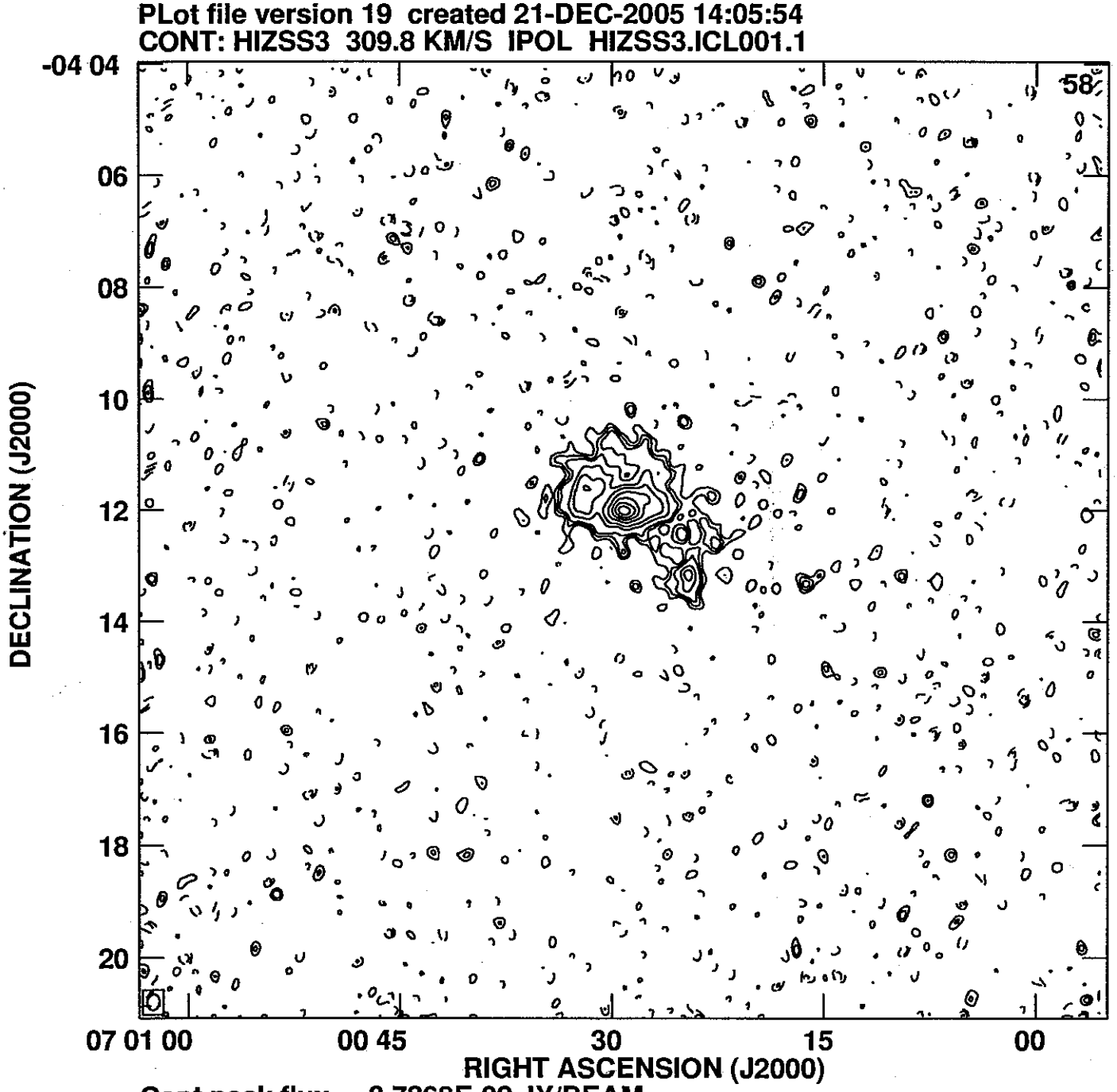
PLot file version 19 created 21-DEC-2005 14:05:54
CONT: HIZSS3 309.8 KM/S IPOL HIZSS3.ICL001.1
-04 04
58
06
08
10
12
14
16
18
20
DECLINATION (J2000)
07 01 00
00 45
30
15
00
RIGHT ASCENSION (J2000)
Cont peak flux = 3.7868E-02 JY/BEAM
Levs = 1.100E-03 * (-5, -4, -3, -2, 2, 3, 4, 7,
10, 15, 20, 25, 30, 35, 40)

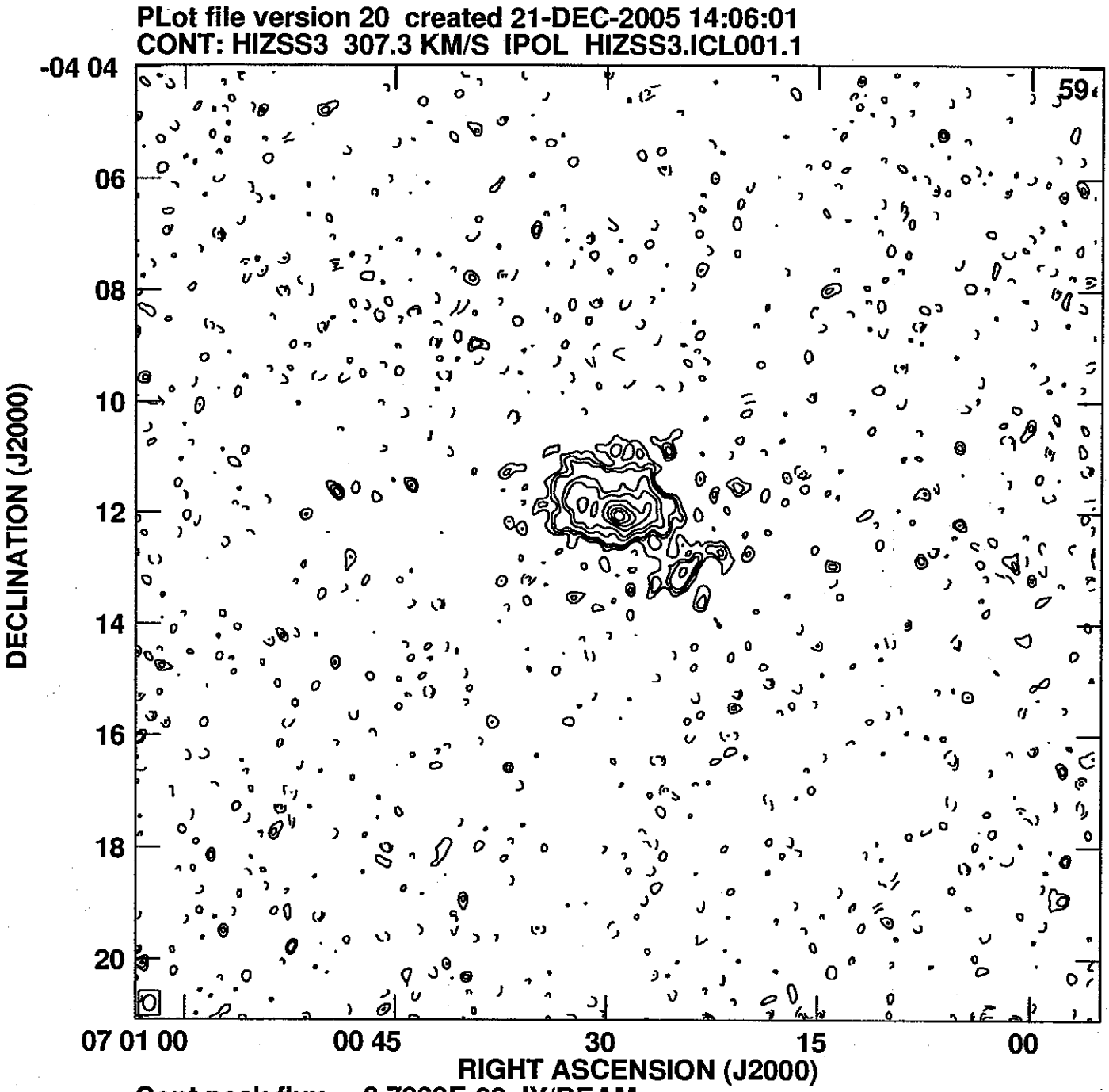
PLot file version 20 created 21-DEC-2005 14:06:01
CONT: HIZSS3 307.3 KM/S IPOL HIZSS3.ICL001.1
-04 04
59
06
08
10
12
14
16
18
20
DECLINATION (J2000)
07 01 00
00 45
30
15
00
RIGHT ASCENSION (J2000)
Cont peak flux = 3.7868E-02 JY/BEAM
Levs = 1.100E-03 * (-5, -4, -3, -2, 2, 3, 4, 7,
10, 15, 20, 25, 30, 35, 40)

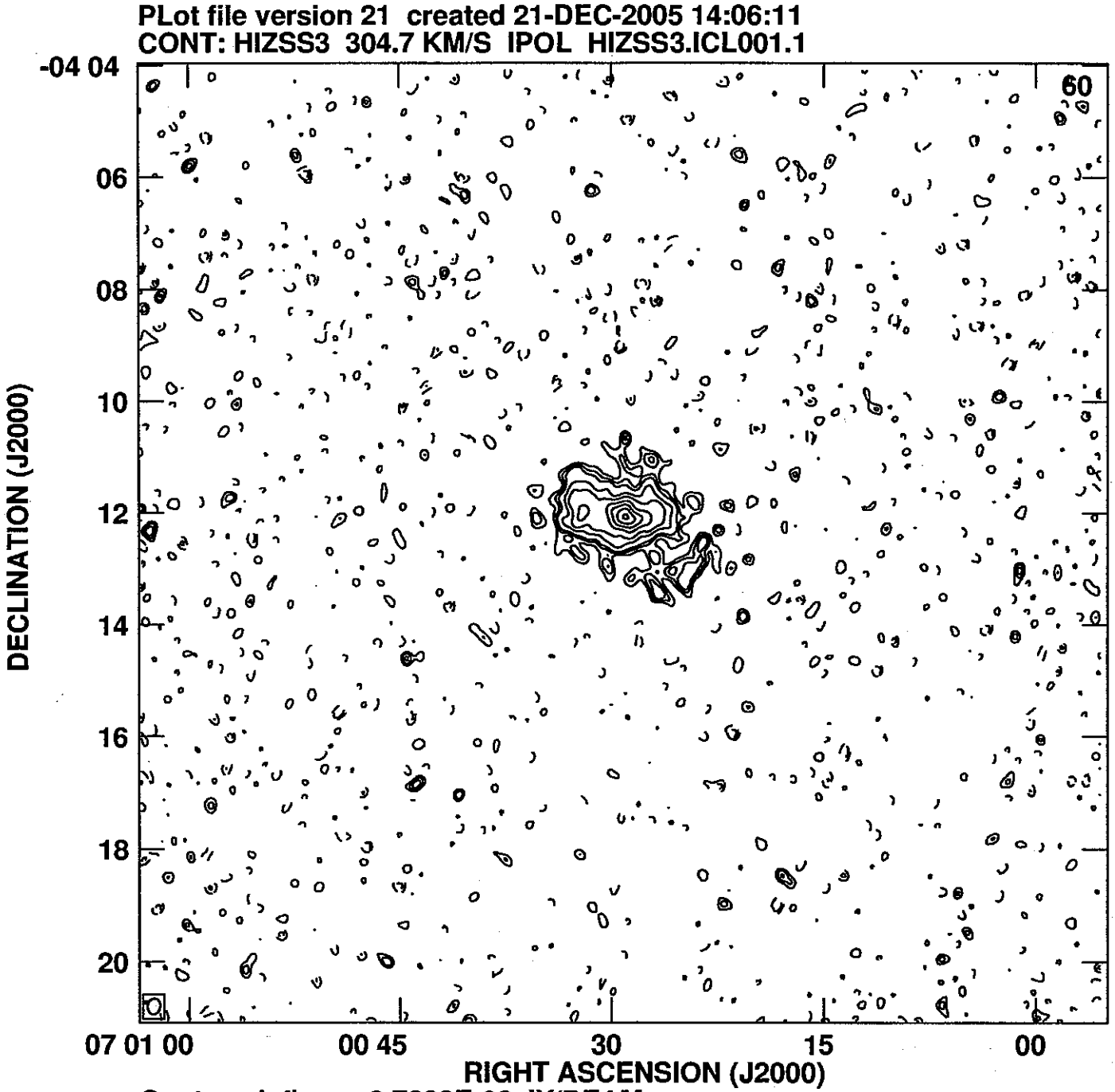
PLot file version 21 created 21-DEC-2005 14:06:11
CONT: HIZSS3 304.7 KM/S IPOL HIZSS3.ICL001.1
-04 04
06
08
10
12
14
16
18
20
60
DECLINATION (J2000)
07 01 00
00 45
30
15
00
RIGHT ASCENSION (J2000)
Cont peak flux = 3.7868E-02 JY/BEAM
Levs = 1.100E-03 * (-5, -4, -3, -2, 2, 3, 4, 7,
10, 15, 20, 25, 30, 35, 40)

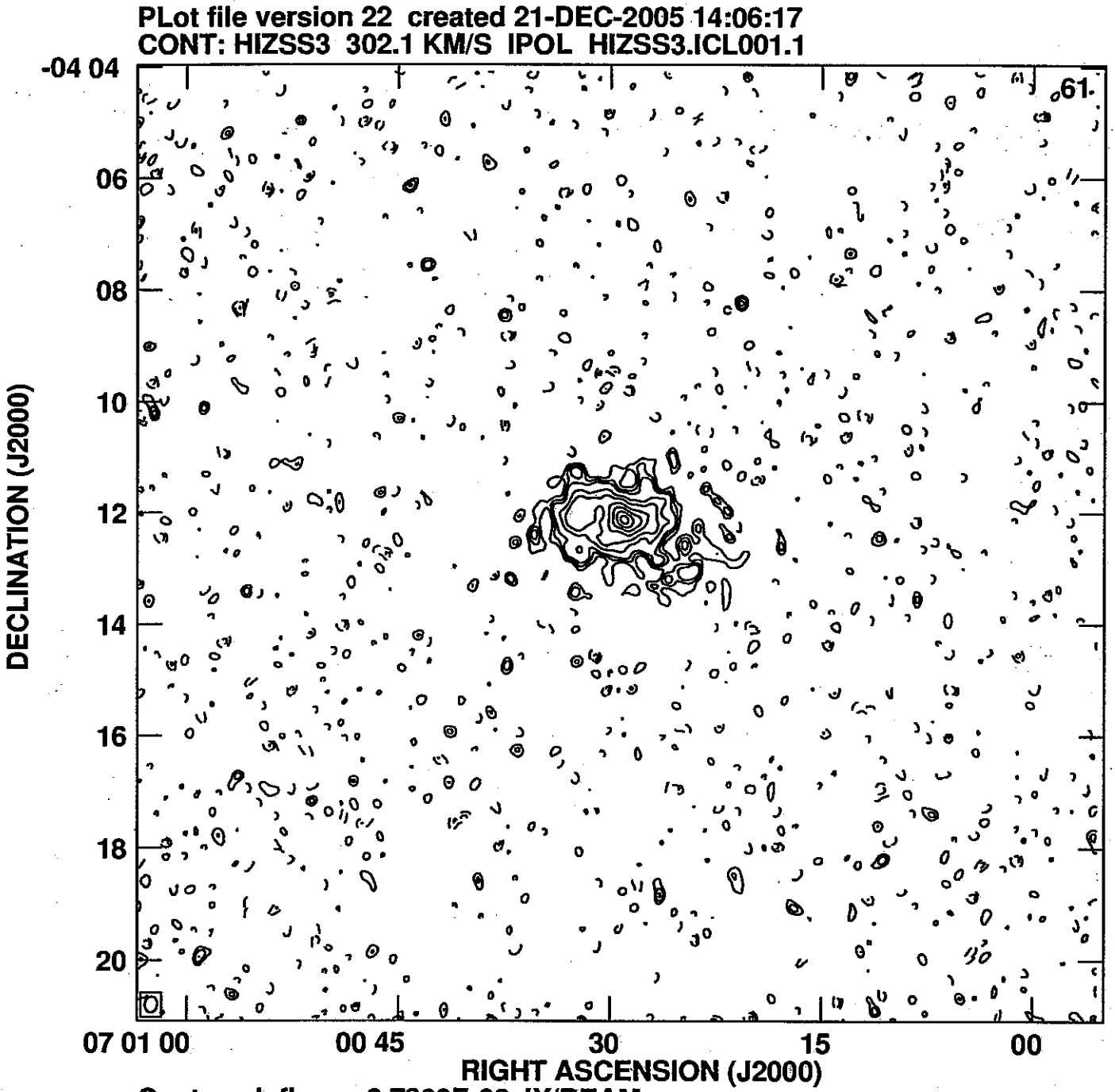
PLot file version 22 created 21-DEC-2005 14:06:17
CONT: HIZSS3 302.1 KM/S IPOL HIZSS3.ICL001.1
-04 04
06
08
10
12
14
16
18
20
61.
DECLINATION (J2000)
07 01 00
00 45
30
15
00
RIGHT ASCENSION (J2000)
Cont peak flux = 3.7868E-02 JY/BEAM
Levs = 1.100E-03 * (-5, -4, -3, -2, 2, 3, 4, 7,
10, 15, 20, 25, 30, 35, 40)

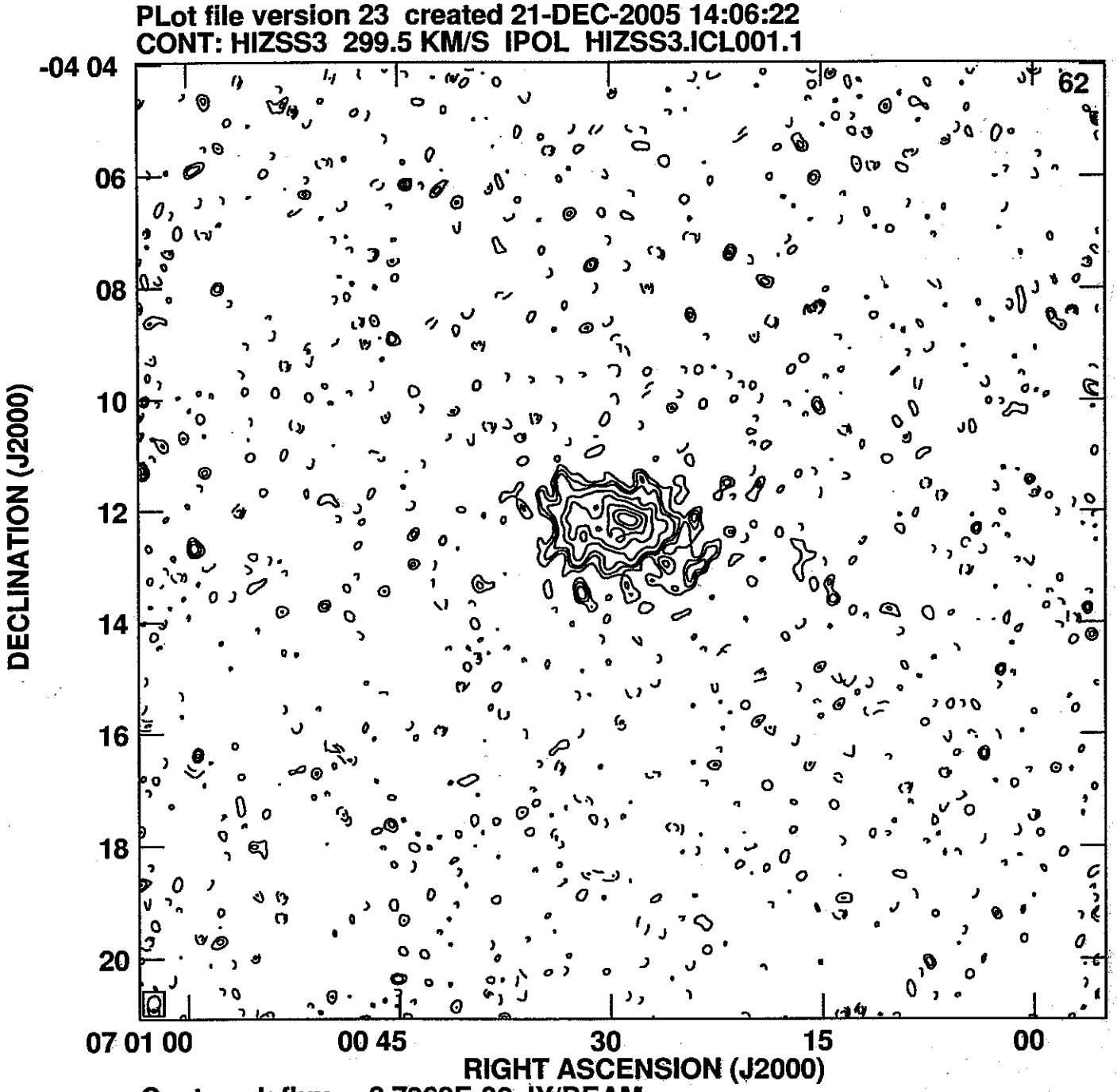
PLot file version 23 created 21-DEC-2005 14:06:22
CONT: HIZSS3 299.5 KM/S IPOL HIZSS3.ICL001.1
-04 04
06
08
10
12
14
16
18
20
62
DECLINATION (J2000)
07 01 00
00 45
30
15
00
RIGHT ASCENSION (J2000)
Cont peak flux = 3.7868E-02 JY/BEAM
Levs = 1.100E-03 * (-5, -4, -3, -2, 2, 3, 4, 7,
10, 15, 20, 25, 30, 35, 40)

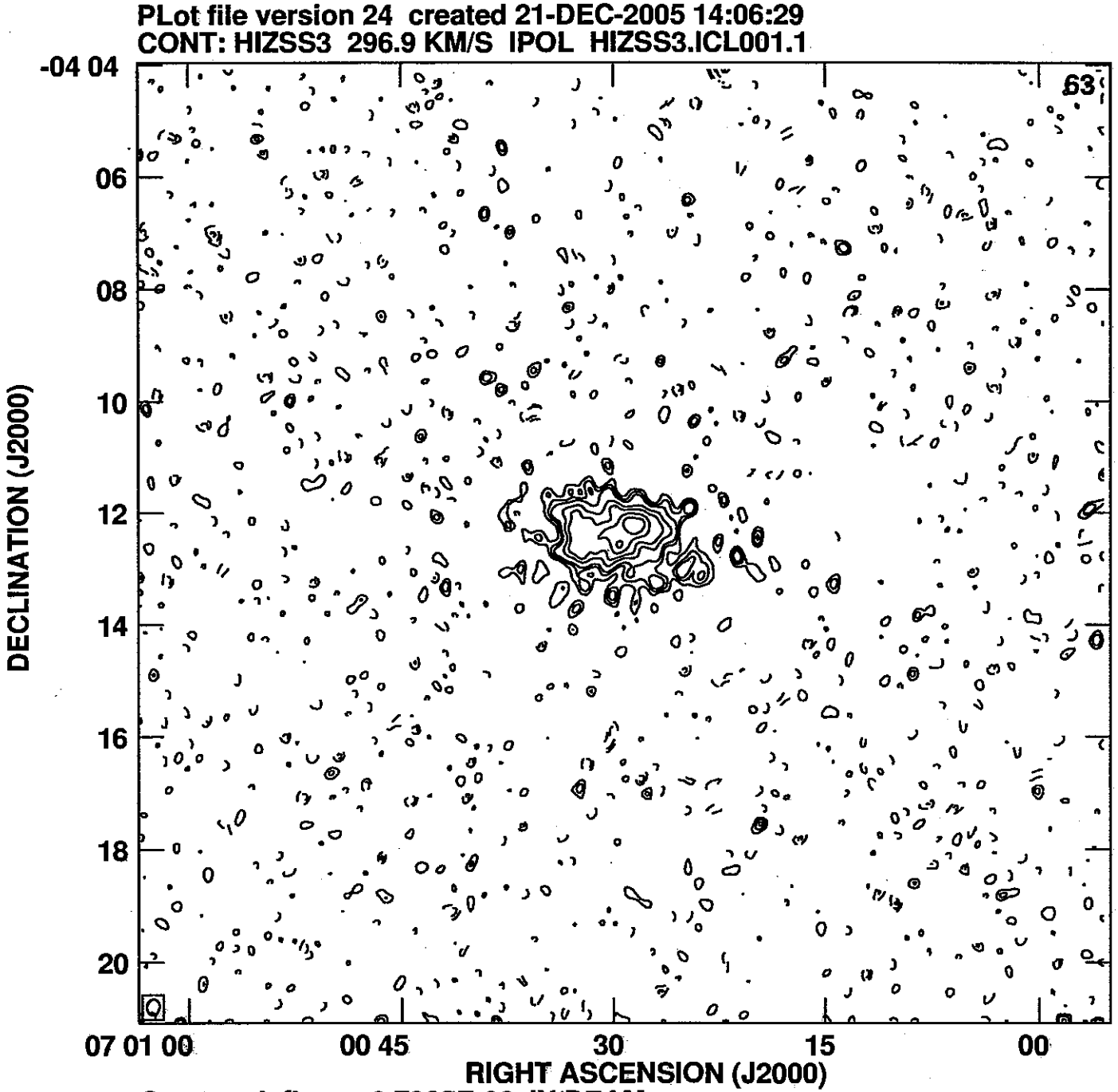
PLot file version 24 created 21-DEC-2005 14:06:29
CONT: HIZSS3 296.9 KM/S IPOL HIZSS3.ICL001.1
-04 04
06
08
10
12
14
16
18
20
DECLINATION (J2000)
07 01 00
00 45
30
15
00
RIGHT ASCENSION (J2000)
Cont peak flux = 3.7868E-02 JY/BEAM
Levs = 1.100E-03 * (-5, -4, -3, -2, 2, 3, 4, 7,
10, 15, 20, 25, 30, 35, 40)

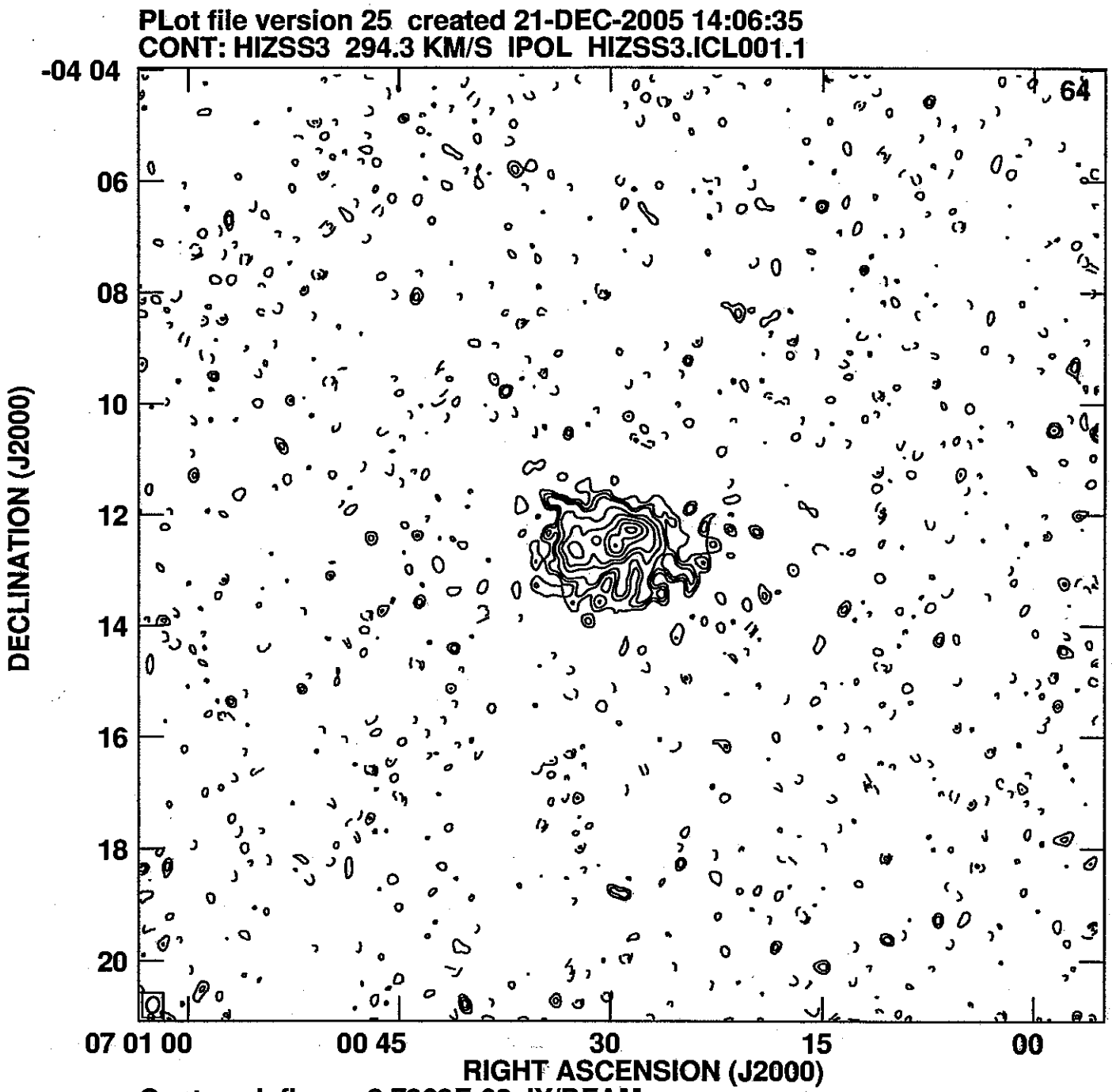
PLot file version 25 created 21-DEC-2005 14:06:35
CONT: HIZSS3 294.3 KM/S IPOL HIZSS3.ICL001.1
-04 04
06
08
10
12
14
16
18
20
64
DECLINATION (J2000)
07 01 00
00 45
30
15
00
RIGHT ASCENSION (J2000)
Cont peak flux = 3.7868E-02 JY/BEAM
Levs = 1.100E-03 * (-5, -4, -3, -2, 2, 3, 4, 7,
10, 15, 20, 25, 30, 35, 40)

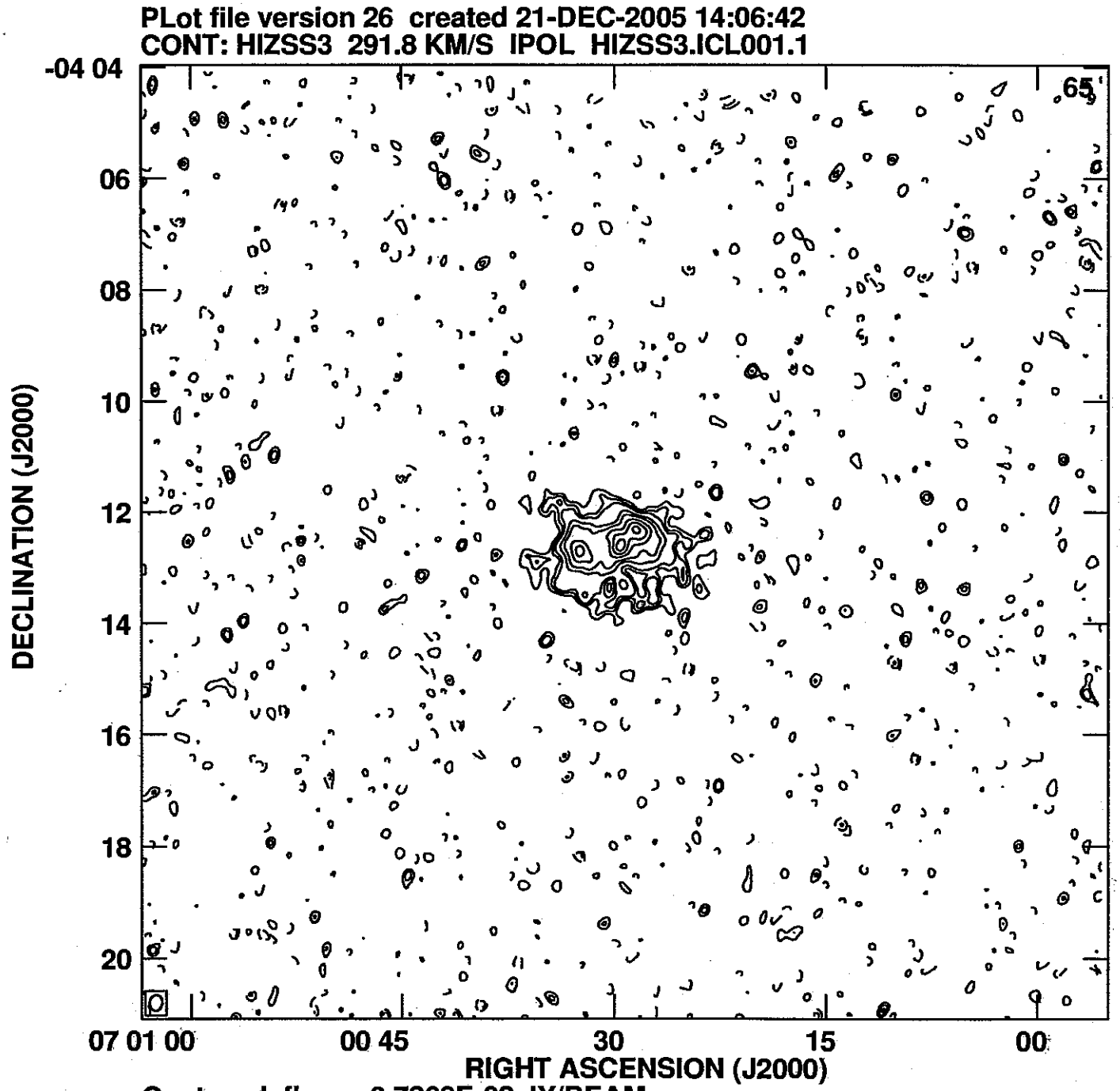
PLot file version 26 created 21-DEC-2005 14:06:42
CONT: HIZSS3 291.8 KM/S IPOL HIZSS3.ICL001.1
-04 04
06
08
10
12
14
16
18
20
DECLINATION (J2000)
07 01 00
00 45
30
15
00
RIGHT ASCENSION (J2000)
Cont peak flux = 3.7868E-02 JY/BEAM
Levs = 1.100E-03 * (-5, -4, -3, -2, 2, 3, 4, 7,
10, 15, 20, 25, 30, 35, 40)

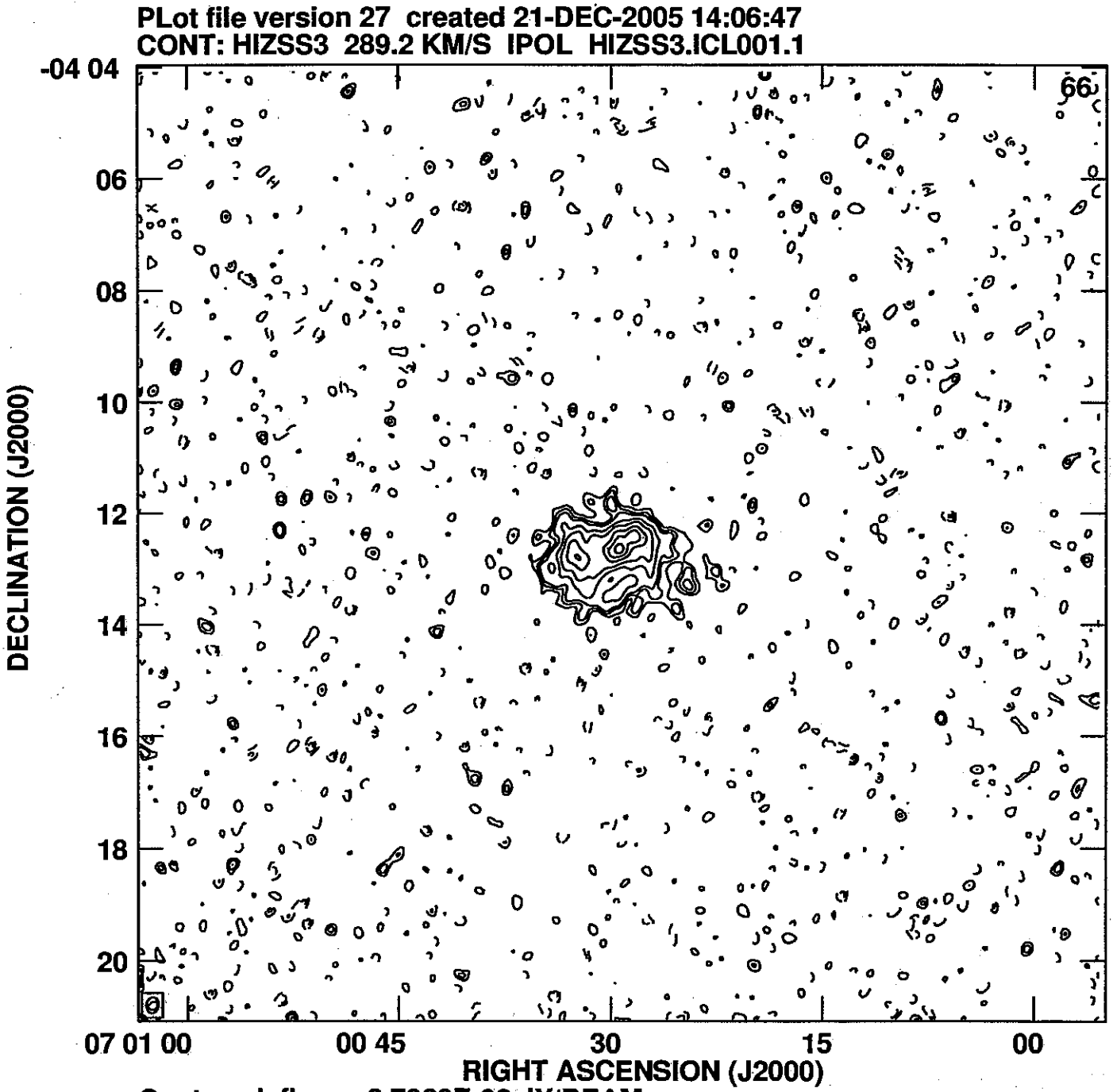
PLot file version 27 created 21-DEC-2005 14:06:47
CONT: HIZSS3 289.2 KM/S IPOL HIZSS3.ICL001.1
-04 04
06
08
10
12
14
16
18
20
DECLINATION (J2000)
07 01 00
00 45
30
15
00
RIGHT ASCENSION (J2000)
Cont peak flux = 3.7868E-02 JY/BEAM
Levs = 1.100E-03 * (-5, -4, -3, -2, 2, 3, 4, 7,
10, 15, 20, 25, 30, 35, 40)

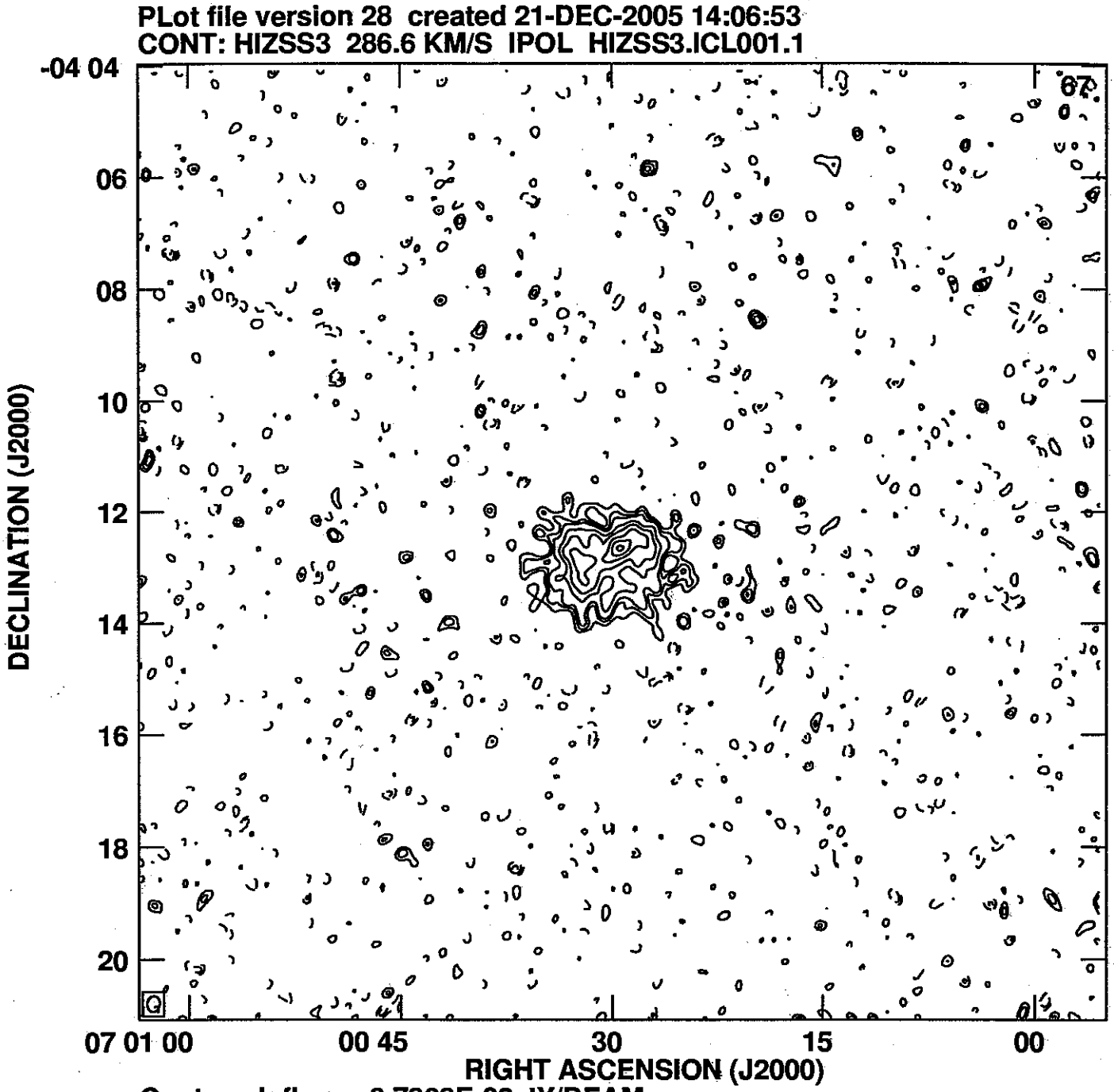
PLot file version 28 created 21-DEC-2005 14:06:53
CONT: HIZSS3 286.6 KM/S IPOL HIZSS3.ICL001.1
-04 04
06
08
10
12
14
16
18
20
DECLINATION (J2000)
07 01 00
00 45
30
15
00
RIGHT ASCENSION (J2000)
Cont peak flux = 3.7868E-02 JY/BEAM
Levs = 1.100E-03 * (-5, -4, -3, -2, 2, 3, 4, 7,
10, 15, 20, 25, 30, 35, 40)

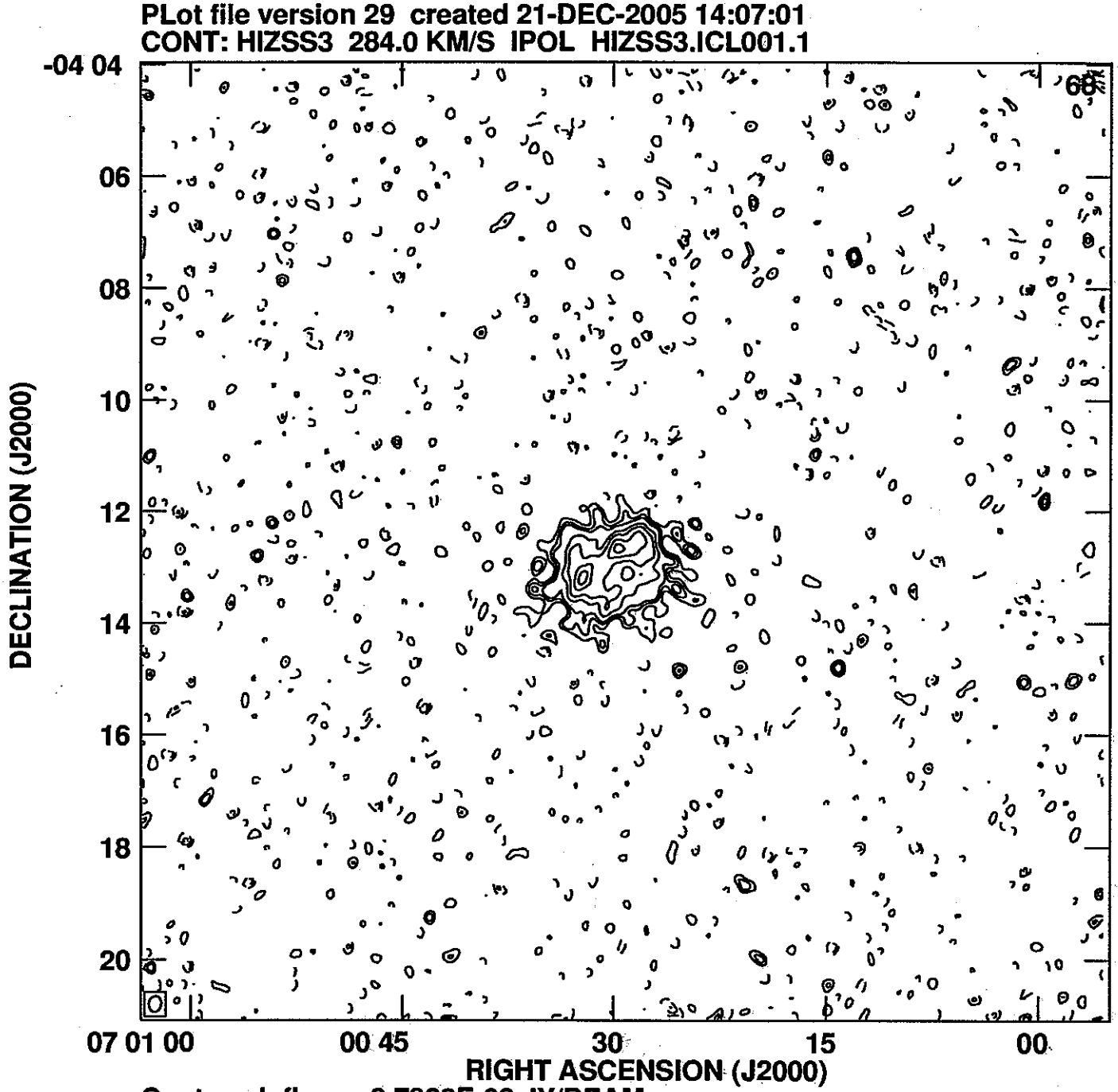
PLot file version 29 created 21-DEC-2005 14:07:01
CONT: HIZSS3 284.0 KM/S IPOL HIZSS3.ICL001.1
-04 04
06
08
10
12
14
16
18
20
DECLINATION (J2000)
07 01 00
00 45
30
15
00
RIGHT ASCENSION (J2000)
Cont peak flux = 3.7868E-02 JY/BEAM
Levs = 1.100E-03 * (-5, -4, -3, -2, 2, 3, 4, 7,
10, 15, 20, 25, 30, 35, 40)

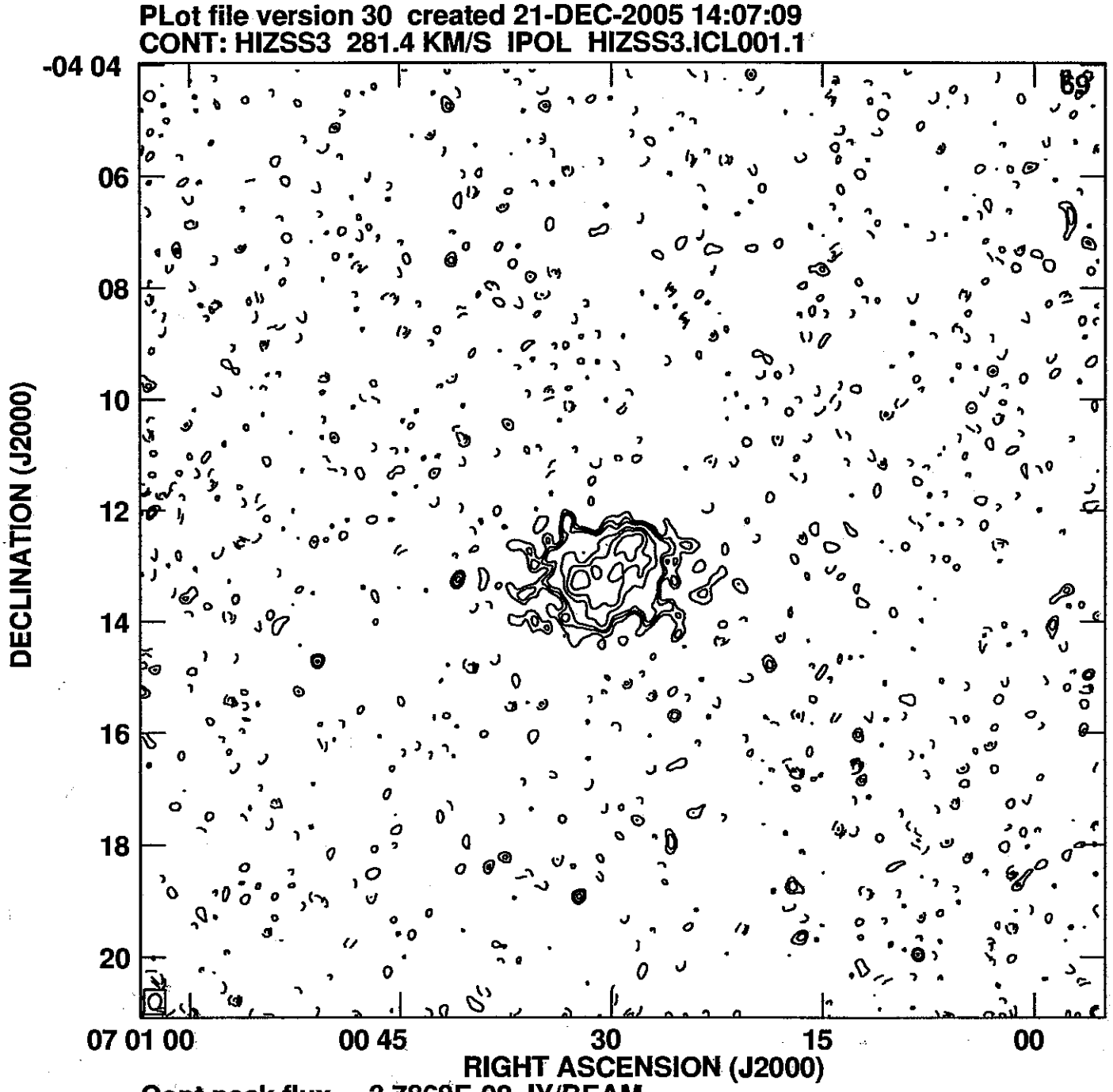
PLot file version 30 created 21-DEC-2005 14:07:09
CONT: HIZSS3 281.4 KM/S IPOL HIZSS3.ICL001.1
-04 04
06
08
10
12
14
16
18
20
DECLINATION (J2000)
07 01 00
00 45
30
15
00
RIGHT ASCENSION (J2000)
Cont peak flux = 3.7868E-02 JY/BEAM
Levs = 1.100E-03 * (-5, -4, -3, -2, 2, 3, 4, 7,
10, 15, 20, 25, 30, 35, 40)

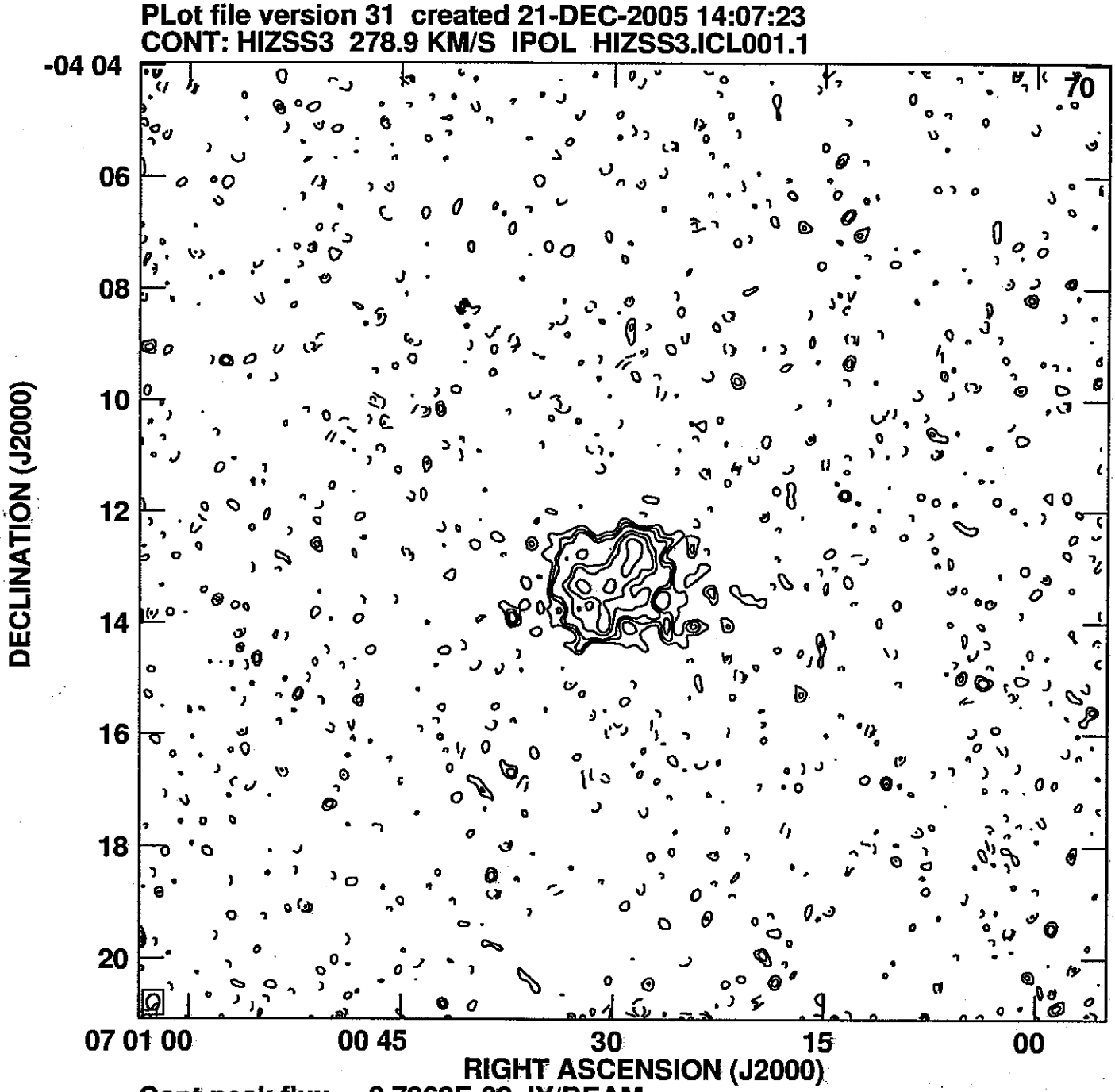
PLot file version 31 created 21-DEC-2005 14:07:23
CONT: HIZSS3 278.9 KM/S IPOL HIZSS3.ICL001.1
-04 04
06
08
10
12
14
16
18
20
70
DECLINATION (J2000)
07 01 00
00 45
30
15
00
RIGHT ASCENSION (J2000)
Cont peak flux = 3.7868E-02 JY/BEAM
Levs = 1.100E-03 * (-5, -4, -3, -2, 2, 3, 4, 7,
10, 15, 20, 25, 30, 35, 40)

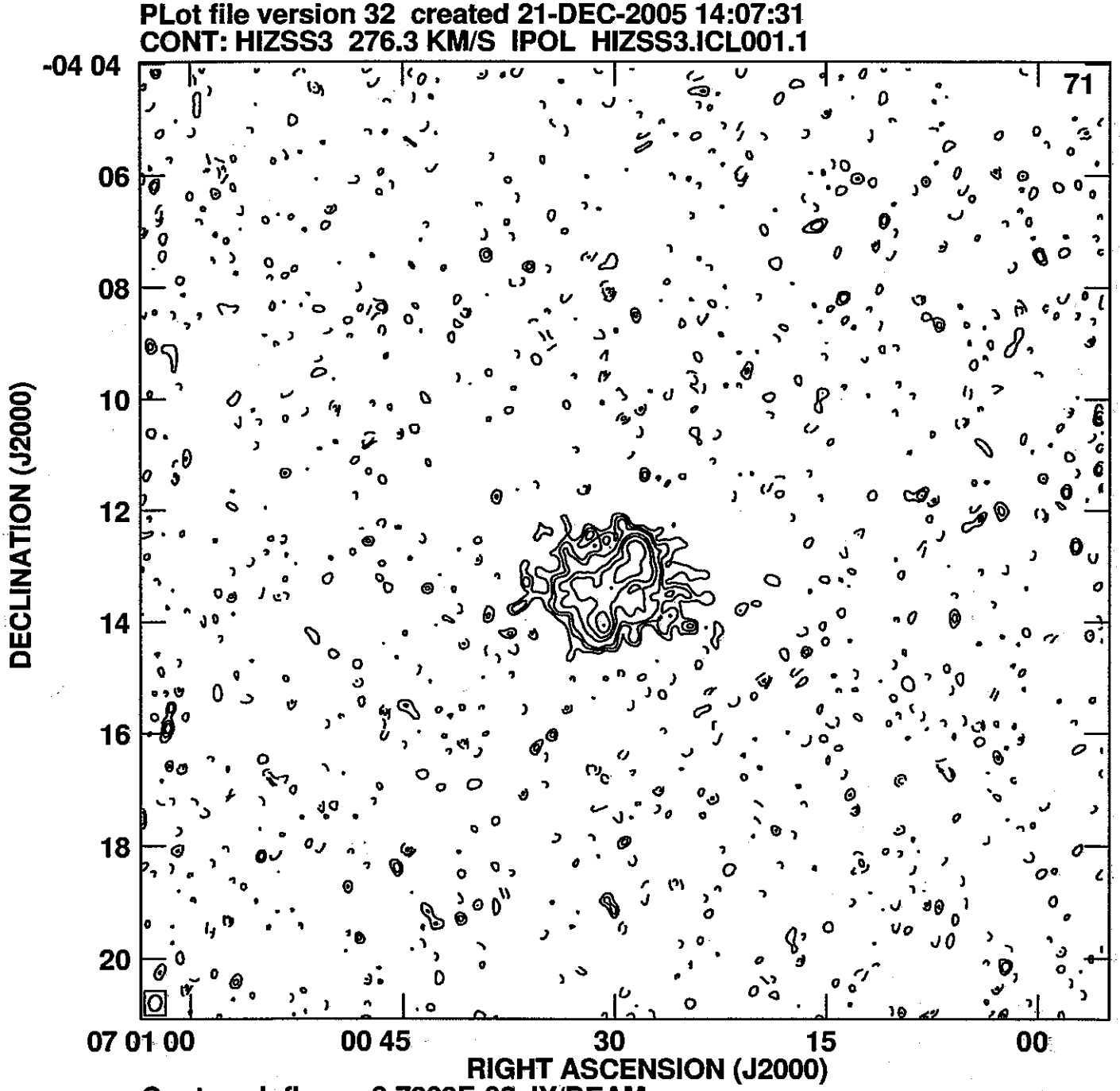
PLot file version 32 created 21-DEC-2005 14:07:31
CONT: HIZSS3 276.3 KM/S IPOL HIZSS3.ICL001.1
-04 04
06
08
10
12
14
16
18
20
71
DECLINATION (J2000)
07 01 00
00 45
30
15
00
RIGHT ASCENSION (J2000)
Cont peak flux = 3.7868E-02 JY/BEAM
Levs = 1.100E-03 * (-5, -4, -3, -2, 2, 3, 4, 7,
10, 15, 20, 25, 30, 35, 40)

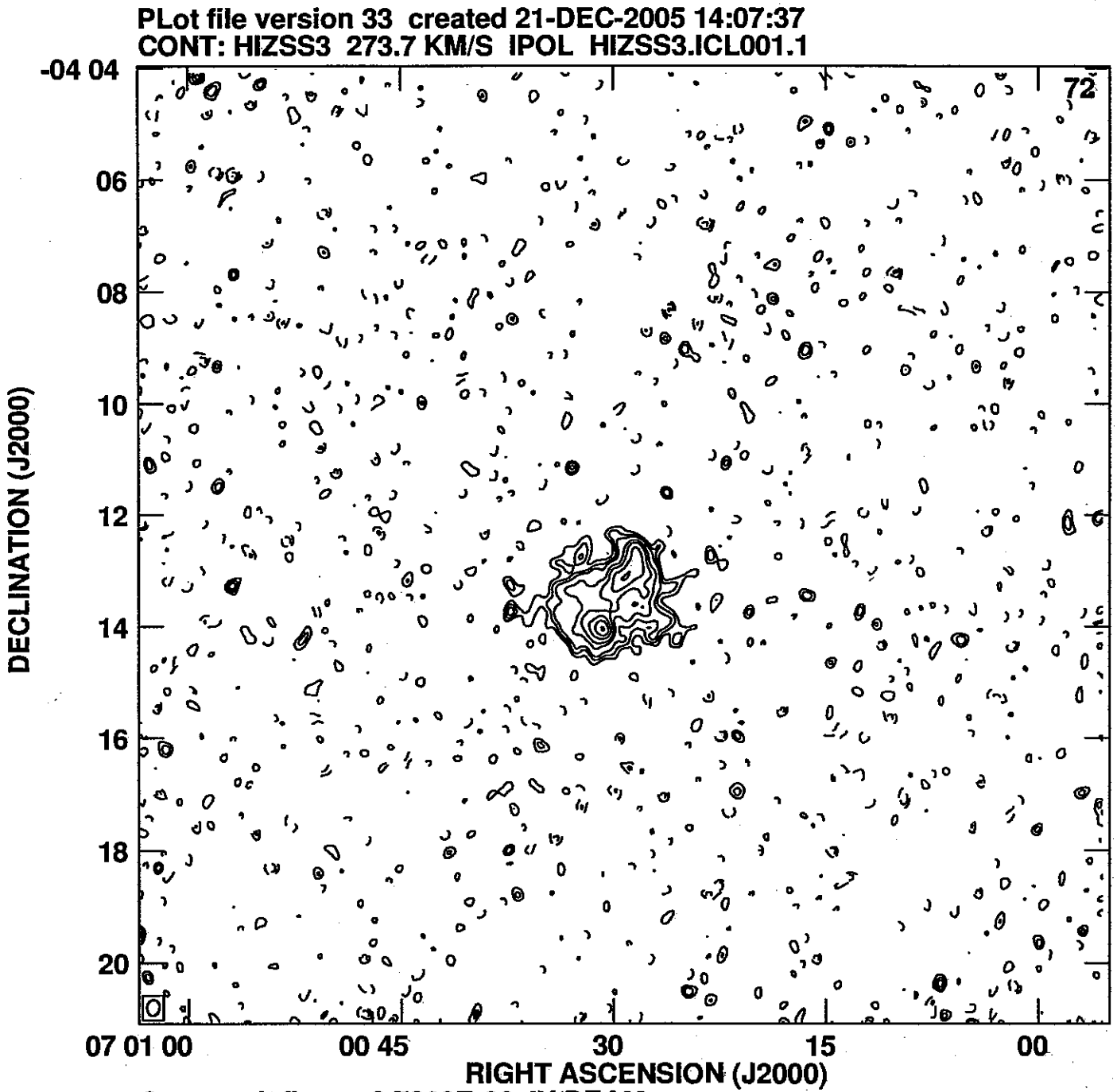
PLot file version 33 created 21-DEC-2005 14:07:37
CONT: HIZSS3 273.7 KM/S IPOL HIZSS3.ICL001.1
-04 04
06
08
10
12
14
16
18
20
72
DECLINATION (J2000)
07 01 00
00 45
30
15
00
RIGHT ASCENSION (J2000)
Cont peak flux = 3.7868E-02 JY/BEAM
Levs = 1.100E-03 * (-5, -4, -3, -2, 2, 3, 4, 7,
10, 15, 20, 25, 30, 35, 40)

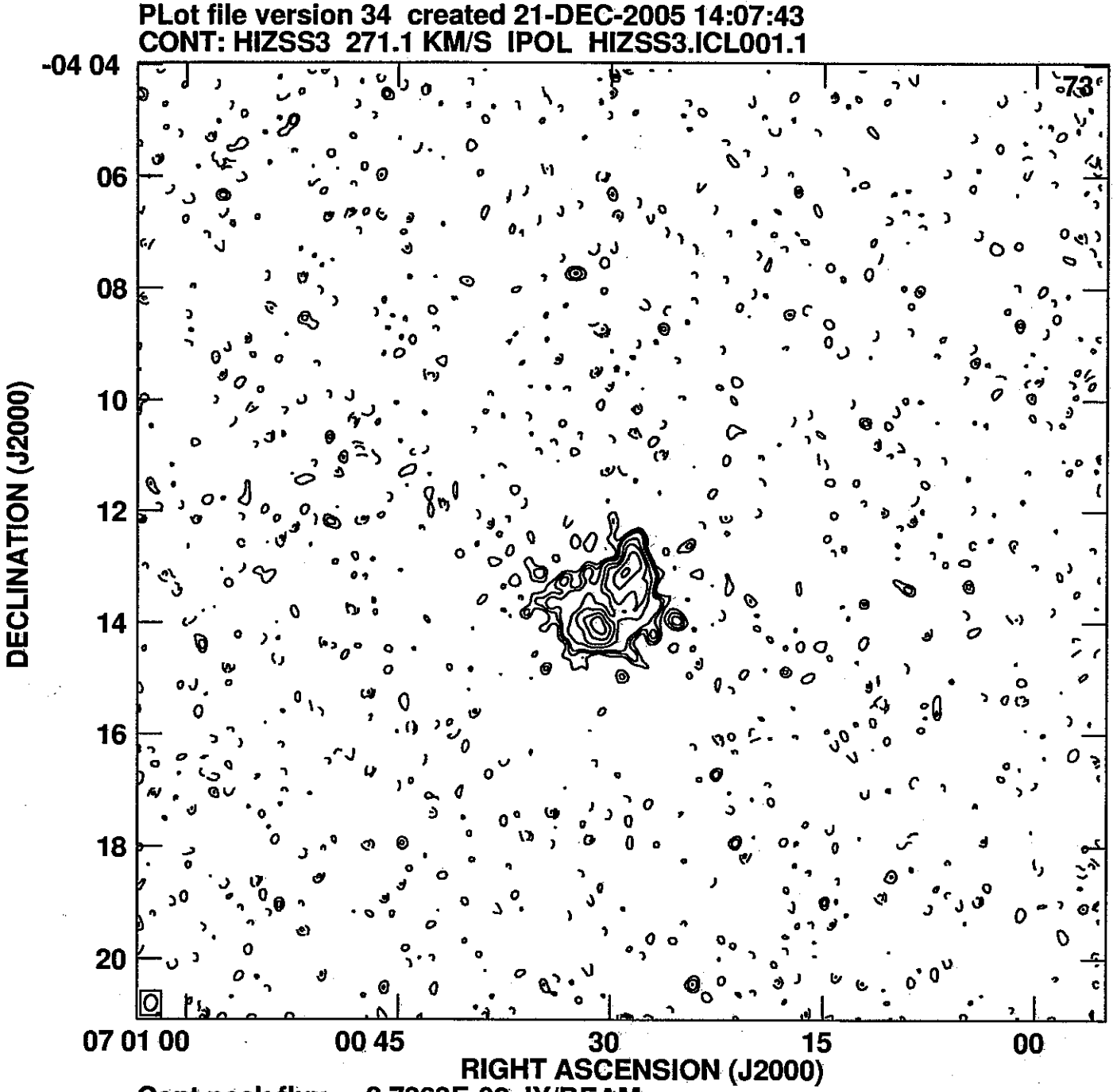
PLot file version 34 created 21-DEC-2005 14:07:43
CONT: HIZSS3 271.1 KM/S IPOL HIZSS3.ICL001.1
-04 04
06
08
10
12
14
16
18
20
DECLINATION (J2000)
07 01 00
00 45
30
15
00
RIGHT ASCENSION (J2000)
Cont peak flux = 3.7868E-02 JY/BEAM
Levs = 1.100E-03 * (-5, -4, -3, -2, 2, 3, 4, 7,
10, 15, 20, 25, 30, 35, 40)

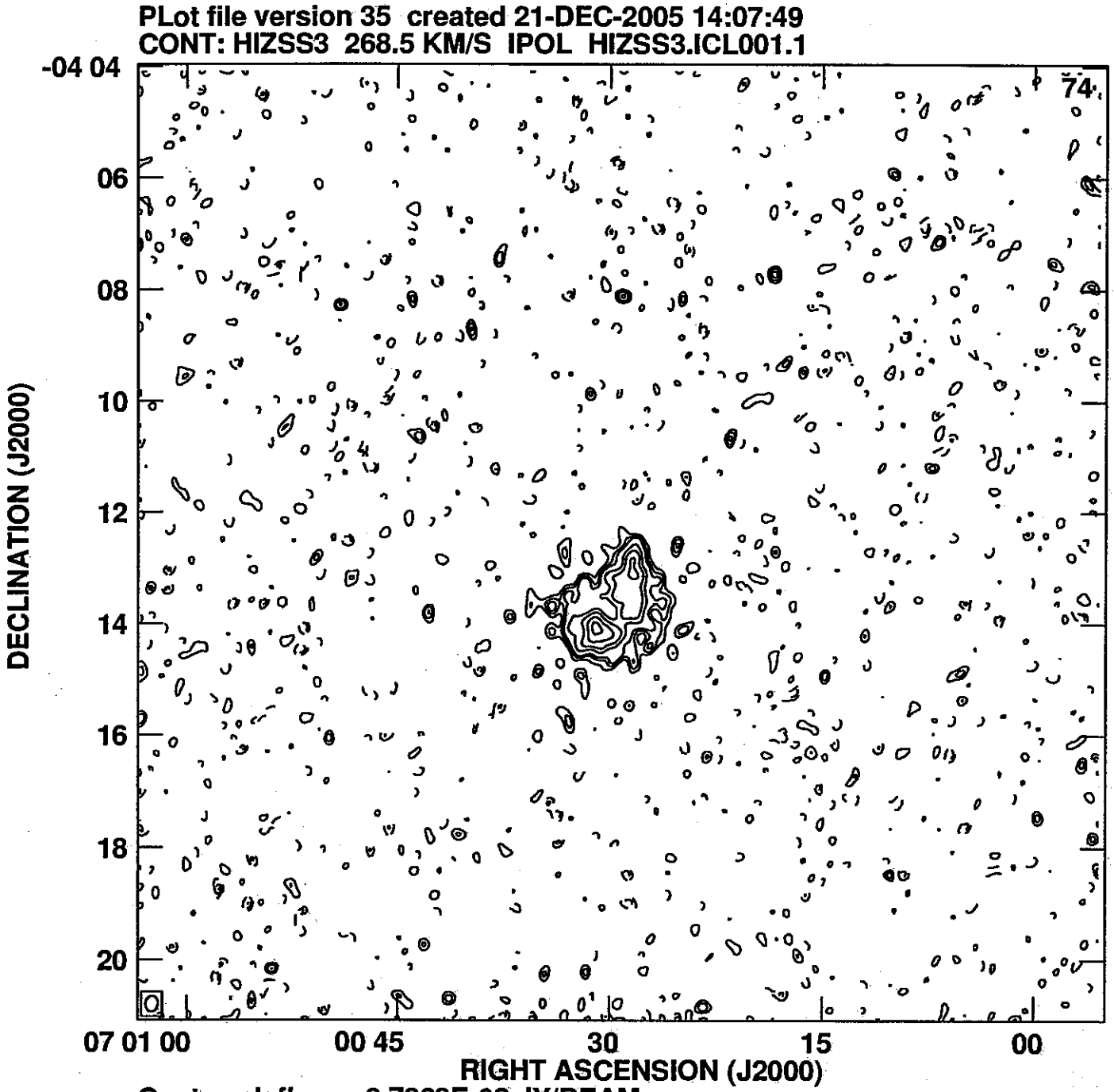
PLot file version 35 created 21-DEC-2005 14:07:49
CONT: HIZSS3 268.5 KM/S IPOL HIZSS3.ICL001.1
-04 04
06
08
10
12
14
16
18
20
74
DECLINATION (J2000)
07 01 00
00 45
30
15
00
RIGHT ASCENSION (J2000)
Cont peak flux = 3.7868E-02 JY/BEAM
Levs = 1.100E-03 * (-5, -4, -3, -2, 2, 3, 4, 7,
10, 15, 20, 25, 30, 35, 40)

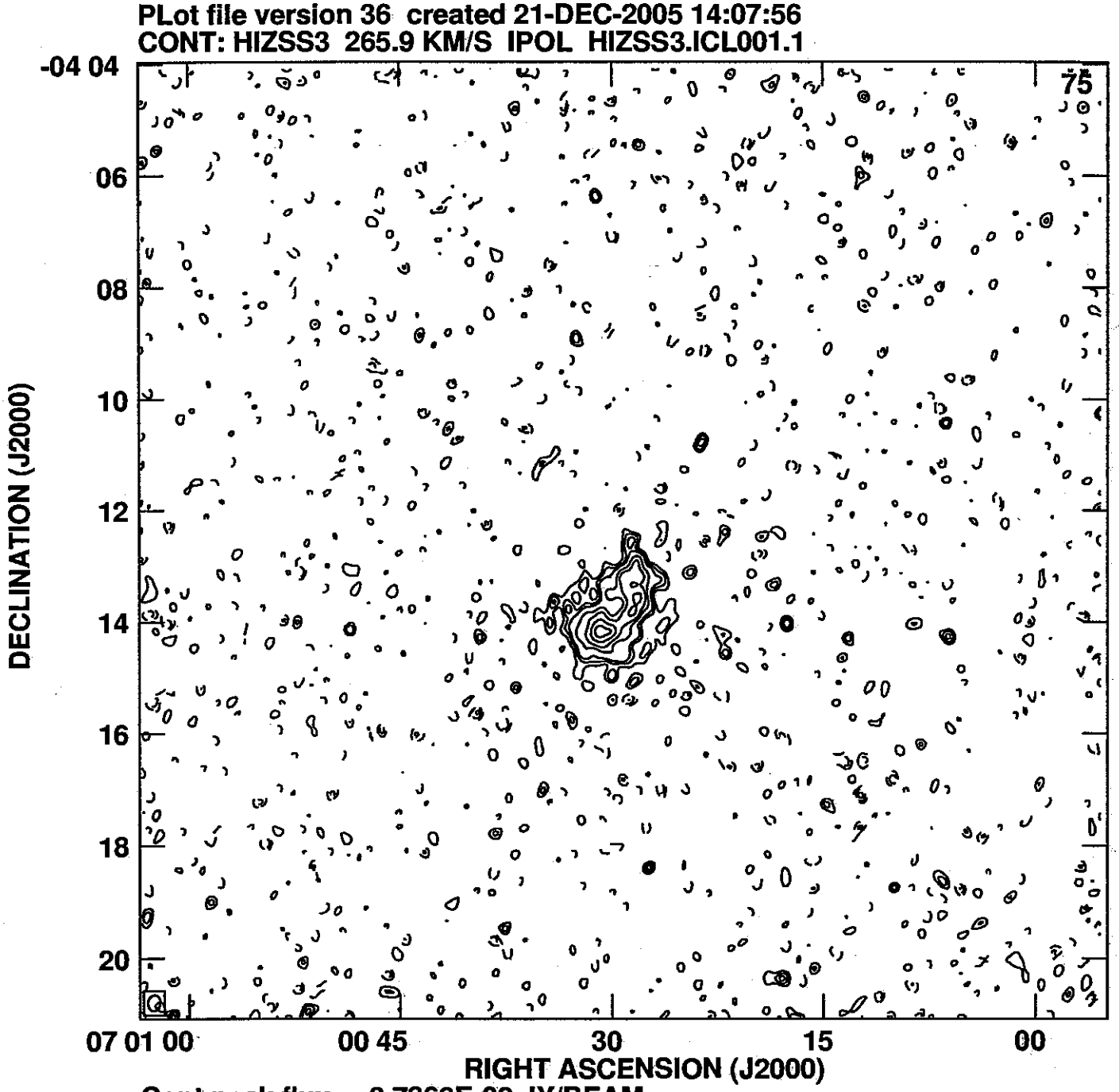
PLot file version 36 created 21-DEC-2005 14:07:56
CONT: HIZSS3 265.9 KM/S IPOL HIZSS3.ICL001.1
-04 04
06
08
10
12
14
16
18
20
75
DECLINATION (J2000)
07 01 00
00 45
30
15
00
RIGHT ASCENSION (J2000)
Cont peak flux = 3.7868E-02 JY/BEAM
Levs = 1.100E-03 * (-5, -4, -3, -2, 2, 3, 4, 7,
10, 15, 20, 25, 30, 35, 40)

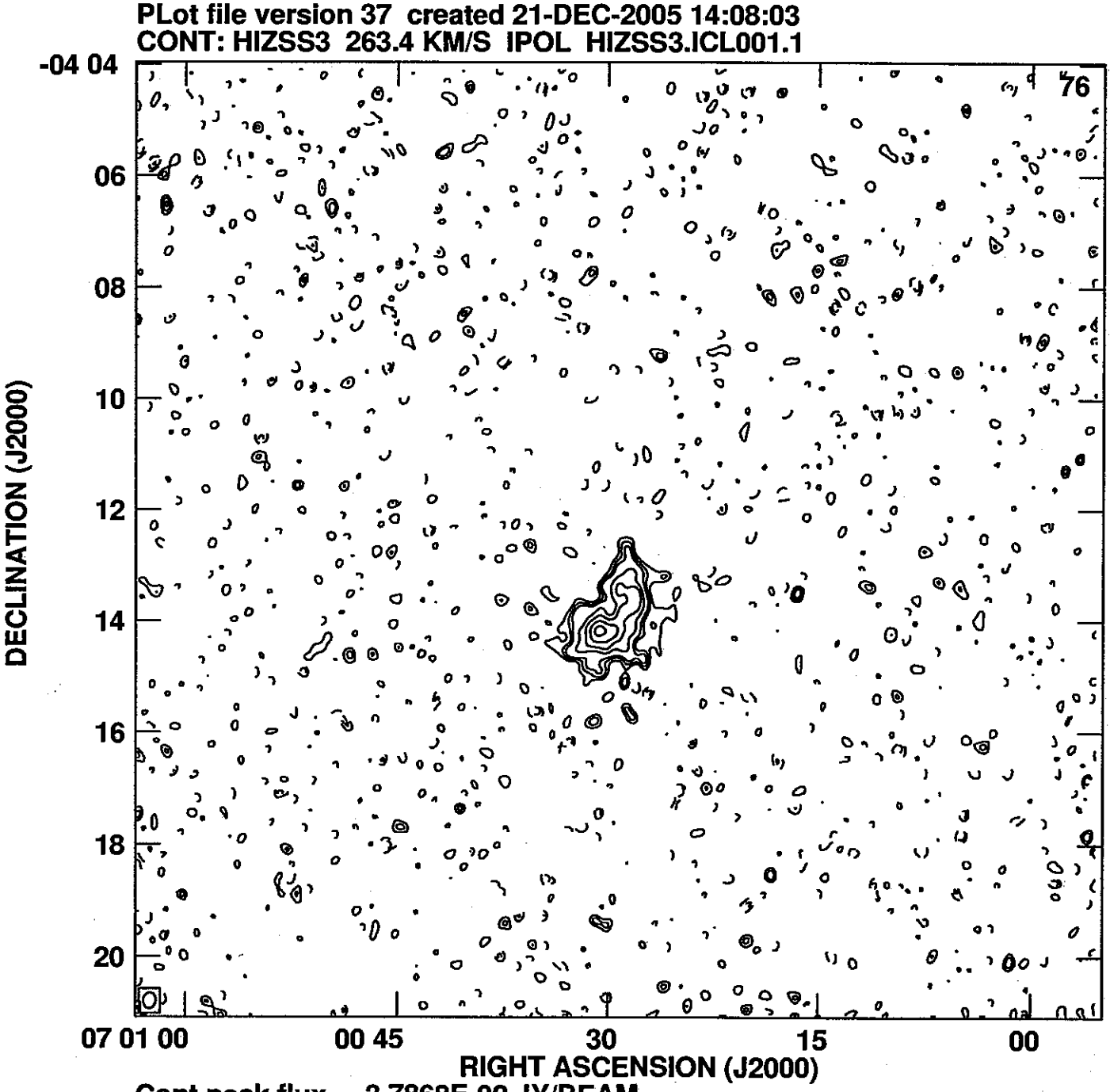
PLot file version 37 created 21-DEC-2005 14:08:03
CONT: HIZSS3 263.4 KM/S IPOL HIZSS3.ICL001.1
-04 04
06
08
10
12
14
16
18
20
76
DECLINATION (J2000)
07 01 00
00 45
30
15
00
RIGHT ASCENSION (J2000)
Cont peak flux = 3.7868E-02 JY/BEAM
Levs = 1.100E-03 * (-5, -4, -3, -2, 2, 3, 4, 7,
10, 15, 20, 25, 30, 35, 40)

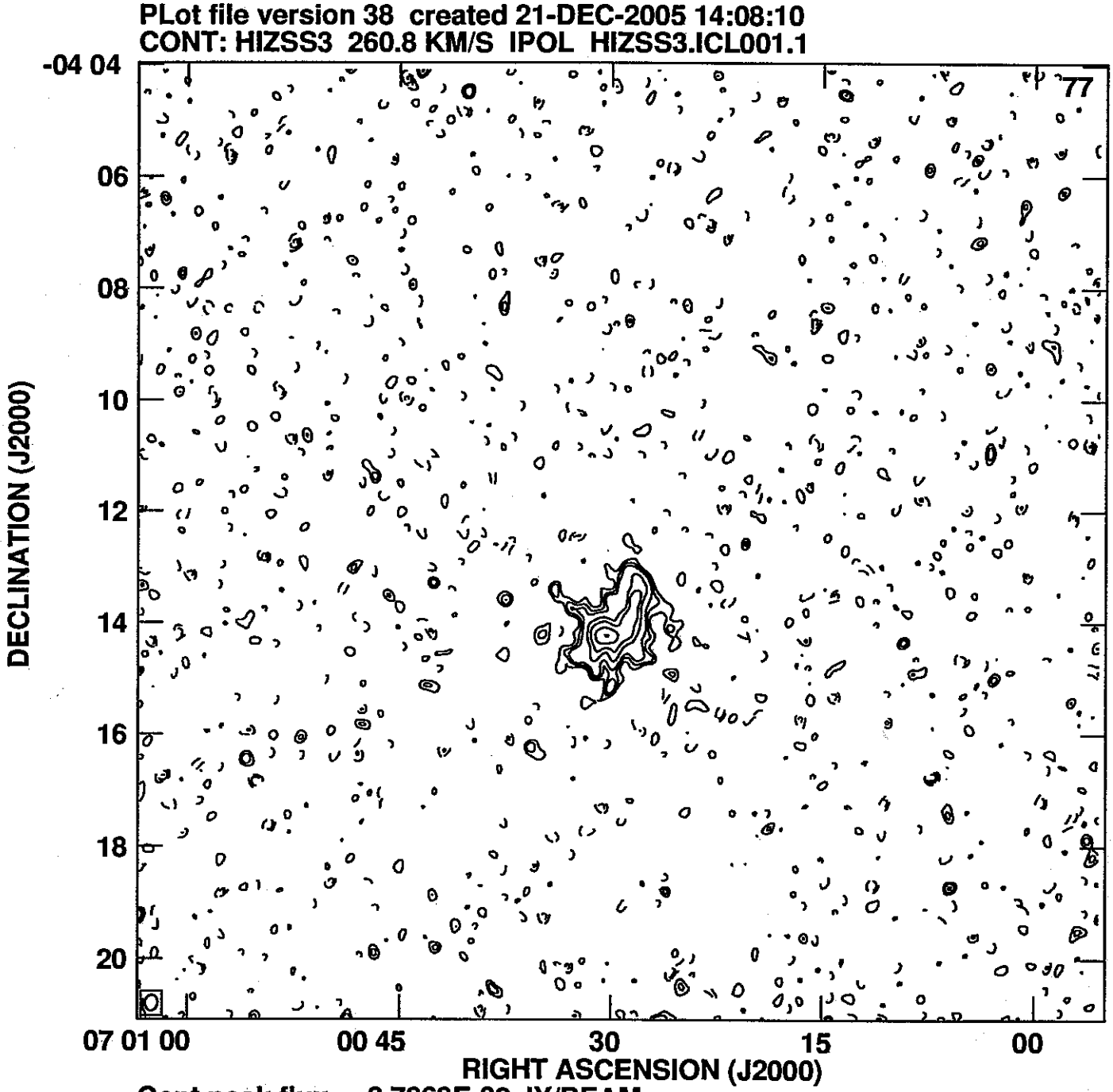
PLot file version 38 created 21-DEC-2005 14:08:10
CONT: HIZSS3 260.8 KM/S IPOL HIZSS3.ICL001.1
-04 04
06
08
10
12
14
16
18
20
77
DECLINATION (J2000)
07 01 00
00 45
30
15
00
RIGHT ASCENSION (J2000)
Cont peak flux = 3.7868E-02 JY/BEAM
Levs = 1.100E-03 * (-5, -4, -3, -2, 2, 3, 4, 7,
10, 15, 20, 25, 30, 35, 40)

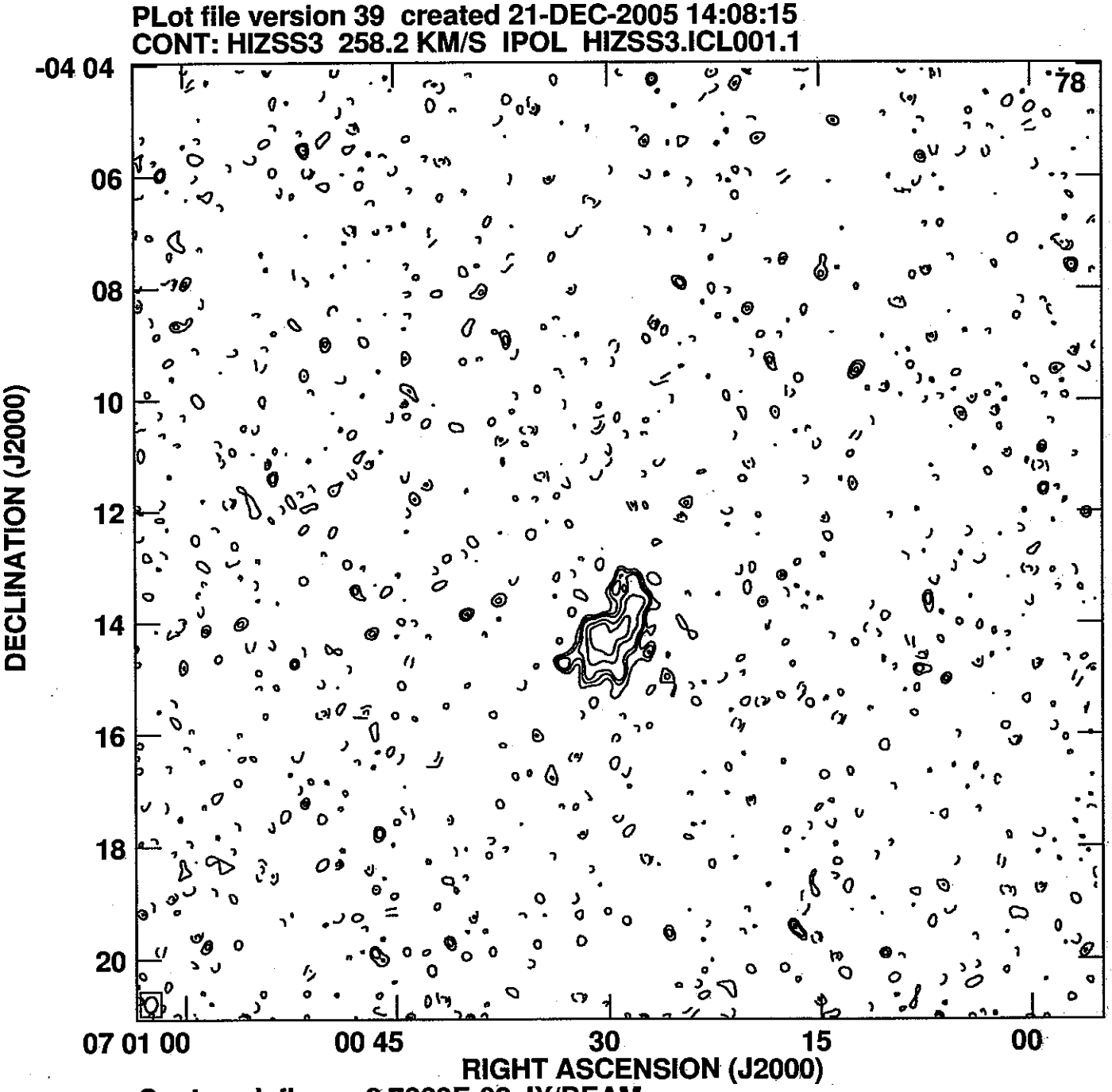
PLot file version 39 created 21-DEC-2005 14:08:15
CONT: HIZSS3 258.2 KM/S IPOL HIZSS3.ICL001.1
-04 04
78
06
08
10
12
14
16
18
20
DECLINATION (J2000)
07 01 00
00 45
30
15
00
RIGHT ASCENSION (J2000)
Cont peak flux = 3.7868E-02 JY/BEAM
Levs = 1.100E-03 * (-5, -4, -3, -2, 2, 3, 4, 7,
10, 15, 20, 25, 30, 35, 40)

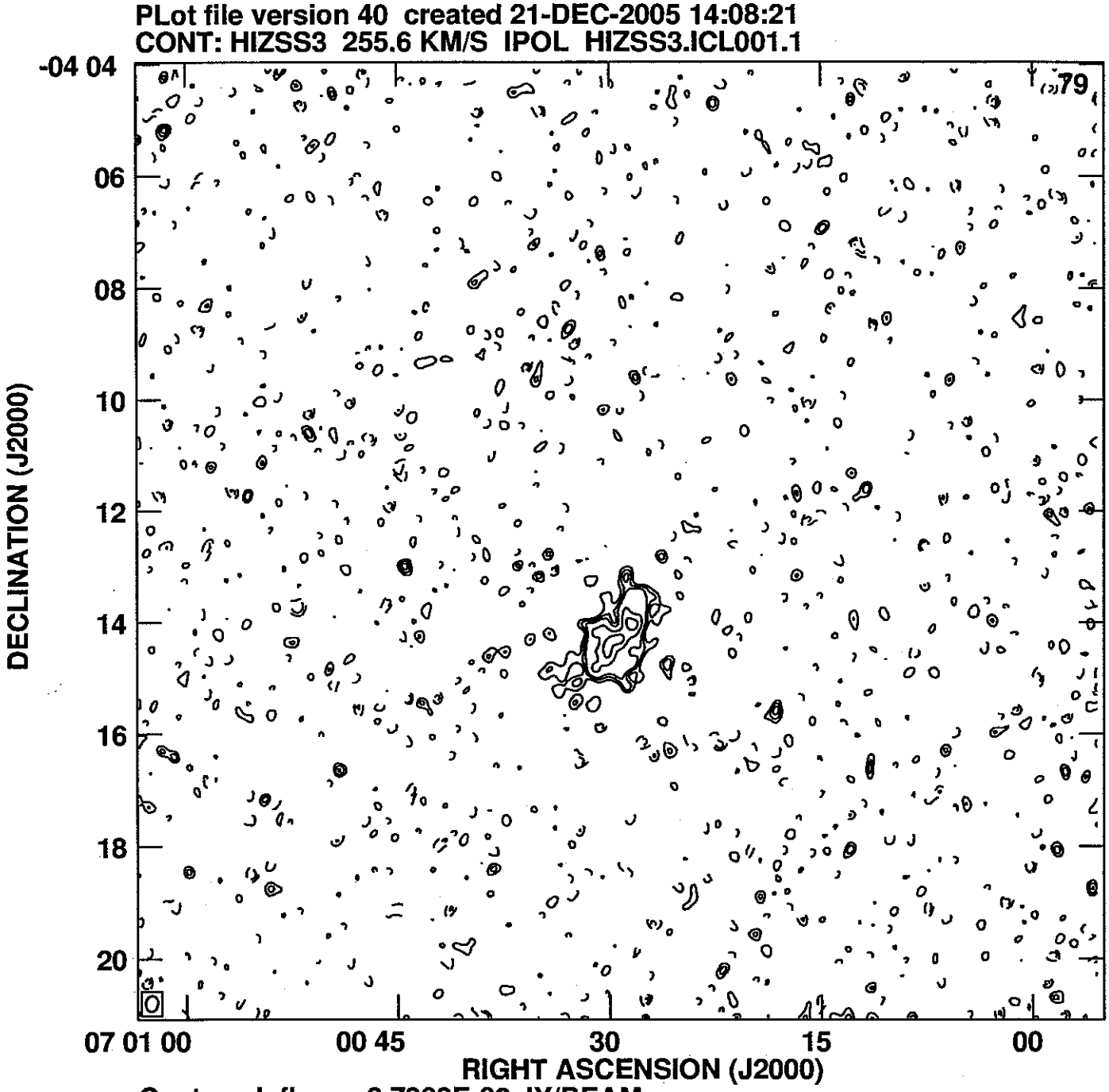
PLot file version 40 created 21-DEC-2005 14:08:21
CONT: HIZSS3 255.6 KM/S IPOL HIZSS3.ICL001.1
-04 04
06
08
10
12
14
16
18
20
DECLINATION (J2000)
07 01 00
00 45
30
15
00
RIGHT ASCENSION (J2000)
Cont peak flux = 3.7868E-02 JY/BEAM
Levs = 1.100E-03 * (-5, -4, -3, -2, 2, 3, 4, 7,
10, 15, 20, 25, 30, 35, 40)

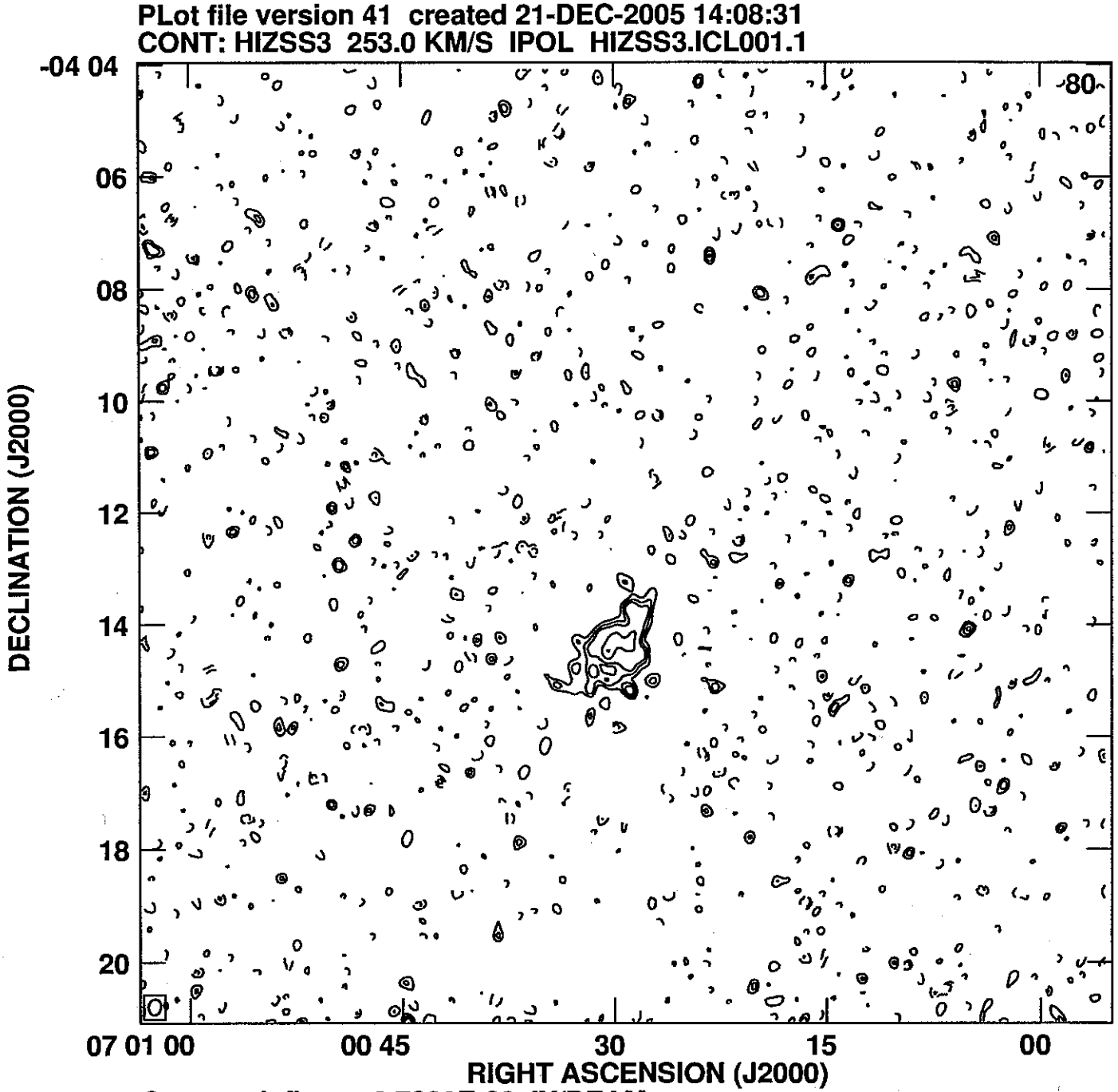
PLot file version 41 created 21-DEC-2005 14:08:31
CONT: HIZSS3 253.0 KM/S IPOL HIZSS3.ICL001.1
-04 04
06
08
10
12
14
16
18
20
80
DECLINATION (J2000)
07 01 00
00 45
30
15
00
RIGHT ASCENSION (J2000)
Cont peak flux = 3.7868E-02 JY/BEAM
Levs = 1.100E-03 * (-5, -4, -3, -2, 2, 3, 4, 7,
10, 15, 20, 25, 30, 35, 40)

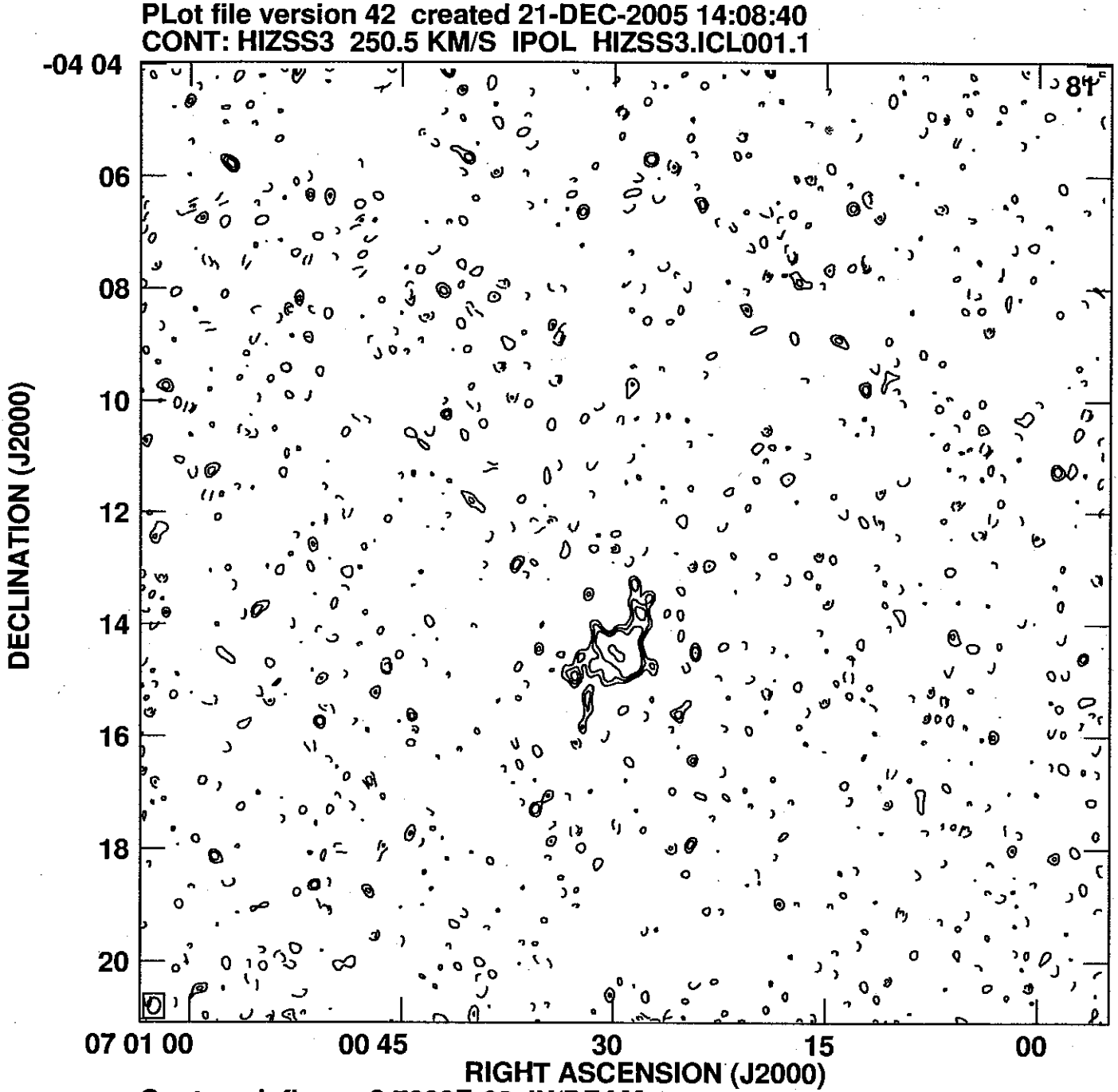
PLot file version 42 created 21-DEC-2005 14:08:40
CONT: HIZSS3 250.5 KM/S IPOL HIZSS3.ICL001.1
-04 04
06
08
10
12
14
16
18
20
DECLINATION (J2000)
07 01 00
00 45
30
15
00
RIGHT ASCENSION (J2000)
Cont peak flux = 3.7868E-02 JY/BEAM
Levs = 1.100E-03 * (-5, -4, -3, -2, 2, 3, 4, 7,
10, 15, 20, 25, 30, 35, 40)

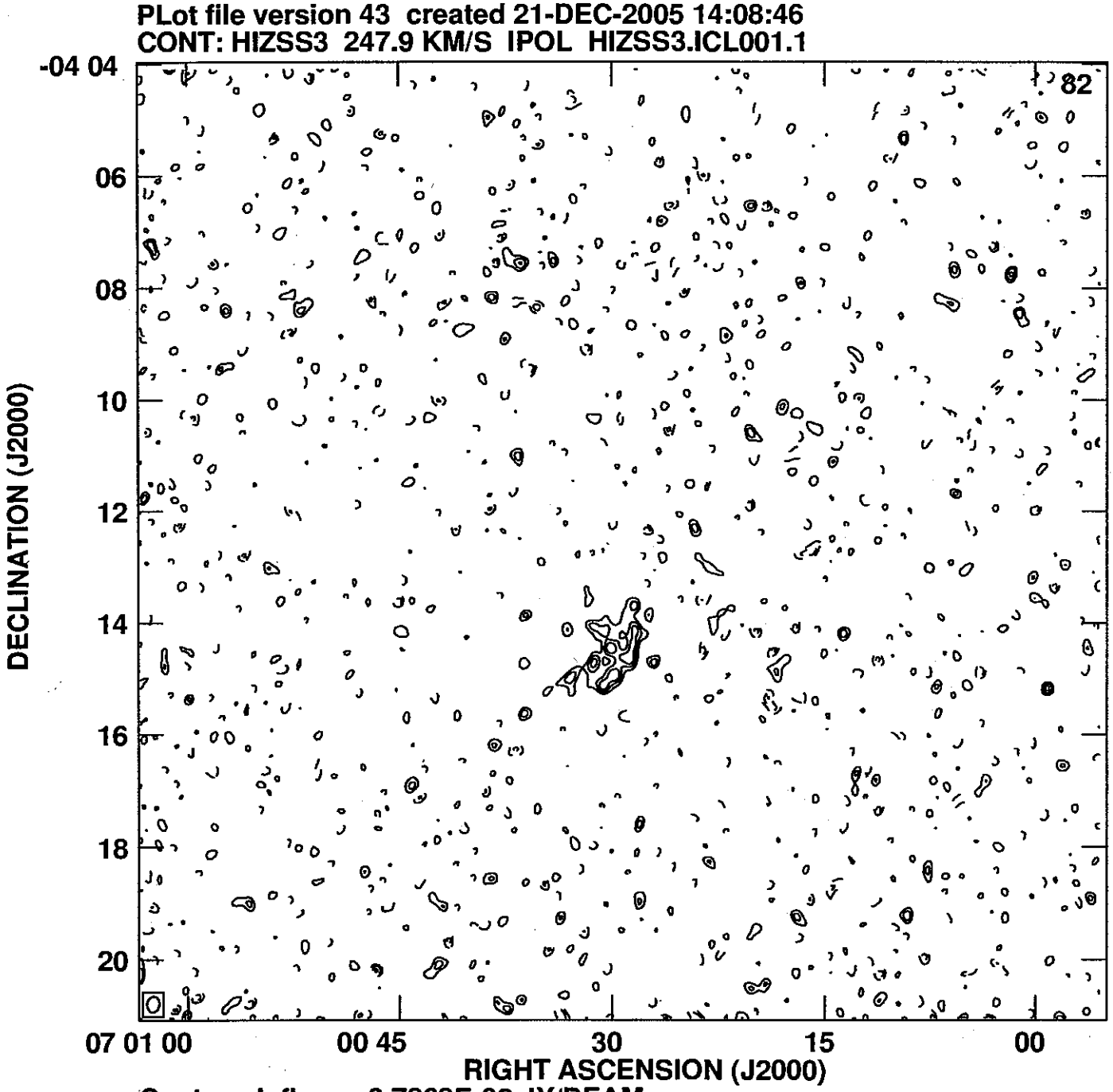
PLot file version 43 created 21-DEC-2005 14:08:46
CONT: HIZSS3 247.9 KM/S IPOL HIZSS3.ICL001.1
-04 04
06
08
10
12
14
16
18
20
82
DECLINATION (J2000)
07 01 00
00 45
30
15
00
RIGHT ASCENSION (J2000)
Cont peak flux = 3.7868E-02 JY/BEAM
Levs = 1.100E-03 * (-5, -4, -3, -2, 2, 3, 4, 7,
10, 15, 20, 25, 30, 35, 40)

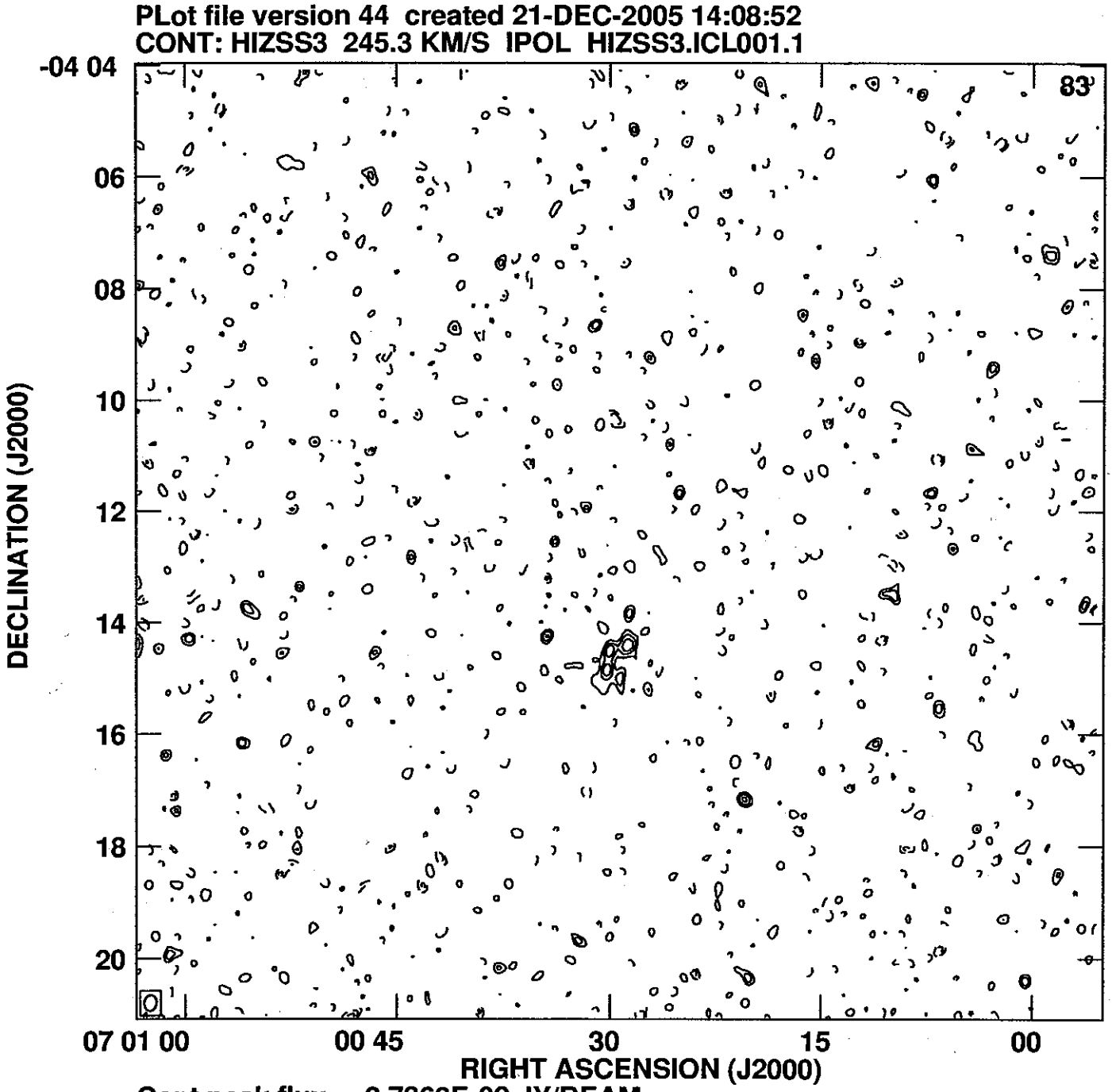
PLot file version 44 created 21-DEC-2005 14:08:52
CONT: HIZSS3 245.3 KM/S IPOL HIZSS3.ICL001.1
-04 04
06
08
10
12
14
16
18
20
83
DECLINATION (J2000)
07 01 00
00 45
30
15
00
RIGHT ASCENSION (J2000)
Cont peak flux = 3.7868E-02 JY/BEAM
Levs = 1.100E-03 * (-5, -4, -3, -2, 2, 3, 4, 7,
10, 15, 20, 25, 30, 35, 40)

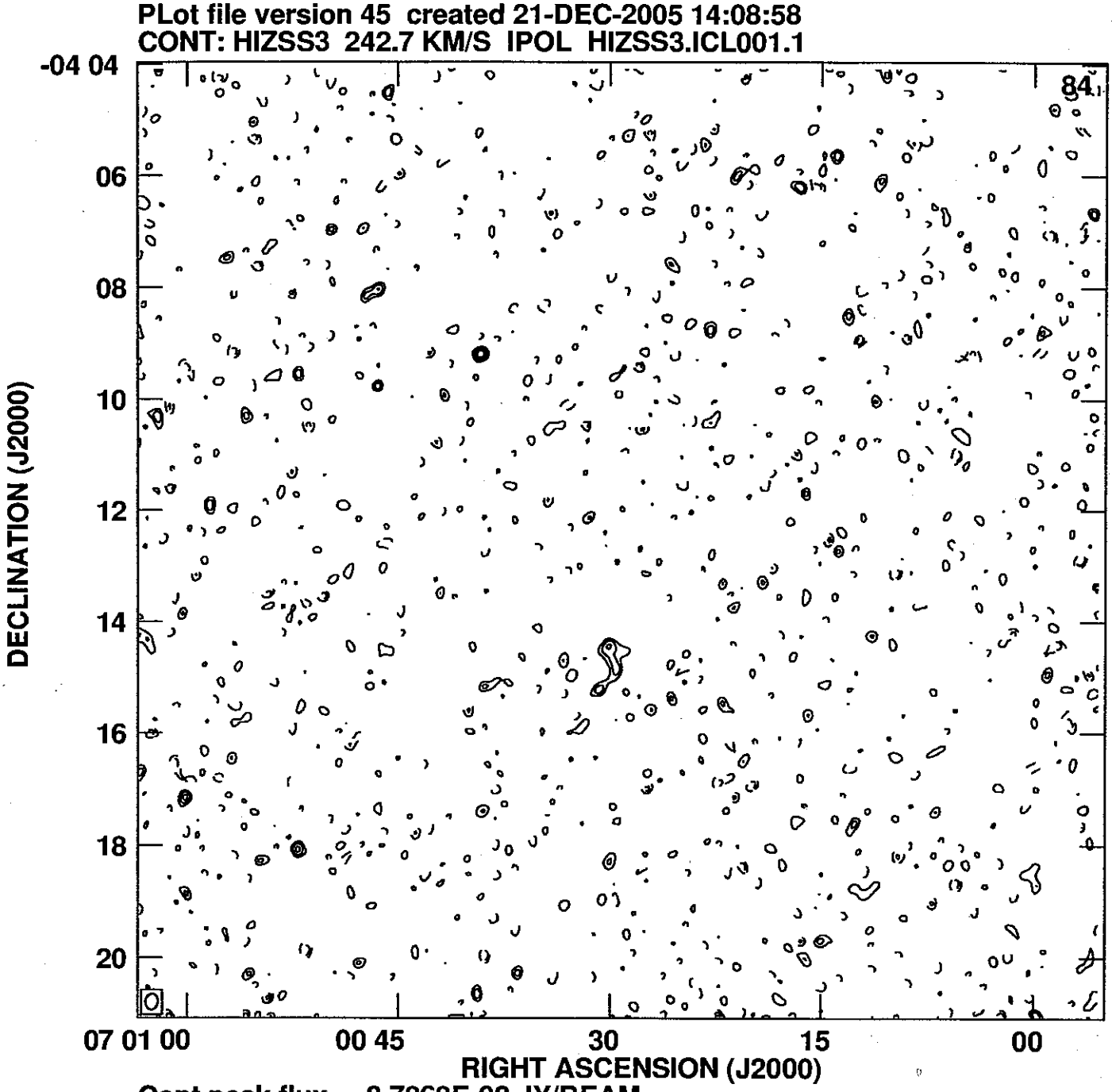
PLot file version 45 created 21-DEC-2005 14:08:58
CONT: HIZSS3 242.7 KM/S IPOL HIZSS3.ICL001.1
-04 04
06
08
10
12
14
16
18
20
DECLINATION (J2000)
07 01 00
00 45
30
15
00
RIGHT ASCENSION (J2000)
Cont peak flux = 3.7868E-02 JY/BEAM
Levs = 1.100E-03 * (-5, -4, -3, -2, 2, 3, 4, 7,
10, 15, 20, 25, 30, 35, 40)

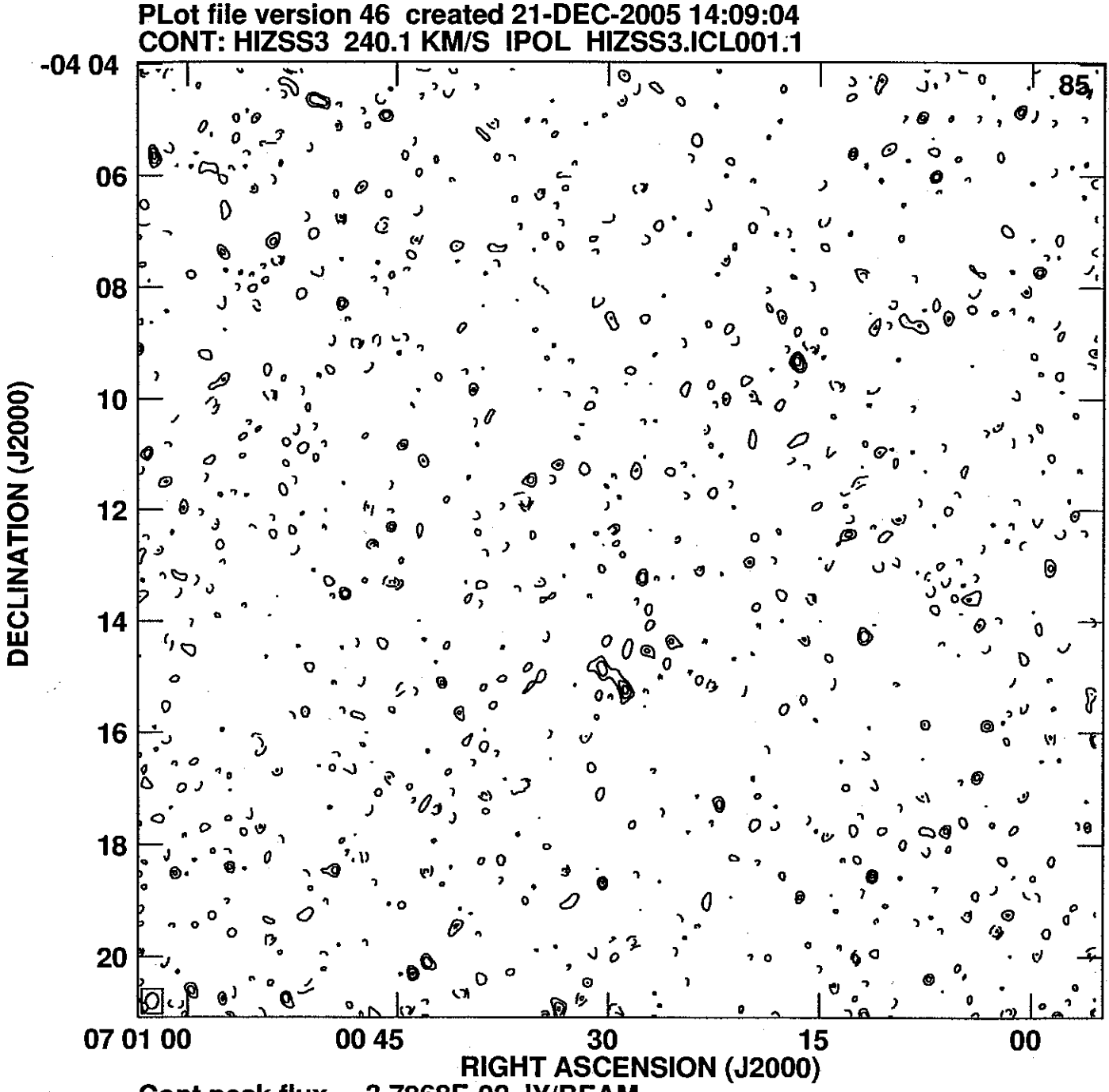
PLot file version 46 created 21-DEC-2005 14:09:04
CONT: HIZSS3 240.1 KM/S IPOL HIZSS3.ICL001.1
-04 04
06
08
10
12
14
16
18
20
DECLINATION (J2000)
07 01 00
00 45
30
15
00
RIGHT ASCENSION (J2000)
Cont peak flux = 3.7868E-02 JY/BEAM
Levs = 1.100E-03 * (-5, -4, -3, -2, 2, 3, 4, 7,
10, 15, 20, 25, 30, 35, 40)

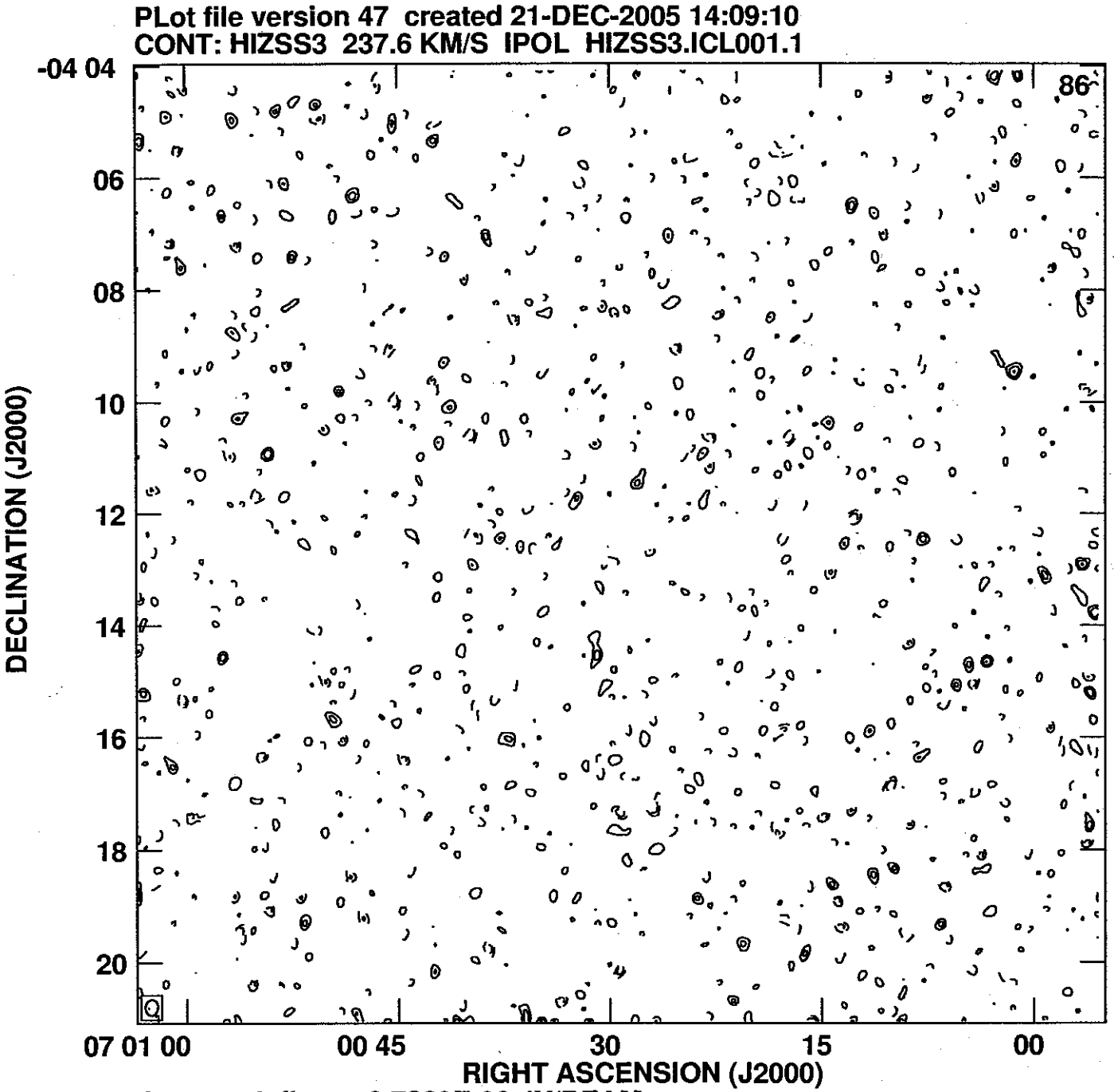
PLot file version 47 created 21-DEC-2005 14:09:10
CONT: HIZSS3 237.6 KM/S IPOL HIZSS3.ICL001.1
-04 04
06
08
10
12
14
16
18
20
DECLINATION (J2000)
07 01 00
00 45
30
15
00
RIGHT ASCENSION (J2000)
Cont peak flux = 3.7868E-02 JY/BEAM
Levs = 1.100E-03 * (-5, -4, -3, -2, 2, 3, 4, 7,
10, 15, 20, 25, 30, 35, 40)

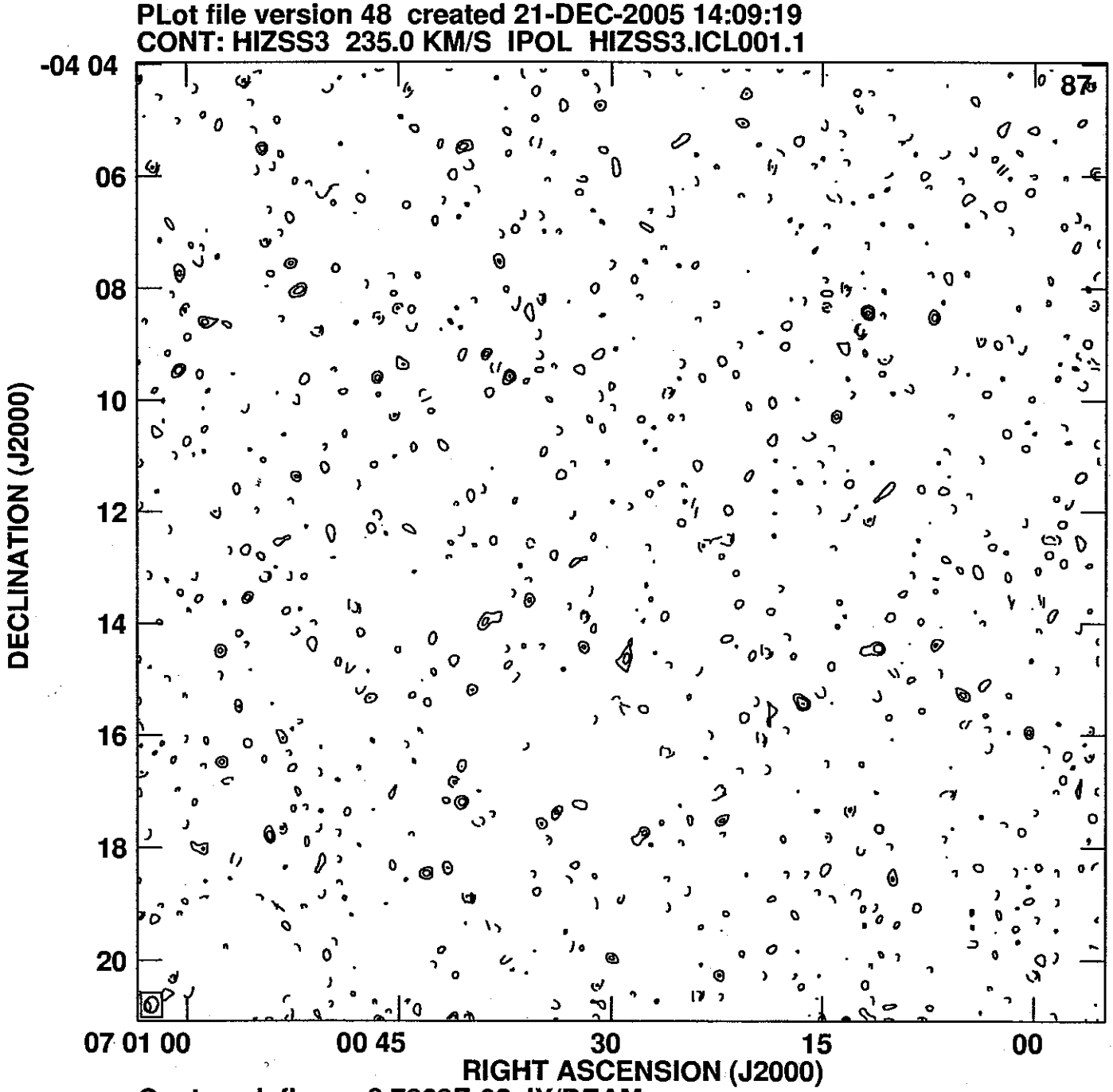
PLot file version 48 created 21-DEC-2005 14:09:19
CONT: HIZSS3 235.0 KM/S IPOL HIZSS3.ICL001.1
-04 04
06
08
10
12
14
16
18
20
DECLINATION (J2000)
07 01 00
00 45
30
15
00
RIGHT ASCENSION (J2000)
Cont peak flux = 3.7868E-02 JY/BEAM
Levs = 1.100E-03 * (-5, -4, -3, -2, 2, 3, 4, 7,
10, 15, 20, 25, 30, 35, 40)

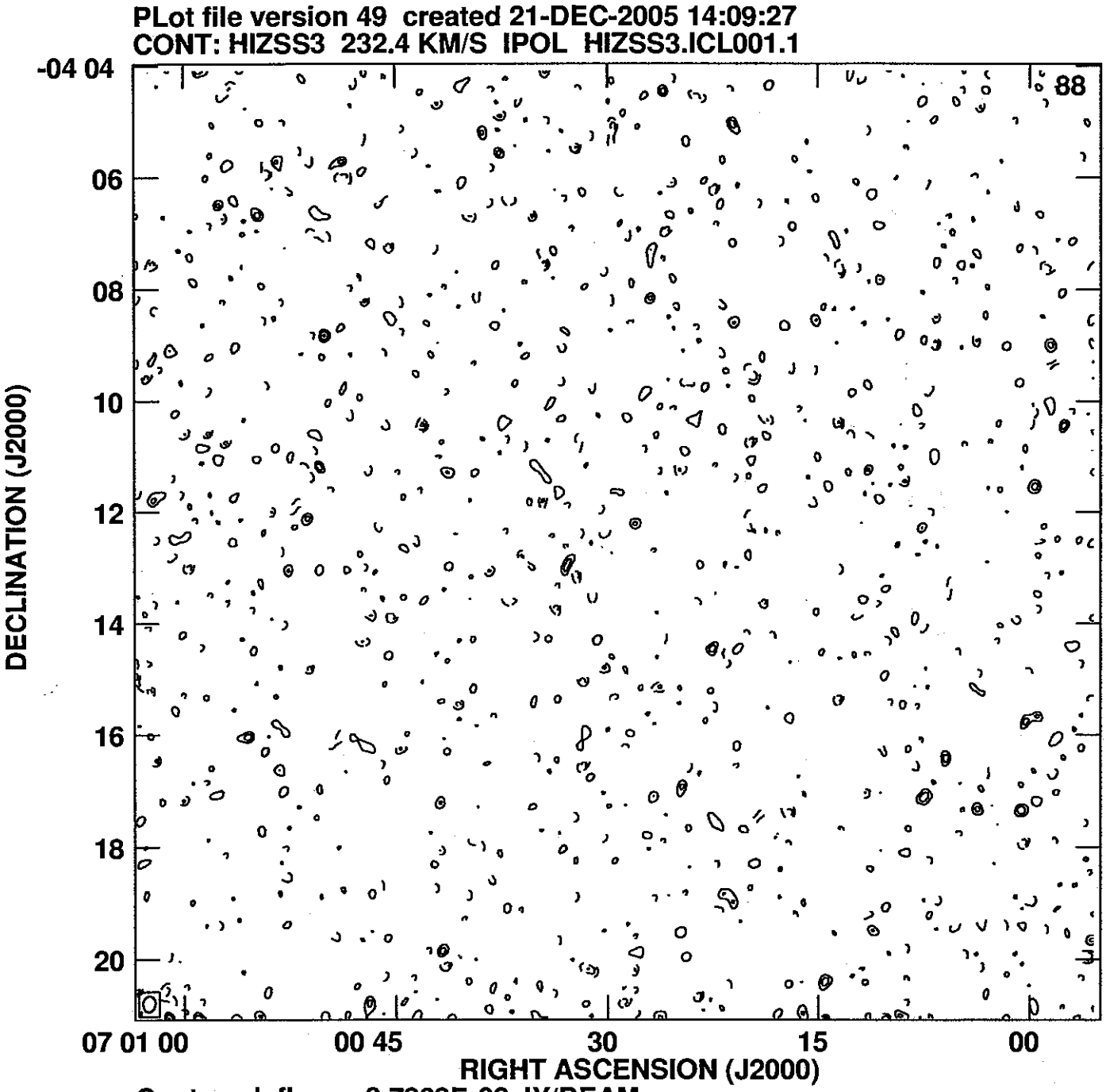
PLot file version 49 created 21-DEC-2005 14:09:27
CONT: HIZSS3 232.4 KM/S IPOL HIZSS3.ICL001.1
-04 04
06
08
10
12
14
16
18
20
88
DECLINATION (J2000)
07 01 00
00 45
30
15
00
RIGHT ASCENSION (J2000)
Cont peak flux = 3.7868E-02 JY/BEAM
Levs = 1.100E-03 * (-5, -4, -3, -2, 2, 3, 4, 7,
10, 15, 20, 25, 30, 35, 40)